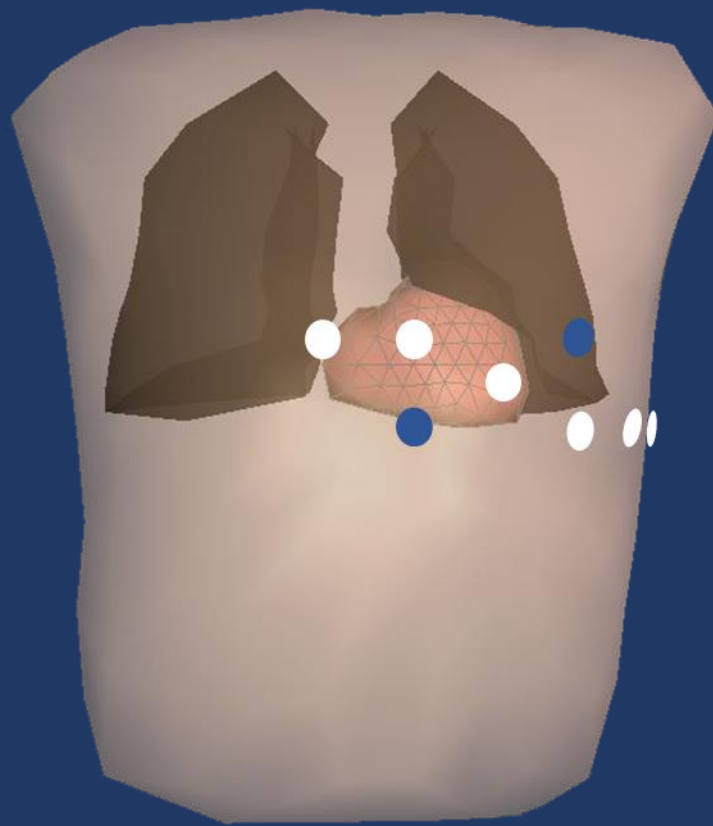


Disease-specific electrocardiographic lead positioning for early diagnosis of arrhythmogenic right ventricular cardiomyopathy

To improve early diagnosis in plakophilin-2 pathogenic variant carriers



Janna Ruisch

Master Thesis Technical Medicine

Medical Sensing & Stimulation

October 27th, 2020

Research committee

Chairman: Prof. Dr. Ir. C.H. Slump

Medical supervisor: Dr. K.P. Loh

Technical supervisor University of Twente: Prof. Dr. Ir. C.H. Slump

Technical supervisor UMC Utrecht: M.J. Boonstra MSc.

Technical supervisor UMC Utrecht: Dr. P.M. van Dam (ECG Excellence BV, Nieuwerbrug)

Process supervisor: N.S. Cramer Bornemann MSc.

External member: Dr. A.T.M. Bellos-Grob

Extra supervisor UMC Utrecht

R.W. Roudijk MSc.

**UNIVERSITY
OF TWENTE.**

ABSTRACT

Background | Arrhythmogenic right ventricular cardiomyopathy (ARVC) is an inherited disease characterized by progressive replacement of cardiomyocytes by fibrofatty tissue which can lead to heart failure or sudden cardiac death. Genetic defects in desmosomal proteins, with plakophilin-2 (PKP2) being the most frequently affected gene, contribute to disease development. Depolarization abnormalities are often the first sign of the disease, even prior to significant structural abnormalities. Early detection of electrical abnormalities might be aided by properly placed electrocardiographic (ECG) leads, like in Brugada syndrome. Therefore, this study aims to identify a better lead configuration to early detect underlying ECG changes in (a)symptomatic PKP2 pathogenic variant carriers.

Method | 67-lead body surface potential maps (BSPM) were obtained in PKP2 pathogenic variant carriers meeting the Task Force Criteria (TFC) for ARVC (ARVC group, n=7), PKP2 pathogenic variant carriers (PKP2 group, n=16) and control subjects with ventricular extrasystoles originated from right ventricular outflow tract (RVOT VES) without signs of structural heart disease (control group, n=9). In these groups, 1) temporal and spatial distribution of integrals in ARVC patients, 2) spatial distribution of (known) diagnostic ECG criteria of ARVC, and 3) additional information about the mean cardiac activation pathway through the cardiac anatomy were investigated.

Results | Depolarization abnormalities, as prolonged initial activation duration, decreased S-wave amplitude and increased RS ratio, were observed around lead V3, V4, L27 (below conventional lead V2), and L40 (above conventional lead V4). Maximum T-wave inversions in ARVC patients were observed in leads located inferior of the conventional lead V2, but no repolarization abnormalities have been observed in ARVC patients without T-wave inversions. Early ECG changes were observed in the initial QRS-segment, which resulted in prolonged initial activation duration and difference in mean cardiac activation pathway through the cardiac anatomy.

Conclusion | Additional ECG lead locations and ECG criteria suggest to be a potential benefit in the early detection of ARVC. Disease manifestation was identified solely on depolarization characteristics, particularly in the initial depolarization segment, whereas the repolarization segment showed not to include additional information for detection of initial disease manifestation. This thesis is a first step toward a disease-specific lead configuration that might improve the screening process for early detection of ARVC in PKP2-pathogenic variant carriers. Future research requires long-term monitoring of pathogenic variant carriers to relate the additional depolarization criteria with onset of disease manifestation.

Index terms

Arrhythmogenic right ventricular cardiomyopathy; plakophilin-2 pathogenic variant; body surface potential mapping; disease-specific lead configuration; early detection

CONTENTS

Abstract.....	V
List of abbreviations	9
Chapter 1 Introduction.....	13
Chapter 2 Pathophysiological background	17
Chapter 3 Technical background	25
Chapter 4 Study aim	35
Chapter 5 PART I: Departure mapping for identification of abnormal electrocardiographic lead positions.....	39
Chapter 6 PART II: Body surface distribution of conventional diagnostic electrocardiographic criteria	51
Chapter 7 PART III: CineECG method to relate mean cardiac activation patterns to cardiac anatomy.....	63
Chapter 8 Validation study	71
Chapter 9 General discussion	79
References	85
Appendix	91
Appendix A - Introduction.....	93
A.1 Prevalence of ECG TFC for ARVC	93
Appendix B – Part I.....	95
B.1 Integrals mapping	95
B.2 Departure mapping	96
Appendix C – Part II.....	97
C.1. Non-existent TAD measurements.....	97
C.2. Spatial distribution of S-wave upstroke.....	97
C.3. Spatial distribution of S-wave amplitude.....	97
C.4. Reproducibility of TAD.....	99
Appendix D – Part III.....	101
D.1. Other ARVC Population.....	101
Appendix E – Computing in Cardiology paper	103

LIST OF ABBREVIATIONS

2D	Two dimensional
3D	Three dimensional
ACM	Arrhythmogenic cardiomyopathy
ARVC	Arrhythmogenic right ventricular cardiomyopathy
AUC	Area under curve
BSPM	Body surface potential map
CVM	Center of ventricular mass
DI	Departure index
DIFC	Desmosome-intermediate filament complexes
DSC2	Desmocollin-2
DSG2	Desmoglein-2
DSP	Desmoplakin
ECG	Electrocardiographic
ECHO	Echocardiography
EDVi	End-diastolic volume index
EF	Ejection fraction
HF	Heart failure
IAD	Initial activation duration
ICD	Implantable cardiac defibrillator
JUP	Junction plakoglobin
LAO	Left anterior oblique
LBBB	Left bundle branch block
LV	Left ventricle
MRI	Magnetic resonance imaging

mTSI	Mean temporal spatial isochrones
PKP2	Plakophilin-2
RAO	Right anterior oblique
RBBB	Right bundle branch block
RMS	Root-mean-square
ROC	Receiver Operating Characteristic
RV	Right ventricle
RVOT	Right ventricular outflow tract
RWA	R-wave amplitude
SCD	Sudden cardiac death
SD	Standard deviation
SE	Sensitivity
SP	Specificity
SWA	S-wave amplitude
TAD	Terminal activation duration
TFC	Task Force Criteria
TWI	T-wave inversion
VCG	Vectorcardiogram
VES	Ventricular extrasystoles
VT	Ventricular tachycardia

CHAPTER 1

Introduction

INTRODUCTION

Arrhythmogenic right ventricular cardiomyopathy (ARVC) is an inherited disease of the heart muscle that predominantly affects the right ventricle (RV).¹ The disease is characterized by progressive loss of RV cardiomyocytes and replacement with fibrous or fibrofatty tissue, that can result in ventricular arrhythmia, sudden cardiac death (SCD), and heart failure (HF).^{1,2} The disease is caused by a genetic defect in cardiac desmosomes, where plakophilin-2 (PKP2) is the most frequently affected gene. Symptom-free pathogenic gene carriers are potentially at risk, because the disease is progressive and can appear late in life.³ The estimated prevalence of ARVC in the general population ranges from 1:1000 to 1:5000.⁴ Eighty percent of diagnosed ARVC patients are <40 years old and males are more frequently affected than females.^{5,6} ARVC is difficult to diagnose due to the heterogeneity of disease presentation. Whereas in 7-23% of the mutation carriers, SCD is the first manifestation of disease, others may never present any signs of disease.^{2,7} A clear association between electrical and structural progression has been observed, where depolarization abnormalities preceded structural abnormalities.⁸ Therefore, early detection should be focused on the detection of electrical abnormalities.

The amount of information obtained with conventional 12-lead electrocardiography (ECG) suffices for most clinical applications. However, in some applications the use of extra ECG leads or other lead locations has proven to increase the detection rate of electrical abnormalities. In this master thesis, 67-lead body surface potential map (BSPM) data was used to design a disease-specific lead configuration for early detection of ARVC in PKP2 pathogenic variant carriers. Furthermore, the novel CineECG technique was used to investigate mean cardiac activation pathways related to the cardiac anatomy. Additional information about ARVC, together with a disease-specific lead configuration, is clinically relevant for: (1) early detection of disease manifestation and monitoring of disease progression, and therefore prevention of the risk of arrhythmia and SCD; and (2) improvement of the screening process in both the hospital ‘financial & time’ aspect and reduced screening load for pathogenic variant carriers at risk for ARVC.

THESIS OUTLINE

The general purpose of this thesis is to design a disease-specific lead configuration for early detection of ARVC in PKP2 pathogenic variant carriers. In **Chapters 2 and 3**, the pathophysiological aspects of ARVC and technical aspects used in the research thesis are elaborated. In **Chapter 2**, the pathophysiological background, encompassing the history, pathophysiology, genetic involvement, ECG waveform features, screening and treatment of ARVC is described. In **Chapter 3**, the BSPM data recording and data processing are described, followed by a comprehensive introduction of the novel CineECG technique. In **Chapter 4**, the study aim, the main research question and sub-questions are presented. In **Chapter 5**, additional temporal and spatial information of ARVC are investigated by displaying abnormalities of integral distributions in BSPM. In **Chapter 6**, the spatial distribution of the current ECG criteria according to the Task Force Criteria for ARVC are investigated. In **Chapter 7**, the novel CineECG is tested as a new tool for identification of initial disease manifestation of ARVC. The results of both **Chapter 5 and 6** are combined to a disease-specific lead configuration that is validated in **Chapter 8** of this thesis. In **Chapter 9**, the major findings and future research are briefly discussed and a final conclusion is drawn.

CHAPTER 2

Pathophysiological background

PATHOPHYSIOLOGICAL BACKGROUND

HISTORY

ARVC is originally described by Fontaine and Marcus in 1982 as arrhythmogenic right ventricle dysplasia (ARVD) (**Figure 2.1**).¹ The disease was initially referred to as dysplasia, because it was thought to be a congenital defect of the RV myocardial development.¹ Since the finding that the disease is caused by a genetic defect in cardiac desmosomes, the disease is re-named as cardiomyopathy.¹ Since 1994, the diagnosis of ARVC was based on the presence of standardized major and minor Task Force Criteria (TFC), including ECG criteria, episodes of ventricular arrhythmias, RV mechanical function and morphology, histopathology, and family history. The diagnosis was fulfilled by the presence of 2 major, or 1 major plus 2 minor criteria, or 4 minor criteria from different categories.^{2,3} However, many parameters were subjective, not evidence based and lacked sensitivity to detect early disease onset in familial members. Since publication of the 1994 Task Force Guidelines, additional ECG criteria have been proposed and the genetic basis of the disease has been recognized (**Figure 2.1**). Besides, experience with quantification of image criteria of ARVC has increased and newer imaging techniques have been introduced, such as contrast-enhanced echocardiography, 3D echocardiography, cardiovascular magnetic resonance with late enhancement, and electroanatomic voltage mapping.⁹ Therefore, Marcus *et al.* proposed modification of the TFC in 2010 by defining normal RV cut off values and properly grading the disease symptoms, with the aim of improving diagnosis and management of ARVC.⁹

PATHOPHYSIOLOGY

The main characteristic of ARVC is RV fibrofatty tissue, which interferes with electrical impulse conduction. Fibrofatty tissue is induced by a genetically abnormal desmosomal protein.³ Desmosomes are intercellular junctions that provide adhesion between cells and are particularly abundant in tissues that are continually assailed by mechanical forces.^{10,11} Desmosomes are composed of desmosome-intermediate filament complexes (DIFC), a network that maintains the integrity of such tissues.¹⁰ DIFC may be divided into three components: two intracellular and one intercellular. In the intercellular region, desmoglein and desmocollin are bound to each other. Intracellularly regions contain the intracellular ends of desmocollin and desmoglein, desmoplakin, plakoglobin and plakophilin. All components of the DIFC must be equally capable of resisting mechanical disruption, and failure of even one of them leads to degeneration of cardiac myocytes with replacement by fat and fibrous tissue.¹⁰ Distribution of degeneration of cardiac myocytes is highly characteristic. In early disease stages, subtle or even

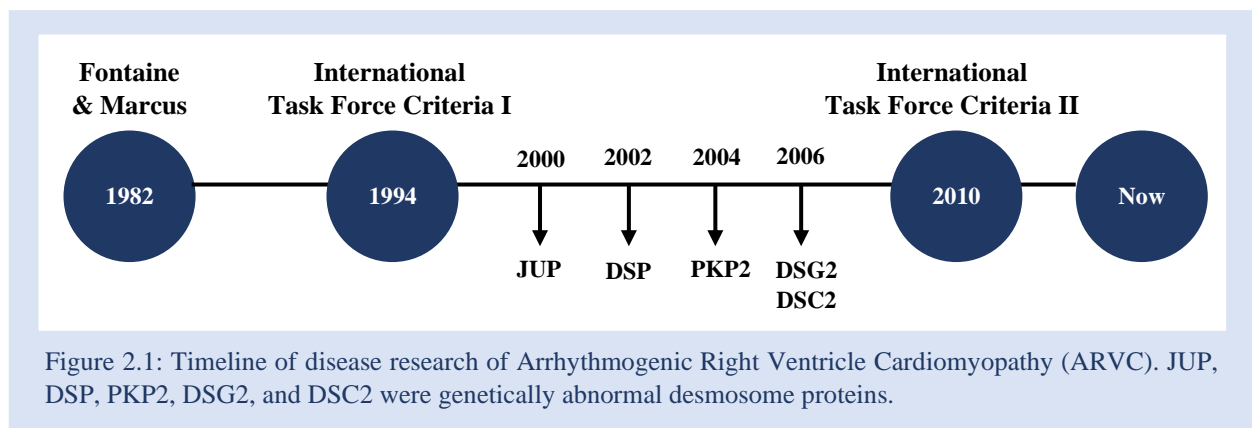


Figure 2.1: Timeline of disease research of Arrhythmogenic Right Ventricle Cardiomyopathy (ARVC). JUP, DSP, PKP2, DSG2, and DSC2 were genetically abnormal desmosome proteins.

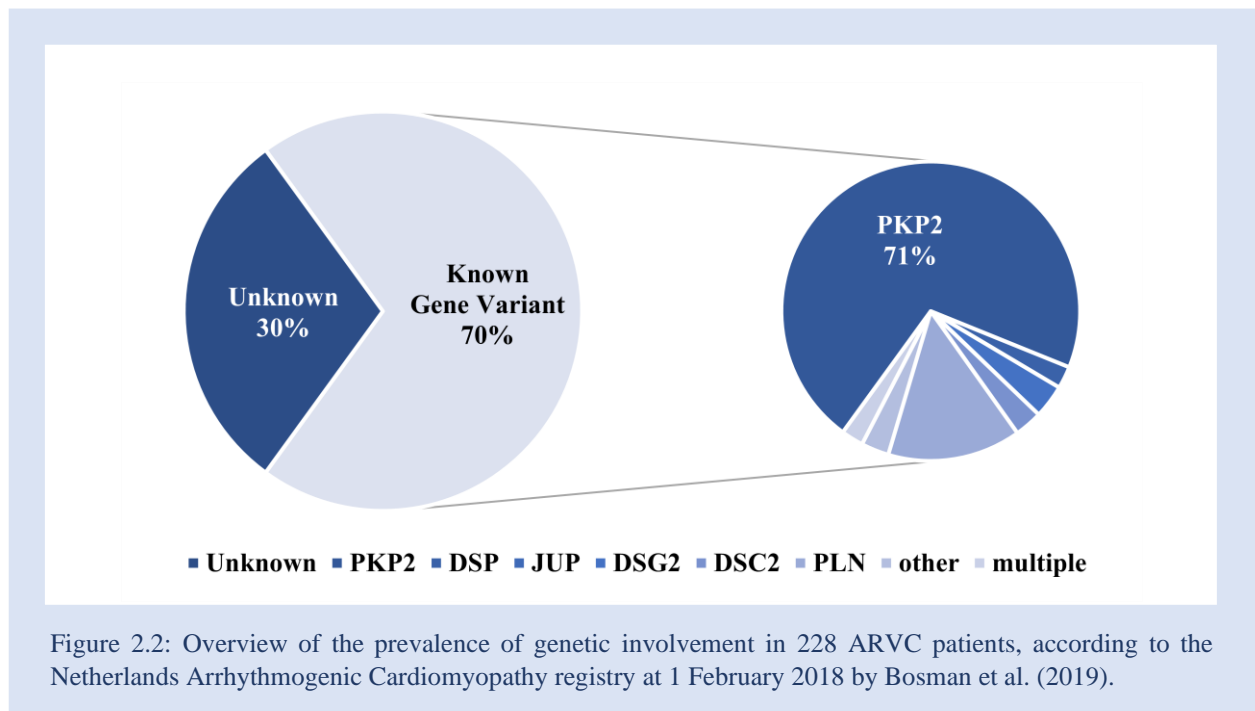
no structural changes may be present in the RV. Most commonly affected were segments with the largest mechanical stress during the cardiac cycle, like the inflow tract, outflow tract or apex of the RV.^{9,12}

GENETIC INVOLVEMENT

Five genes encoding important desmosomal proteins are thought to account for the disease in approximately 70% of ARVC patients.^{11,13} As can be observed in **Figure 2.1**, junction plakoglobin deletion encoded by JUP was the first found dominant gene (2000), followed by a discovery of pathogenic variants in desmoplakin encoded by DSP (2002), plakophilin-2 by PKP2 (2004), desmoglein-2 by DSG-2 (2006) and desmocollin-2 by DSC-2 (2006).^{3,11} Cox *et al.*¹⁴ and Bosman *et al.*¹³ designed the Netherlands Arrhythmogenic Cardiomyopathy registry, which contained 850 individual patient records at 1 February 2018. Among the individual patient records, 228 individual patients met the definite ARVC diagnosis according to the TFC for ARVC. An overview of the genetic involvement within ARVC patients can be found in **Figure 2.2**. In 70% of all ARVC patients a genetic variation is known, with PKP2 being the most frequently affected gene, present in up to 71% of ACM patients with a known variation. Comprehensive pathogenic variant screening of known ARVC genes can detect genetic abnormalities in at least 40-50% of family members.^{2,3} Cascade genetic screening of family members is therefore important, because it allows early identification of symptom-free carriers. Symptom-free pathogenic variant carriers are potentially at risk because of the progressive character of the disease and therefore life-long clinical assessment is needed.³

ELECTROCARDIOGRAPHIC CRITERIA

In the TFC for ARVC, electrophysiological criteria of ARVC are based on depolarization or conduction, repolarization, and arrhythmic features.⁹ Abnormalities were subdivided into major and minor categories. The ECGsim software package, available from www.ecgsim.org and free of charge, was used to simulate the depolarization and repolarization abnormalities in a 12-lead ECG (V1-V3) (**Figure 2.3**).



Depolarization abnormalities

Depolarization abnormalities that can be detected in 12-lead ECGs are a prolonged terminal activation duration (TAD) and epsilon waves in the right precordial leads.⁹ Prolonged TAD reflects RV activation delay in the transmural or endocardial region of the RV base (**Figure 2.3; lead V1**). TAD was first proposed by Cox *et al.* in 2008 and was added to the TFC for ARVC in 2010.¹⁵ The ECG criterium was a refinement from the S-wave upstroke criterium that was reported by Nasir *et al.* in 2004.¹⁶ The S-wave upstroke was defined as the duration from the nadir of the S-wave up to the isoelectric line, where the TAD was defined as the duration from the nadir of the S-wave to the end of all depolarization deflections. Therefore, TAD also includes late fractional signals and epsilon waves. Both parameters were considered abnormal when exceeding the duration of 55ms in lead V1, V2 or V3. In the simulation model, TAD can be prolonged due to RV activation delay in (1) the transmural region or (2) the endocardial region of the RV base. In the first case, RV activation delay causes epsilon waves that resulted in a prolonged TAD measurement (**Figure 2.3; lead V1**). In the second option, RV activation delay causes late activation propagating from epi- to endocardium, that corresponds to an increased S-wave amplitude in V1. As can be observed in **Appendix A.1**, the prevalence of prolonged TAD in ARVC patients was reported to be between 22% and 66%, with a pooled prevalence of 41% (38% - 44%). Specificity was only reported by Jain *et al.* and corresponded to 89% (77% - 100%).

Epsilon waves are electrical potentials of small amplitude that occur at the end of a QRS complex in the right precordial leads (**Figure 2.3, lead V2**).² In the simulation model, epsilon waves in lead V2 were observed at delayed depolarization activation in a transmural area located at the RVOT. Delayed depolarization activation located in other areas than the ventricular base do not present as epsilon waves in lead V2. Epsilon waves, caused by late activation potentials, are potential substrates for re-entry ventricular tachycardia (VT).⁵ Epsilon waves are not often observed in the conventional 12-lead ECG, as was visualized in **Appendix A.1**. The prevalence of epsilon waves in ARVC patients was reported to be between 6% and 56%, with a pooled prevalence of 16% (14% - 17%). Yet, the ECG criterion is very specific in ARVC patients and observation of the depolarization abnormality in the right precordial leads (V1 through V3) corresponds to a major criterion. Garcia-Niebla *et al.*¹⁷ demonstrated that the prevalence of epsilon waves may be underestimated in the conventional 12-lead ECG because of its frequency rate. Conventional 12-lead ECG use 40Hz low-pass filtering to reduce muscle noise, but the low cutoff frequency might attenuate or remove the presence of epsilon waves.¹⁷

Repolarization abnormalities

Detection of repolarization abnormalities are expressed by the presence of inverted T-waves, with T-wave inversions in the right precordial leads (V1 through V3) in the absence of complete RBBB being a major criterion.⁹ Repolarization abnormalities are an early and sensitive electrocardiographic marker for diagnosis of ARVC.⁹ T-wave inversions have been shown to be more common in patients with advanced RV dysfunction and may even extent to the left precordium.^{18,19} The presence of T-wave inversions can be caused by a prolonged repolarization phase within the transmembrane potential (**Figure 2.3; third row**), or a delayed repolarization phase that could be the direct effect of delayed depolarization (at a constant refractory period). T-wave inversions were observed when these transmembrane abnormalities were applied in a transmural or epicardial region in the RV base. Enlargement of the abnormal region (**Figure 2.3; second column**) corresponds to T-wave inversions present in more precordial leads. Conversely, a prolonged repolarization phase in the endocardial area of the RV base

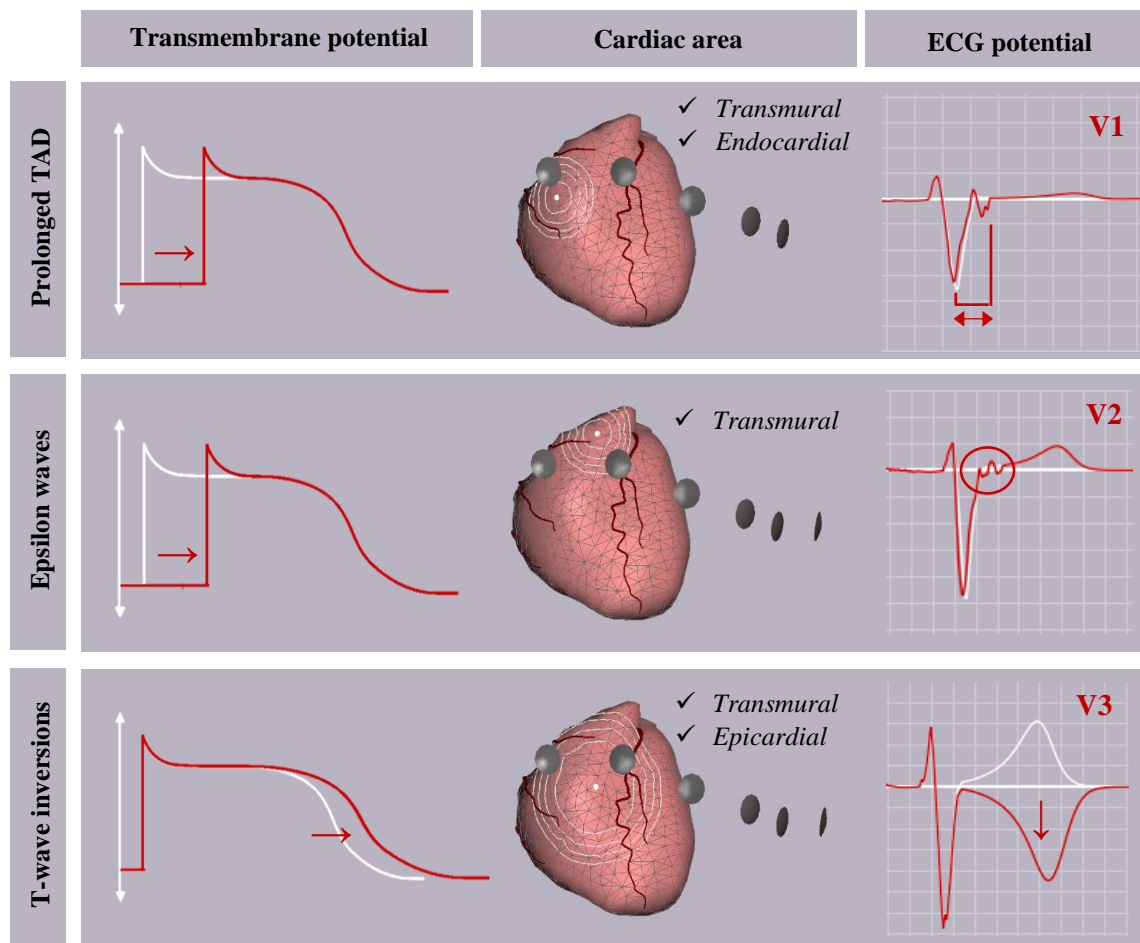


Figure 2.3: Simulated electrocardiographic (ECG) potentials of prolonged terminal activation duration (TAD; first row), epsilon waves (second row) and T-wave inversions (third row). Transmembrane potentials (TMP; first column) and ECG potentials (third column) were visualized in normal situation (white). Besides, abnormal TMP (red) originated in single cardiac region (second column; white circle) is simulated. Abnormal TMP could be applied endocardial, epicardial or transmural. Diseased regions that cause the visualized abnormal ECG signals (red) were indicated with ✓.

corresponds to increased positive T-waves. T-wave inversions through V4 are related to LV involvement and can be used as a marker of poor prognosis.²⁰

As can be observed in **Appendix A.1**, in the last fifteen years the prevalence of T-wave inversion in V1 through V3 in ARVC patients was reported to be between 26% and 80%, with a pooled prevalence of 65% (95% CI: 62 – 67%). Specificity was only determined in two reports with a pooled specificity of 98% (95% CI: 93 – 100%). A wide range in sensitivity was observed, that might be explained by differences in follow-up after diagnosis. The presence of PKP2 pathogenic variants corresponds to higher sensitivity (80%) for T-wave inversions compared to no PKP2 pathogenic variant (47%).¹⁵ No differences in the prevalence of T-wave inversions were found between men and women, according to Bauce et al (2008).²¹

Arrhythmic features

With regard to arrhythmic features, the presence of non-sustained or sustained VT with left bundle-branch morphology with superior axis, indicates origin of the VT in the inferior RV and is defined as a major criterion for ARVC.⁹ VTs are observed in 50-80% of patients with ARVC.⁵ Ruwald *et al.* (2015) showed that VT and SCD were developed at an earlier age in patients participating competitive sports compared with patients who participated in recreational sport or inactive patients.²² Therefore exercise restriction is a recommended lifestyle modification for subjects at risk.

SCREENING & TREATMENT

Nowadays, the screening process includes clinical and family history, physical examination, chest radiograph, 12-lead ECG, 24-hour ambulatory ECG, signal-averaged ECG, stress test, and 2D echocardiography. Patients in whom non-invasive assessment is inconclusive might require further examination by contrast-enhanced MRI, contrast angiography, and endomyocardial biopsy.³ In case of ARVC diagnosis, patients will be treated to (1) reduce the mortality from SCD or death from HF, (2) to prevent or decelerate disease progression, and (3) to improve quality of life by reducing symptoms.¹ Therapeutic options consist of lifestyle modifications (exercise restriction), pharmacological treatment, radiofrequency ablation, implantation of cardioverter defibrillator, and even cardiac transplantation.^{1,23}

CHAPTER 3

Technical background

TECHNICAL BACKGROUND

BODY SURFACE POTENTIAL MAPPING

BSPM uses multi-lead ECGs to portray cardiac electrical information on a map representing the body surface. The noninvasive technique visualizes the spatial variation of potentials over the body surface. Often a sequence of time instants throughout the cardiac cycle is used to image the spatial variation of potentials over the body surface.²⁴ BSPM focuses on the magnitude, location, gradient, and migration of potential extrema as well as the shape and dynamics of iso-potential contours throughout the cardiac cycle, where conventional ECG relies on the interpretation of waveform features.²⁵

The origins of BSPM go back to 1888, when Waller described a diagram showing the potential distribution he expected on the body.^{24,26} The beginning of modern measurements of surface maps were described in 1952, but limitations in recording technology resulted in a lengthy task of construction of maps for a single subject. Since the advent of electronic amplifiers and laboratory computers, the time required to record a map has been significantly reduced.^{24,25} Despite the fact that many changes in map patterns have been observed in cardiac patients,²⁴ routine use of BSPM in clinical practice is limited due to the complexity and the high amount of leads.²⁷ Currently many lead systems are in use in the research environment, differing in lead locations and in the number of leads used.²⁷ Lead systems of 64, 120, 129, 192 or even 242 torso leads are used to measure electrophysiologic potentials, where more recording sites result in higher spatial resolution.^{25,27} Leads can be placed in separated rows and columns over the thorax or based on the potential gradient distribution. When taking the potential gradient distribution into account, the spatial lead density is increased in the precordial region and reduced on the posterior surface.²⁵

BSPM are often represented in the form of isopotential contour patterns or isopotential maps, to visualize the pattern of the voltage potentials (mV). Isopotential maps can focus on different parts of the ECG data, as P-wave, QRS-complex and T-wave. In these maps, maxima and minima can be identified.²⁴ In addition to isopotential maps, similar map types of preprocessed ECG data can be displayed. For diagnostic purposes, difference maps and departure maps have been used.²⁵ Difference maps portray differences with respect to reference data, which can correspond to the mean potential value in some appropriate population group, or to the mean potential value measured at a reference time.²⁷ In departure maps, the difference maps are scaled by the standard deviation of the reference data. Such maps identify areas on the body surface that depart significant from the reference data.²⁷

DATA ACQUISITION

In this thesis, a 67-lead BSPM system was used manufactured by Biosemi (Amsterdam, The Netherlands, <https://www.biosemi.com/>). For each subject, 64 precordial and 3 limb lead sites were recorded using a 24-bit ActiveTwo AD converter, with a sample rate of 2048Hz and a built-in first-order 3600Hz anti-aliasing filter. Wilson's central terminal was used as reference potential. ActiView LabVIEW software was used as acquisition program to display all channels on screen and save the digitized data in bitmap distribution format (BDF).^{28,29}

The 64 precordial leads (disposable 3M Red Dot) were placed in vertical strips of 28cm over the thorax, with individual leads indicated by numbered dots (**Figure 3.1**). The left and right half shows lead locations at the

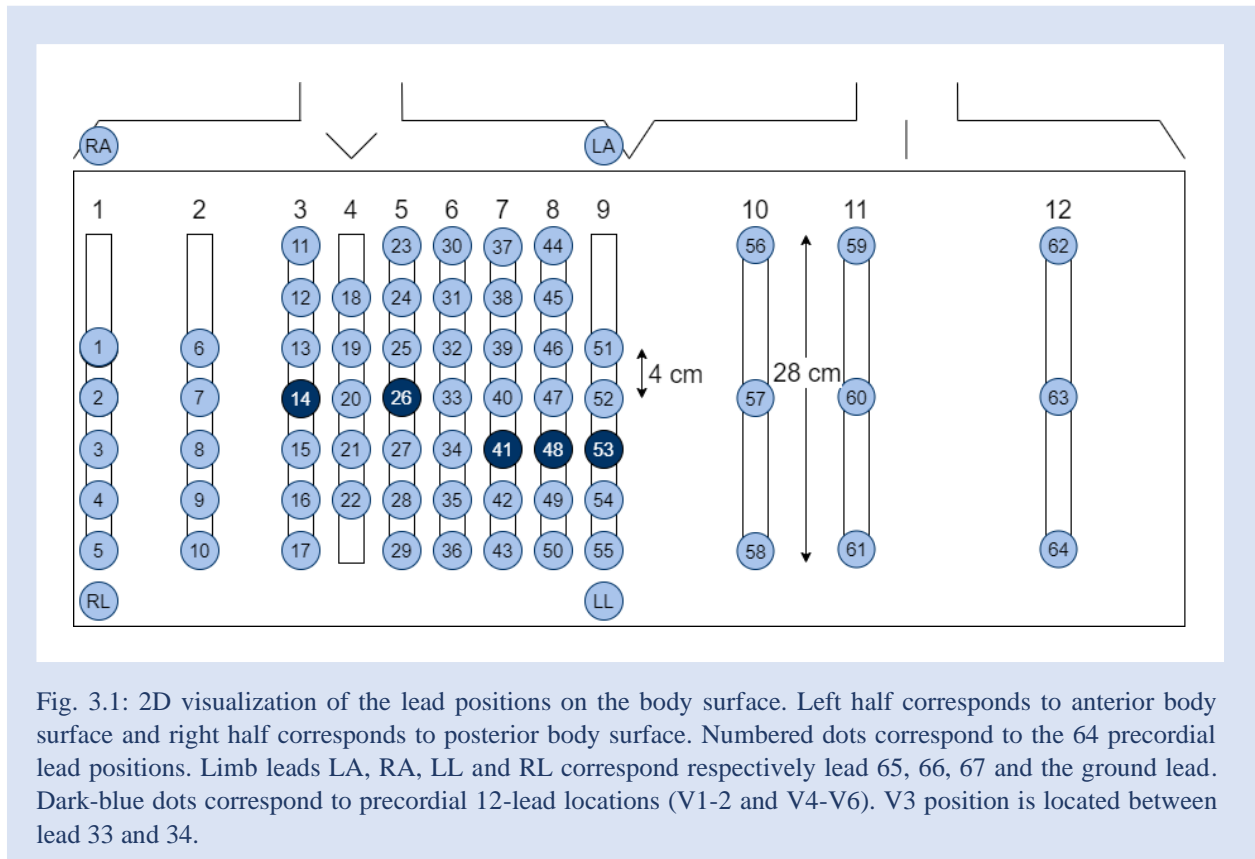


Fig. 3.1: 2D visualization of the lead positions on the body surface. Left half corresponds to anterior body surface and right half corresponds to posterior body surface. Numbered dots correspond to the 64 precordial lead positions. Limb leads LA, RA, LL and RL correspond respectively lead 65, 66, 67 and the ground lead. Dark-blue dots correspond to precordial 12-lead locations (V1-2 and V4-V6). V3 position is located between lead 33 and 34.

anterior and posterior body surface, respectively. Nine vertical strips were placed on the anterior body surface with strip 4 located at the sternum. Leads were separated 4cm from each other. Strip 3 and 5-9 are located at the same sagittal axis as the conventional 12-lead ECG leads, where lead 14, 26, 33-34, 41, 48 and 53 corresponds to conventional lead V1-V6. Conventional lead V3 position is located between lead 33 and 34. Three vertical columns were placed at the back.

Four minutes of BSPM were acquired from all leads for each subject in supine position. Due to an improvement in the recording protocol during the inclusion period, few subjects were recorded only during normal breathing conditions, where other subjects were recorded with the improved recording protocol. In the improved recording protocol, the patients received breathing instructions. Briefly, the breathing instructions included ten second recording at end-inspiration, ten second recording at end-expiration and 40 seconds interval of normal breathing conditions.

STUDY SUBJECTS

The study population consisted of 26 PKP2 pathogenic variant carriers, who underwent series of clinical tests to ascertain the fulfillment of the TFC for ARVC, and 12 patients with symptomatic right ventricular outflow tract ventricular extrasystoles (RVOT VES). ARVC was diagnosed based on the TFC for ARVC. Exclusion criteria were complete right bundle branch block (QRS width > 120ms) and other underlying diseases that affect ECG morphologies. The RVOT VES subjects were considered to be control subjects, where subjects that showed signs of heart failure or conduction abnormalities were excluded from the study (QRS width > 120ms, LV ejection

Table 3.1: Patient characteristics of the seven individual PKP2 pathogenic variant carriers that met the Task Force criteria for ARVC.

VARIABLES	N1	N2	N3	N4	N5	N6	N7
Age at BSM, y	17	47	59	61	20	28	19
Duration after diagnosis, y	2	4	5	0	3	12	0
Gender	M	F	M	M	F	M	F
ICD, y	2013	-	2015	-	-	2013	-
BSPM CHARACTERISTICS							
QRS width (ms)	107	94	116	94	104	105	101
STT segment length (ms) #	323	334	334	360	288	347	387
PQ interval (ms)	190	210	200	200	190	150	230
TASK FORCE CRITERIA *							
I. Structural alterations	++	++	++	+		++	++
II. Tissue characterization							
III. Repolarization abnormalities	++	++	++		+	++	
IV. Depolarization abnormalities	+	+	+				
V. Arrhythmias	+	++	++	+	+	++	
VI. Family history	++	++	++	++	++	++	++
TOTAL MAJOR CRITERIA	3	4	4	1	1	4	2
TOTAL MINOR CRITERIA	2	1	1	2	2	0	0
TFC SCORE	8	9	9	4	4	8	4

determined before normalization preprocessing step

* determined at date of BSM measurement from clinical data. ++ = major criterion. + = minor criterion. Definite ARVC is defined as modified TFC score ≥ 4 , with TFC score = $2 \cdot \text{Major} + 1 \cdot \text{Minor}$;

fraction (LVEF) $<45\%$, RVEF $<45\%$, RV end-diastolic volume index (EDVi) $> 110\text{ml}/\text{m}^2$). All subjects underwent recording in sinus rhythm.

Three PKP2 pathogenic variant carriers (with prolonged QRS width) and three control subjects (with signs of heart failure) were excluded from the study. The final study population consisted of 23 PKP2 pathogenic variant carriers, whereof seven patients met the TFC for ARVC. Individual ARVC subject characteristics can be found in **Table 3.1**. ARVC was defined as the modified TFC score ≥ 4 , with TFC score = $2 \cdot \text{Major} + 1 \cdot \text{Minor}$. Subject characteristics of each group can be found in **Table 3.2**. For all subject characteristics, heart function and BSPM characteristics, normal distribution was found across the ARVC, PKP2 and CONTROL group. From sixteen PKP2 pathogenic variant carriers, all subjects carried a pathogenic variation associated with ARVC (major criteria) and three subjects showed >500 ventricular extrasystoles per 24 hours (minor criteria).

DATA PROCESSING

For every subject, data preprocessing and beat selection from BSPM data was performed in MATLAB (version R2019a). Pre-processing of BSPM data consisted of several steps (**Figure 3.2**). First, the BSPM measurements were down-sampled to a sampling frequency of 1000Hz. Here, *resample* function was used that applied a default

Table 3.2: Group characteristics of the arrhythmogenic right ventricular cardiomyopathy group, PKP2 group and CONTROL group.

VARIABLES	ARVC (n=7)	PKP2 (n=16)	CONTROL (n=9)
Age (y)	35.9 ± 17.9	37.7 ± 17.0	33.6 ± 12.5
Male	4 (57.1)	5 (31.3)	3 (33.3)
ICD	3 (42.9)	0 (0)	0 (0)
Task Force Criteria	6.6 ± 2.4	2.2 ± 0.4	-
Duration after diagnosis, y	3.7 ± 3.8	-	-
HEART FUNCTION			
LV EDV index (ml/m ²)	93.3 ± 15.4	94.1 ± 11.4	94.8 ± 16.5
LV EF (%)	58.7 ± 4.6	55.4 ± 4.4	53.8 ± 5.3
RV EDV index (ml/m ²)	129.0 ± 39.7 # %	91.7 ± 13.3	92.0 ± 14.3
RV EF (%)	40.9 ± 13.1	56.2 ± 6.2	53.1 ± 6.4
ECG			
QRS width (ms)	103.0 ± 7.7	105.9 ± 5.7	104.8 ± 8.8
STT segment length (ms)	339.0 ± 30.9	341.6 ± 30.3	329.6 ± 29.8
PQ interval (ms)	195.7 ± 24.4	185.3 ± 31.1	186.7 ± 25.5
Heart rate (bpm)	61.2 ± 9.9	60.8 ± 11.2	62.6 ± 8.8

Abbreviations: ICD = implantable cardioverter-defibrillator, LV = left ventricle, RV = right volume, EDV = end-diastolic volume, EF = ejection fraction;

Subject characteristics were determined at date of BSM measurement. Heart function was determined from magnetic resonance imaging. ECG characteristics were determined from BSPM data.

ARVC vs CONTROL, significant difference

% ARVC vs PKP2, significant difference

FIR antialiasing lowpass filter (Kaiser window with cut-off frequency $f_c = \pi/\max(p,q)$ rad/sample, with $p=2048$ and $q=1000$).

Next, two moving average filters were applied to remove the high-frequency and low-frequency signals. First a moving average low pass filter was used with window size $M = 20$ ms, which corresponds with 50Hz moving average low-pass filter. Second, a high pass filter was applied by subtracting a moving average low pass filter from the data. Here, a window size $M = 10.000$ ms was used, which corresponds to 0.1Hz moving average low-pass filter. The result of the moving average lowpass filter can be observed in a five second data preview in **Figure 3.2 (step 2)** and the result of both filter methods can be found in **Figure 3.2 (step 3)**.

Data preprocessing was pursued with a baseline correction using spline function to interpolate over the P-wave onsets in the filtered signal. P-wave onsets were manually determined, by defining the PQ-interval within the root-mean-square (RMS) signal of all 67 leads:

$$x_{RMS} = \sqrt{\frac{1}{n} \sum_{i=1}^n x_i^2} \quad (3.1)$$

where n corresponds to 67 electrodes and x corresponds to the recorded lead signal i . Default PQ-interval was set at 260ms. In **Figure 3.2 (step 3)**, an example of the spline interpolation through P-wave onsets is shown. Baseline

correction was applied by subtracting the baseline from the filtered signal, that resulted the start- and end-potential of every beat corresponding to 0mV.

After baseline correction, ten consecutive sinus beats were selected during resting respiration. In case ventricular extrasystoles were present in the data that limited selection of consecutive sinus beats, ten not consecutive sinus beats were manually selected. ECG annotations were collected for every beat by manually assigning the QRS-onset, T-wave end, QRS-offset, T-wave apex, U-wave apex and U-wave end at the RMS signal of all 67 leads. When U-waves were present, the end T-wave was measured in the nadir of the curve between the T- and U-wave. Both ECG signals and ECG annotations were outputs of the preprocessing. Visualization of the RMS signal of all 67 leads and the corresponding ECG annotations can be observed in **Figure 3.2 (step 4)**. From left to right, QRS-onset, QRS-end, T-wave apex and T-wave end were marked with black dots.

DATA SEGMENTATION

In this study, both the QRS-segment and STT-segment are analyzed separately as T-wave morphology varies with changes in heart rate. At increased heart rate, the T-wave morphology is more symmetrical and shows an increase in amplitude.³⁰ Therefore, the averaged beat was segmented in a QRS-segment and STT-segment (**Figure 3.3**).

First, all ten beats were aligned at QRS-apex of the RMS, as this reflects time of maximum ventricular activation. Next, leads with noise were assumed to have bad electrode-skin interface and were removed from the dataset. Mean SD of all ten beats were analyzed in leads with noise and an adequate cut-off value of 0.04mV was defined for the classification of a bad lead measurement. In **Figure 3.3 (step 2)**, ten beats of a bad data measurement (lead 28) is shown together with its horizontal neighbor leads (lead 22 and 35). In lead 28, the mean SD exceeded 0.04mV, and therefore the data in this lead was removed. Per subject, 0 to 3 leads were removed. Next, the ten consecutive beats were averaged. The QRS-complex was segmented by

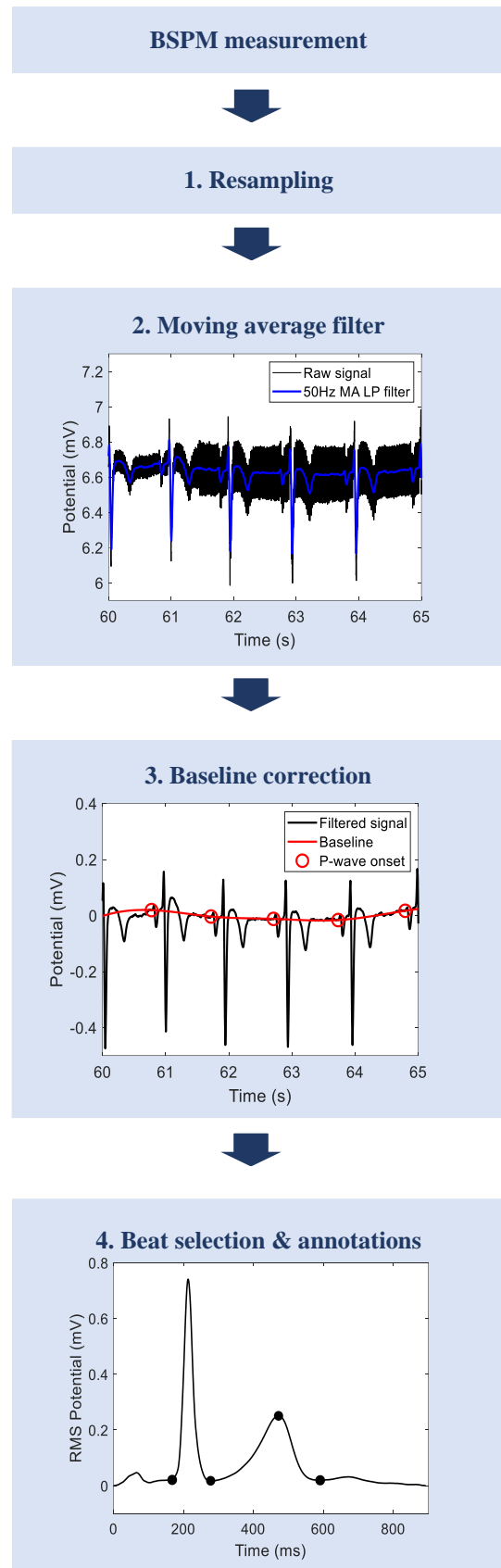


Fig 3.2. The preprocessing steps of body surface potential map measurements. In step 2 and 3, the potentials of lead 14 (V1) is shown.

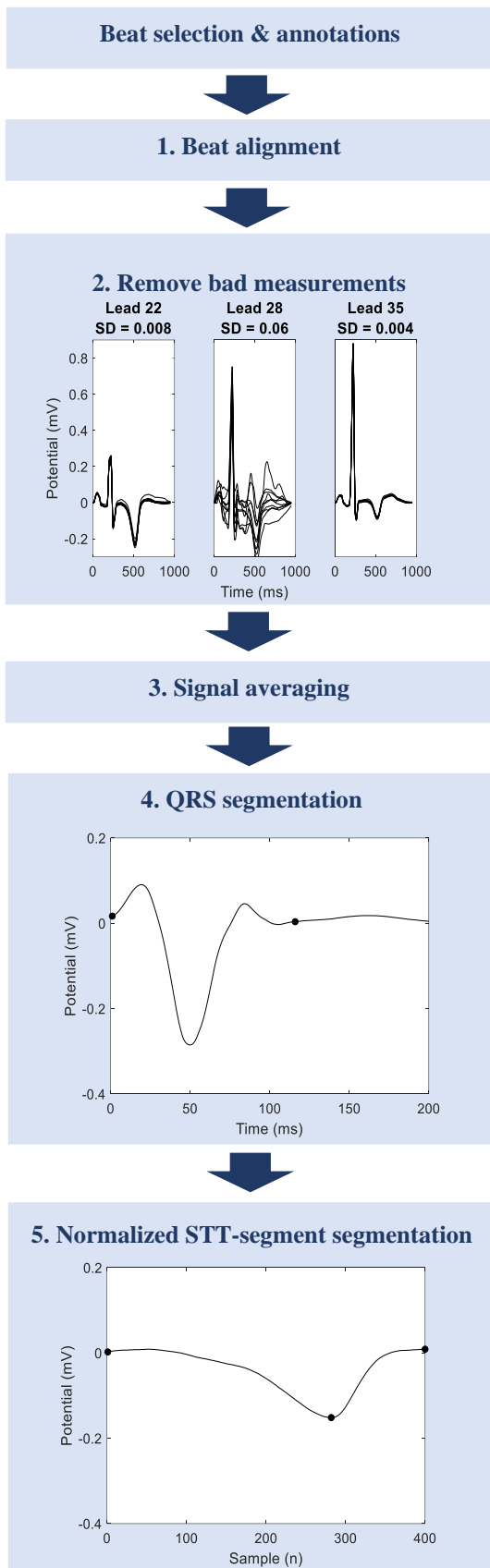


Fig 3.3. The process from beat selection toward the QRS- and STT-segment. QRS- and STT-segment of lead 14 (V1) were shown.

extracting the first 200ms after QRS onset. It is assumed that heart rate does not influence the QRS-complex morphology. In **Figure 3.3 (step 4)**, an example of a segmented QRS-complex of lead V1 is shown, with two black dots referring to QRS-onset and QRS-offset.

The heart rate does influence the STT-segment morphology, and more precisely the interval from QRS-offset to T-wave apex.³¹ It was hypothesized that the interval from T-apex to the end of the T-wave might not be affected by change in heart rate. Therefore, the interval from QRS-offset to T-wave apex, determined in the RMS of the STT-segments, were normalized to create STT-intervals with equal lengths of 400 samples. *Resample* function was used that applied an FIR antialiasing lowpass filter and compensates for the delay introduced by the filter. The Kaiser window, with cut-off frequency $\pi/\max(p,q)$, was used to design the lowpass filter. Here, p and q correspond to the sample size of the old and new STT-interval, respectively. The index of T-wave apex was determined as the steepest slope in the cumulative sum of the baselined STT-segment. In **Figure 3.3 (step 5)**, an example of a normalized, segmented STT-segment of lead V1 is shown, with three black dots referring to the QRS-offset, T-wave apex and T-wave end. Note that, due to normalization within the STT-segment, the time unit (ms) is changed to samples (n).

CINEECG

The novel CineECG method relies on a combination of the vectorcardiogram (VCG) and patient-specific anatomical modeling. The method, developed by ECG Excellence BV, computes the mean position of the all electrically active myocardial tissue through the heart during the QRST-complex, called mean temporo-spatial isochrone (mTSI).³² A main advantage of this technique is the ability to relate electrical signals to the cardiac anatomy, which makes characterization and localization of small areas of conduction delay and local ischemia most likely to be enhanced. A visualization of the work-flow of the technique can be found in **Figure 7.1**.

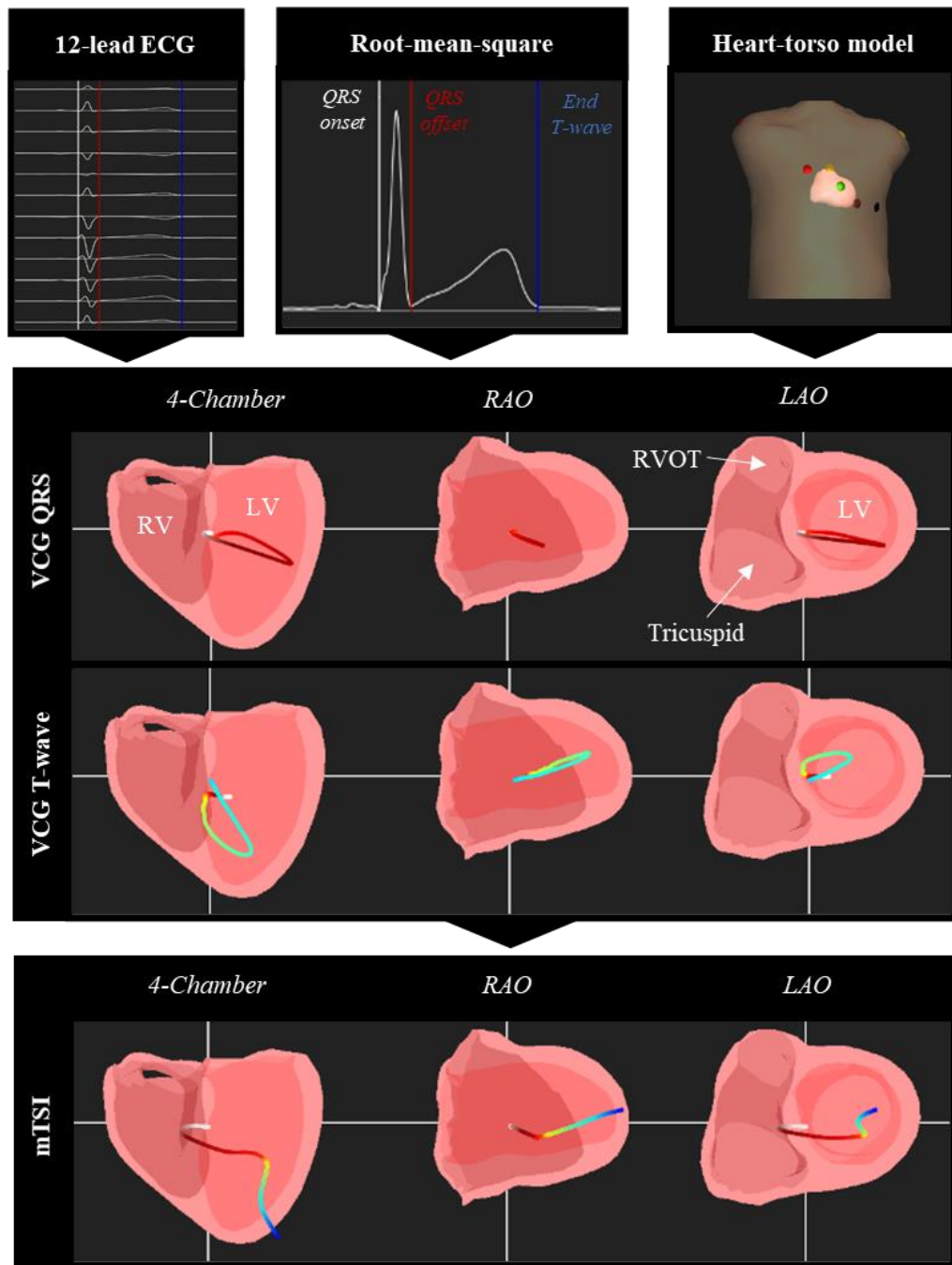


Figure 7.1: Visualization of computation of mean temporal spatial isochrone (mTSI) trajectory from 12-lead ECG and patient-specific heart- and torso model in CineECG. 12-lead ECG was converted to vectorcardiogram (VCG), using the root-mean-square (RMS) of all leads to annotate QRS-onset (white), QRS-offset (red) and end T-wave (blue). mTSI trajectory was constructed from VCG using different propagation velocities in the QRS- and STT-segment. mTSI was colored from white to red (QRS-onset to QRS-offset) and red to blue (QRS-offset to end T-wave). VCG and mTSI were visualized in 4 chamber view, right anterior oblique (RAO) view, and left anterior oblique (LAO) view.

VCG represents the mean direction of activation at each time instant of the QRS or STT-segment and was derived from the 12-lead ECG while taking the precordial lead positions on the thorax into account:

$$VCG(t) = \sum_{el=1}^9 \alpha_{el} ecg_{el}(t) \cdot |r_{el} - r_{ref}| \quad (3.2)$$

where $|r_{el} - r_{ref}|$ is the normalized vector between the reference position and the lead position on the thorax. The reference position was initially set to the center of the ventricular mass (CVM). $ecg_{el}(t)$ is the potential value at of the ECG at a lead at sample t . The mTSI over time is derived from VCG, assuming a constant propagation velocity:

$$mTSI(t + 1) = mTSI(t) + v \cdot \frac{VCG(t)}{\|VCG(t)\|} \quad (3.3)$$

where the VCG signal is normalized and multiplied by the constant propagation velocity to compute the 3D mTSI position in time. In the QRS-segment, a propagation velocity of 0.7 m/s was used.^{33,34} Velocities at ST-segment and 50ms prior to T-wave end (terminal T-wave) were set initially to 0.2 m/s and 0.35 m/s, respectively.³⁵ Propagation velocity in ST-segment and T-wave were stepwise decreased if the mTSI trajectory propagated outside the patient-specific cardiac model. Normal His-Purkinje activation was assumed in all subjects and therefore the CVM was used as start point from the mTSI.³⁶

CineECG aims to facilitate the interpretation of 12-lead ECG signals in relation with cardiac anatomy. Recently, the technique showed to improve (early) localization of late QRS electrical activity to RVOT in patients with Brugada Syndrome.³⁷ Here, CineECG even classified Ajmaline-positive patients, who only had non-diagnostic pattern on baseline ECG. These results substantiates that the novel CineECG technique might detect subtle QRS electrical changes that were not observed in the 12-lead ECG. Detection and localization of late RV activation potentials, that is also present in ARVC patients, might be improved using this novel technique.

CHAPTER 4

Study aim

STUDY AIM

ARVC is a complex disease due to its clinical heterogeneity, thereby making clinical definition and diagnosis difficult.^{2,13} The new 2010 TFC for ARVC represent a step forward in the attempt to identify individuals with ARVC, but mostly the diagnosis will reflect a variable degree of probability that depends on the clinical context.² With the absence of a single diagnostic test, detection of ARVC can be a diagnostic challenge leading to delayed treatment.² Early diagnosis may prevent arrhythmias or SCD and makes early treatment and reduction disease progression possible. This study aims to identify better lead locations and additional ECG criteria to improve early diagnosis of ARVC in PKP2 pathogenic variant carriers.

This thesis is divided into three parts. In the first part, the departure mapping technique was used to visualize significant differences in potentials between ARVC patients, PKP2 pathogenic variant carriers and controls. Part II will focus on the current ECG TFC for ARVC. In Part II, CineECG was used to investigating the mean cardiac activation pathway related to cardiac anatomy and gain additional information about ARVC. The results will be discussed and validated to eventually present a final product that needs to be further investigated and validated in a larger clinical setting.

RESEARCH QUESTIONS

AIM To identify better ECG lead positioning and additional ECG criteria for early diagnosis of ARVC in PKP2 pathogenic variants carriers.

Sub Questions

Part I To what extent provides the departure mapping technique additional information about the temporal and spatial distribution of potentials in ARVC?

Part II To what extent can identification of (known) diagnostic ECG criteria of ARVC be improved using better lead locations instead of the conventional 12-lead ECG?

Part III To what extent provides the novel CineECG method additional information about mean cardiac activation pattern in ARVC patients?

DESIGN ASPECTS

The current study ultimately aims to improve early ECG-based diagnosis of ARVC in PKP2 pathogenic variant carriers. Three different sub-questions will be investigated to gain insight in ARVC and identify early disease-specific abnormalities in PKP2 pathogenic variant carriers, to eventually design a disease-specific ECG configuration that can be used by clinicians. Therefore, the product of this thesis has to meet some design aspects, that will be described in this section.

Implementation of disease-specific lead configurations for better detection of ARVC in clinics is approachable, because of the fact that other lead configurations were already used for the diagnosis of diseases like Brugada Syndrome or Myocardial Infarction.^{38,39} In other words, the use of disease-specific lead positions for better

detection of ARVC abnormalities does not need purchasing new techniques or intensive training of the clinicians in interpreting the data. The conventional ECG technique can be used, using different electrode positions.

This study purposes a first step toward implementation of disease-specific lead configuration. Two main design aspects have to be taken into account. At first, lead positions found in this study require higher sensitivity and specificity compared to the conventional 12-lead ECG positions. Second, requirements for additional found ECG criteria for ARVC are debatable, because of the limited ECG criteria that are currently available in the TFC for ARVC. High specificity is required, but here the cut-off value is also debatable. The diagnostic values of current ECG criteria can be found in Appendix A.1, from which depolarization criteria show low sensitivity. Diagnostic ECG values of Brugada Syndrome during provocation test (SE 77-80%, SP 80-94.4%)^{40,41}, myocardial infarction at (1) ST-elevation (SE 65%, SP 79%)⁴², (2) fragmented QRS (SE 68%, SP 80%), and (3) Q-waves (SE 51%, SP 97%)⁴³ can be used as reference cut-off values for sensitivity and specificity. Besides diagnostic values of an abnormal ECG at myocarditis (SE 47-77%)^{44,45} or sarcoidosis (SE 20-31%)⁴⁶ might be interested to take into account, as these diseases can overlap with the diagnostic criteria of ARVC.

CHAPTER 5

PART I

Departure Mapping for Identification of Abnormal Electrocardiographic Lead Positions

*Toward a Disease-specific Lead Configuration for Arrhythmogenic Right Ventricular
Cardiomyopathy*

Introduction

Nowadays, diagnosis of arrhythmogenic right ventricular cardiomyopathy (ARVC) is based on a complex set of major and minor criteria from different diagnostic modalities, but diagnosis remains a clinical challenge due to heterogeneous clinical presentation. Mast *et al.*⁸ have determined the association between structural and electrical progression in 85 ARVC patients. The study showed that significant structural right ventricular (RV) progression, such as RV enlargement and RV mechanical dysfunction, was associated with prior depolarization abnormalities.⁸ In other words, assuming electrical abnormalities arise prior to mechanical abnormalities, detection and screening of electrical abnormalities seems to be important for early diagnosis of ARVC.

The amount of information obtained with conventional 12-lead electrocardiography (ECG) suffices for most clinical applications. However, in some applications the use of extra ECG leads or other lead locations on the chest has proven to increase the detection rate of ECG abnormalities. For example in the European Society of Cardiology guidelines (2017), it is recommended to consider the use of additional posterior chest wall leads (V7-V9) in patients with high suspicion of posterior myocardial infarction or additional right precordial leads (V3R and V4R) in patients with inferior myocardial infarction.³⁹ Also, for the diagnosis of Brugada Syndrome it is strongly recommended to use one or more leads among right precordial leads V1 and/or V2 positioned in the second or third intercostal space.^{4,38} In both examples, body surface potential maps (BSPM) were used to identify additional diagnostic information that was not present in conventional 12-lead ECGs.

BSPM is a noninvasive technique that uses multi-lead ECGs to image cardiac electrophysiologic information on a potential map representing the body surface. The technique focuses on the magnitude, location and migration of potential extrema where 12-lead ECG is only a subset of the BSPM and majorly relies on patterns of the ECG signals including amplitudes, duration and morphologies.²⁵ Physicians correlate the change in ECG patterns to electrophysiological information. In other words, for clinicians it is very time consuming and therefore not feasible to interpret ECG morphologies from all leads in the BSPM data.

To investigate early electrical abnormalities of ARVC in PKP2 pathogenic variant carriers, integral

maps from BSPM data can be compared with each other. From the integral maps a mean potential direction of activation can be derived. The extent of deviation of integrals from the normal range of the reference group can be determined and visualized in a departure map. Essentially, the departure map needs a normal control group. The departure map was first proposed by Flowers *et al.* in 1976, where the departure value was determined that expressed the voltage (x) out of the normal range: $x - (\bar{x} \pm 2 \text{SD})$, where \bar{x} and SD correspond to the mean and standard deviation voltages from a reference group, respectively. In 1990, Ikeda *et al.* proposed the departure index, to assess the deviation of potentials equivalently in different leads: $(x - \bar{x}) / \text{SD}$.⁴⁷ The index defines the extent of deviation from the normal range of a reference group and therefore a departure index exceeding ± 2 times SD can be defined as significantly different.

In the present study, the departure mapping technique was used to investigate the temporal and spatial distribution of body surface map potentials in ARVC patients and PKP2 pathogenic variant carriers compared to a control group. Departure mapping was performed over integrals of the QRS- and STT-segment. This study aims to identify abnormal ECG lead positions in both ARVC patients and PKP2 pathogenic variant carriers that might express early electrical abnormalities.

Method

Study population

The study population consisted of 23 PKP2 pathogenic variant carriers and nine control subjects with symptomatic ventricular extrasystoles originating in the right ventricular outflow tract (RVOT VES). Patients without right bundle branch block (QRS width <120ms) and no other structural diseases that affect ECG morphology apart from ARVC symptoms were included in this study. Subjects with RVOT VES were considered to be control subjects, where subjects without signs of heart failure were included in the study (QRS width <120ms, LV ejection fraction (EF) >45%, RVEF >45%, RV end-diastolic volume index <110ml/m²).

The study was approved by the Medical Ethics Committee of University Medical Center Utrecht (17/907) and informed consent was obtained from each subject before enrolment.

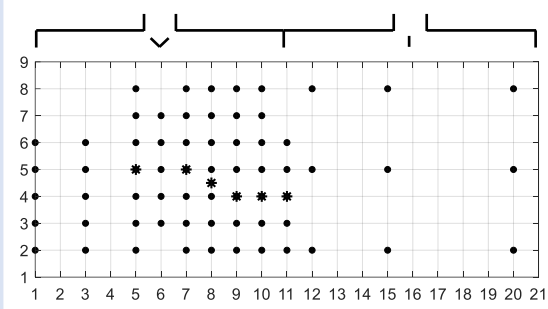


Figure 5.1: Visualization of 9×21 matrix that was determined to visualize the body surface potential map (BSPM) results. Column 1-11 and 11-21 correspond to the anterior and posterior body surface, respectively. Black dots refer to the 64 torso lead locations of the BSPM measurement. Black stars refer to the conventional 12-lead ECG positions, where V1-V2 and V4-V6 were included in the 64 torso leads.

Body surface potential mapping

67-lead BSPM were obtained in each subject, consisting of 64 torso and 3 limb leads. A 2D visualization of the 64 torso lead positions can be observed in **Figure 5.1**, where column 1-11 corresponds to the anterior body surface and column 11-21 corresponds to the posterior body surface. The anterior body surface includes 55 leads, that were placed in nine vertical strips with strip 4 located at the sternum. Electrodes were separated 4cm in the vertical strip from each other. Strip 3 and 5-9 are located at same sagittal axis as the conventional precordial ECG leads. The posterior body surface includes 9 leads, that were placed in three vertical columns.

Body surface potentials were recorded (Biosemi, Amsterdam, The Netherlands) simultaneously with Wilson's central terminal as reference. BSPM recordings were digitized using a 24-bit AD-converter and sampling rate of 2048Hz per channel. BSPMs were down-sampled to 1000Hz and were filtered with a moving average low-pass filter (window size 0.02s) and high-pass filter (window size 10s). Per subject, ten consecutive sinus beats obtained during resting respiration were averaged. Leads with noise were removed. QRS-onset, QRS-offset, T-wave apex and end T-wave were manually annotated using the root mean square (RMS) of all leads (**Figure 5.2**). QRS- and STT-segments were segmented from the BSPM for all subjects. It was hypothesized that the STT-segment might be affected by heart rate, therefore the STT-segments

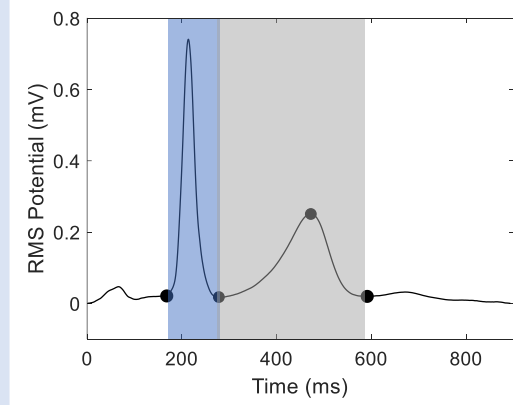


Figure 5.2: Visualization of segmentation of QRS-segment (blue) and STT-segment (grey) in root-mean-square (RMS) of all 64 precordial leads. Black dots correspond to (from left to right) manually annotated QRS-onset, QRS-offset, T-wave apex and T-wave end.

were normalized to equal lengths of 400samples. Extensive details about the signal preprocessing steps can be found in **Chapter 3**.

Data analysis

For each subject, definite integrals of the QRS-segment and STT-segment were determined in each lead, with integral defined as the signed area of the region bounded by its graph. For both segments, the lead potentials were integrated over the total segment, resulting in the QRS- and STT-integrals. Besides, the terminal QRS- and STT-integrals were determined, where the lead potentials were integrated from the peak in the RMS-segment to the end of the RMS-segment. The departure map analysis was utilized to identify integrals on body surface leads that differ significantly from the reference data. The departure index (DI) was calculated for each integral of each lead of subject A by:

$$DI = \frac{I_A - \mu_B}{\sigma_B} \quad (5.1)$$

where I_A equals the integrals of an individual subject A, μ_B is the mean integral of group B and σ_B is the

Table 5.1: Departure index (DI) determined for three different group combinations.

DI	Subject A	Group B
1	ARVC	PKP2
2	ARVC	CONTROL
3	PKP2	CONTROL

SD of the integrals in group B. The difference in integrals is significant when the integral of subject A deviates more than two SD from the normal range of group B. In other words, the integral of subject A differs significantly when the departure index exceeds ± 2 . Different patient groups were compared with each other (**Table 5.1**).

Abnormal ECG lead potentials of both the QRS- and STT-segment that showed high significant difference in integrals were visualized and clinically interpreted. Abnormal ECG lead positions in ARVC patients and PKP2 pathogenic variant carriers were noted to be of value for a disease-specific lead configuration.

Data visualization

The data was visualized in a 9×21 matrix displaying the anterior and posterior body surface (**Figure 5.1**). The dotted cross-sections correspond to measured 64 torso lead locations. Limb leads were excluded in the visualization. Individual departure maps were determined, where significant different lead positions ($DI > \pm 2$) were summed to visualize similarities within a group. The summation was visualized in a filled 2D contour plot, using a colormap from 0 to the number of subjects in group A. 2D contour plots of significantly increased ($DI > +2$) and decreased ($DI < -2$) integrals, i.e. integrals that exceeded twice the SD of the control group, were visualized separately.

Statistical analysis

Continuous variables, expressed as mean \pm SD, were compared using Student's *t* test for normally distributed continuous variables. Categorical variables, expressed as frequency (%), were compared using χ^2 or Fisher's exact test. A *p*-value of 0.05 or less was considered statistically significant.

Results

From all PKP2 pathogenic variant carriers, seven subjects met the TFC for ARVC. Patient characteristics are stated in **Table 5.2**.

The overall results display that lead 40 shows highest significance in terminal QRS-integrals and lead 22 shows highest significance in terminal STT-integrals. At all seven ARVC patients and 25% of the PKP2 pathogenic variant carriers, terminal QRS-integrals show significant increased values in lead 40, above the conventional V4 lead position. The terminal STT-integrals show significant increased values in 56% (9/16) of the PKP2 pathogenic variant

carriers in lead 22, but significant decreased values in 71% (5/7) of the ARVC patients. In **Table 5.3**, the presence of significance ($DI > \pm 2$) in lead 22 and 40 were summarized for all PKP2 pathogenic variant carriers, with the first seven subjects corresponding to the carriers meeting the TFC for ARVC. The presence of significant difference in terminal QRS- or STT integrals is denoted with a plus-sign.

QRS-segment

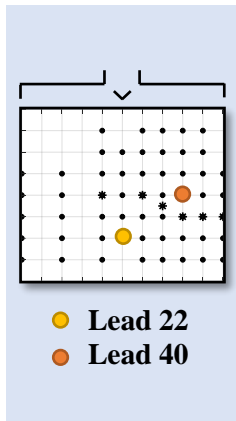
Averaged QRS-integrals were determined in all leads for every subject (**Appendix B.1; Figure B.1**). Departure maps were determined per individual (**Appendix B.2; Figure B.3**) and all individual departure maps were merged per group to visualize the summed individual departure map per group. **Figure 5.3A** shows the summed individual departure maps of $DI > +2.0$ and $DI < -2.0$ separately when comparing the averaged QRS-integrals between the groups.

Four out of seven ARVC patients visualize significant different QRS-integrals in lead 40 and 46 (above conventional lead V4 and V5) compared to the control group. Three out of 16 PKP2 pathogenic variant carriers showed different QRS-integrals in lead 46 and 47, compared to controls. ARVC vs. PKP2 portrayed an area of different integrals in lead 26 and 27 (at-below conventional lead V2).

Table 5.2: Patient group characteristics

Group	ARVC n=7	PKP2 n=16	CONTROL n=9
Male	4	5	3
Age (y)	36 \pm 18	38 \pm 17	34 \pm 13
TFC (#)	6.6 \pm 2.4	2.2 \pm 0.4	-
Onset diagnosis (y)	3.7 \pm 3.8	-	-
QRS width (ms)	103 \pm 8	106 \pm 6	105 \pm 9
Heart rate (bpm)	61 \pm 10	61 \pm 11	63 \pm 9
LV EDVI (ml/m2)	93 \pm 15	94 \pm 11	95 \pm 17
LV EF (%)	59 \pm 5	55 \pm 4	54 \pm 5
RV EDVI (ml/m2)	129 \pm 40	92 \pm 13	92 \pm 14
RV EF (%)	41 \pm 13	56 \pm 6	53 \pm 6

Abbreviations: ARVC = Arrhythmogenic Right Ventricular Cardiomyopathy; PKP2 = Plakophilin-2; TFC = Task Force Criteria; LV = left ventricle; EDVI = end diastolic volume index; EF = ejection fraction; RV = right ventricle.



		ARVC							PKP2															
		1	2	3	4	5	6	7	8	9	10	11	12	13	14	15	16	17	18	19	20	21	22	23
Terminal QRS-integral	DI > +2	+									→	+	+			+	+							
	DI < -2	+	+	+			+	+						←	←									
Terminal STT-integral	DI > +2							+			+	↑		→		+	+	+	+	+	+	↑	+	+
	DI < -2																							

Table 5.3: Overview of significant differences in terminal QRS-integrals (lead 40; orange) and terminal STT-integrals (lead 22; yellow) in all 23 PKP2 pathogenic variant carriers, compared to the control group. First seven subjects correspond with PKP2 pathogenic variant carriers meeting the Task Force Criteria for ARVC. Subjects that showed no significant difference in the lead position but in adjacent leads, were noted with arrow pointing to the significant different adjacent lead.

At the terminal QRS-integrals, more individual ARVC patients showed different integrals compared to the control group (Figure 5.3B). All seven ARVC patients showed increased terminal QRS-integrals in lead 34 and 40. Four out of 16 PKP2 pathogenic variant carriers showed different terminal QRS-integrals in lead 40 compared to controls.

QRS-potentials of lead 40 were visualized for ARVC patients, PKP2 pathogenic variant carriers and the averaged control group (Figure 5.4). All potentials were shifted to the left with an interval corresponding to the index of the apex of RMS (RMS_{apex}), i.e. RMS_{apex} corresponded to 0ms. The visualization ensures averaged QRS-integrals to correspond with the integral of both negative and positive time intervals and the terminal QRS-integrals to correspond with the integral of the positive time interval. The time index of RMS_{apex} for ARVC, PKP2 and control subjects were 47.9 ± 3.5 ms, 52.3 ± 4.1 ms, and 53.0 ± 9.3 ms, respectively.

STT-segment

Averaged STT-integrals were determined in all leads for every subject (Appendix B.1; Figure B.2). Departure maps were determined per individual (Appendix B.2; Figure B.3) and all individual departure maps were merged per group to visualize the summed individual departure map per group. Figure 5.5A shows the summed individual departure maps of $DI > +2.0$ and $DI < -2.0$ separately when comparing the averaged STT-integrals between the groups.

Four out of seven ARVC patients show decreased integrals in lead 27 and 34 (below

conventional lead V2 and V3) compared to controls. Besides, four ARVC patients showed significant increased integrals in lead 59 (on the upper back) and in lead 12 (above conventional lead V1). Six out of 16 PKP2 pathogenic variant carriers showed increased integrals in lead 21, 22 and 28 (below conventional lead V2) compared to controls. ARVC vs. PKP2 portrayed equal located significant differences compared to ARVC vs. CONTROL. At the terminal STT-integrals, five individual ARVC patients showed significant lower integrals in lead 22 compared to controls (Figure 5.5B). Besides, nine PKP2 pathogenic variant carriers show significantly increased integrals around lead 22 (below conventional lead V1-V2).

STT-potentials of lead 22 were visualized for ARVC patients, PKP2 subjects and the averaged control group (Figure 5.6). All potentials were shifted to the left with an interval corresponding to the index of the RMS_{apex} . The sample index of RMS_{apex} in the STT-segment for ARVC, PKP2 and CONTROL subjects were respectively 296.1 ± 18.8 , 281.8 ± 18.9 , and 290.3 ± 8.5 samples.

Discussion

The purpose of this study was to investigate BSPM data in ARVC patients, PKP2 pathogenic variant carriers and control subjects, to identify lead positions that might express early disease abnormalities. Departure maps were determined to visualize significant differences within the QRS-segment and STT-segment between the groups. The main results show lead 34 and 40 contains highest significance in terminal QRS-integrals and lead 22

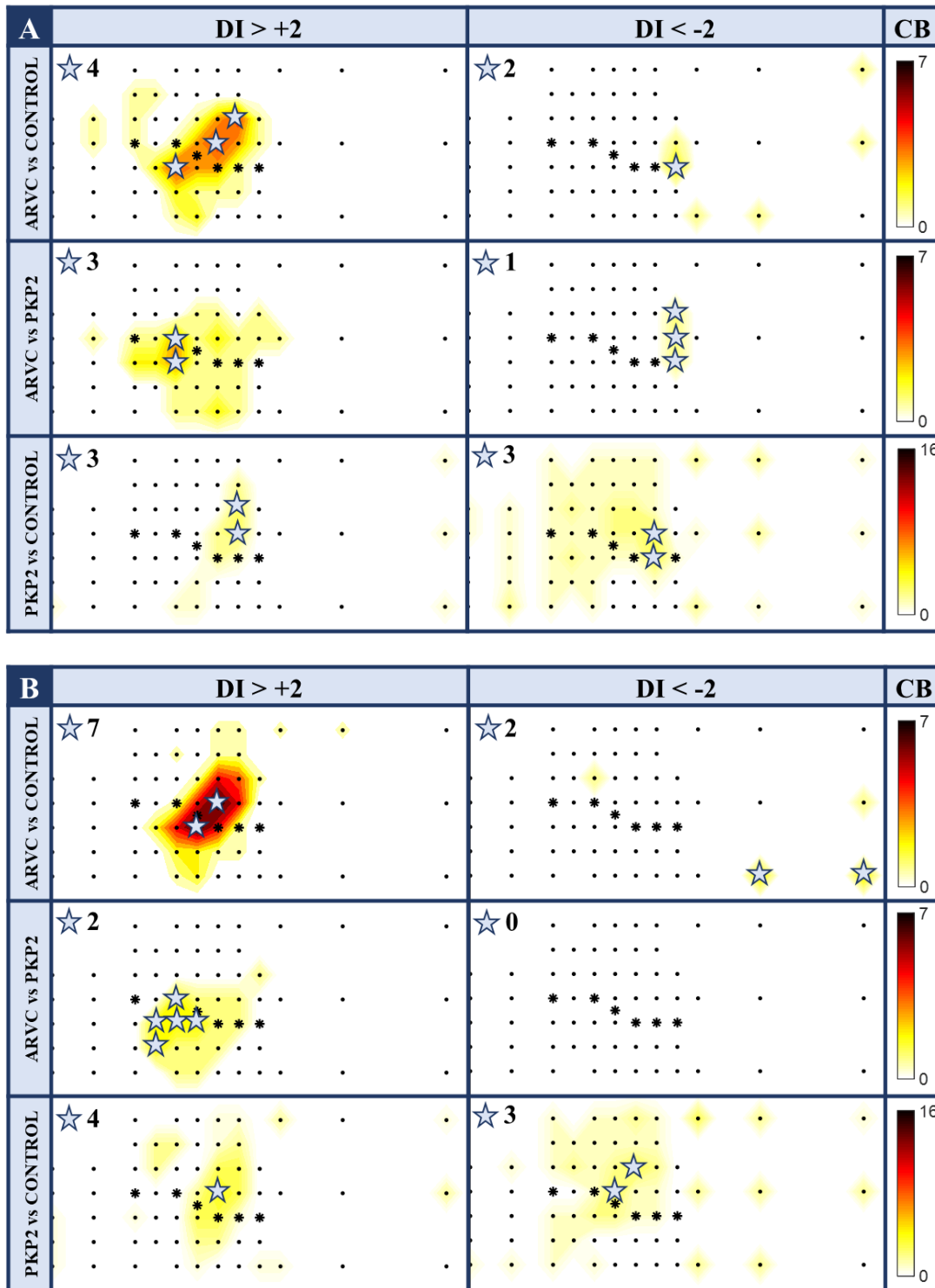


Figure 5.3: Summed individual departure maps for (A) QRS-integrals and (B) terminal QRS-integrals. Filled contour map that visualizes the summation of body surface leads that show (left) significant higher ($DI > +2.0$) and (right) significant lower ($DI < -2.0$) integrals. Each row refers to the groups that were compared with each other. Black dots represent BSPM lead locations and black stars represent conventional 12-lead ECG positions. V1-2 and V4-6 of the 12-lead ECG were measured within the BSPM. Values in left-upper corner represent maximum summation of leads that show significant difference within the contour map. CB = Color bar. DI = Departure index.

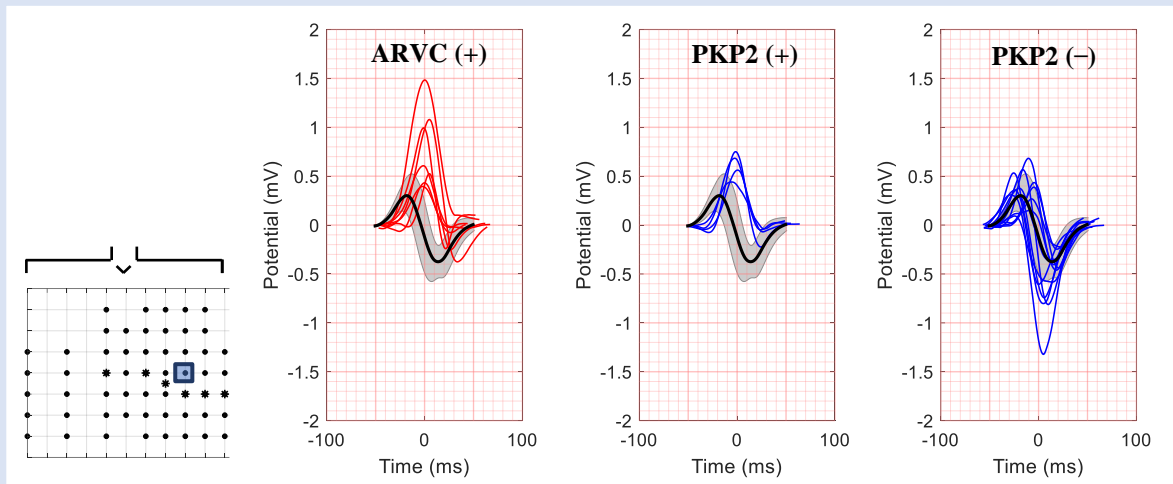


Figure 5.4: Electrophysiologic potentials of lead 40 that shows high significant differences within the summed individual departure maps. QRS-potentials of ARVC patients (red), PKP2 subjects (blue) and averaged controls (black; mean \pm SD). (+) corresponds to subjects that show significant differences in lead 40, (-) do not show significant differences. For each subject, the potentials were shifted over the X-axes with index of the $-RMS_{peak}$.

shows highest significance in terminal STT-integrals. Where Marcus *et al.* noted repolarization abnormalities to be an early and sensitive criteria in ECG of ARVC patients,⁹ the results indicate changes in the terminal QRS-integrals and increased terminal STT-integrals to occur before T-wave inversions (**Table 5.3**).

QRS-segment

Despite the heterogenous clinical presentation of ARVC, same significant differences were found in all seven ARVC patients and even in 25% PKP2 pathogenic variant carriers in lead 40. The result suggests early depolarization abnormalities in PKP2 pathogenic variant carriers that not met the TFC for ARVC, which is in accordance with previous studies that show absence of symptoms appeared to be a poor index for disease severity. Besides, depolarization abnormalities could be detected prior to structural abnormalities and the occurrence of the first VT episode.⁴⁸ Screening for early depolarization abnormalities in PKP2 gene variant carriers might prevent arrhythmia or SCD by starting medical treatment in patients at risk.

Minimum values of the averaged QRS-integrals over the BSPM were significant higher in ARVC patients compared to PKP2 subjects and controls, where position of minimum averaged QRS-integrals did not differ between groups (**Appendix B.1; Figure B.1**). At terminal QRS-integrals, highest significant difference in integrals was observed in lead 40 in both ARVC and PKP2 subjects (**Figure**

5.3B). Significant difference in terminal QRS-integrals can be explained by shift in R-wave apex (**Figure 5.4**). QRS-complexes of ARVC subjects show R-wave apex located around 0ms where control subjects show R-wave apex around -20ms. These changes were also observed in 25% of PKP2 pathogenic variant carriers. Therefore, prolonged R-wave apex duration and decreased S-wave amplitude might be criteria that improve the classification of ARVC in PKP2 pathogenic variant carriers.

The increased terminal QRS-integrals, i.e. prolonged R-wave apex duration and decreased S-wave amplitude, in lead 40 might be explained by late RV activation (**Figure 5.7**). The ECGsim software package, available from www.ecgsim.org and free of charge, was used to simulate the ECG changes that were observed within the QRS-complex. The delayed ventricular activation was adjusted in two different epicardial cardiac regions by decreasing the epicardial propagation velocities up to 25% of the normal (0.7 m/s) propagation velocities. An affected region at RV anterior-septal region on the left anterior coronary (LAD) resulted in local increased R-wave amplitudes and prolonged R-wave apex durations in lead 27 (**Figure 5.7; upper row**). An affected region at LV mid-lateral wall corresponded to similar but smaller depolarization changes in lead 40, where these changes were also noted in surrounded leads (**Figure 5.7; bottom row**).

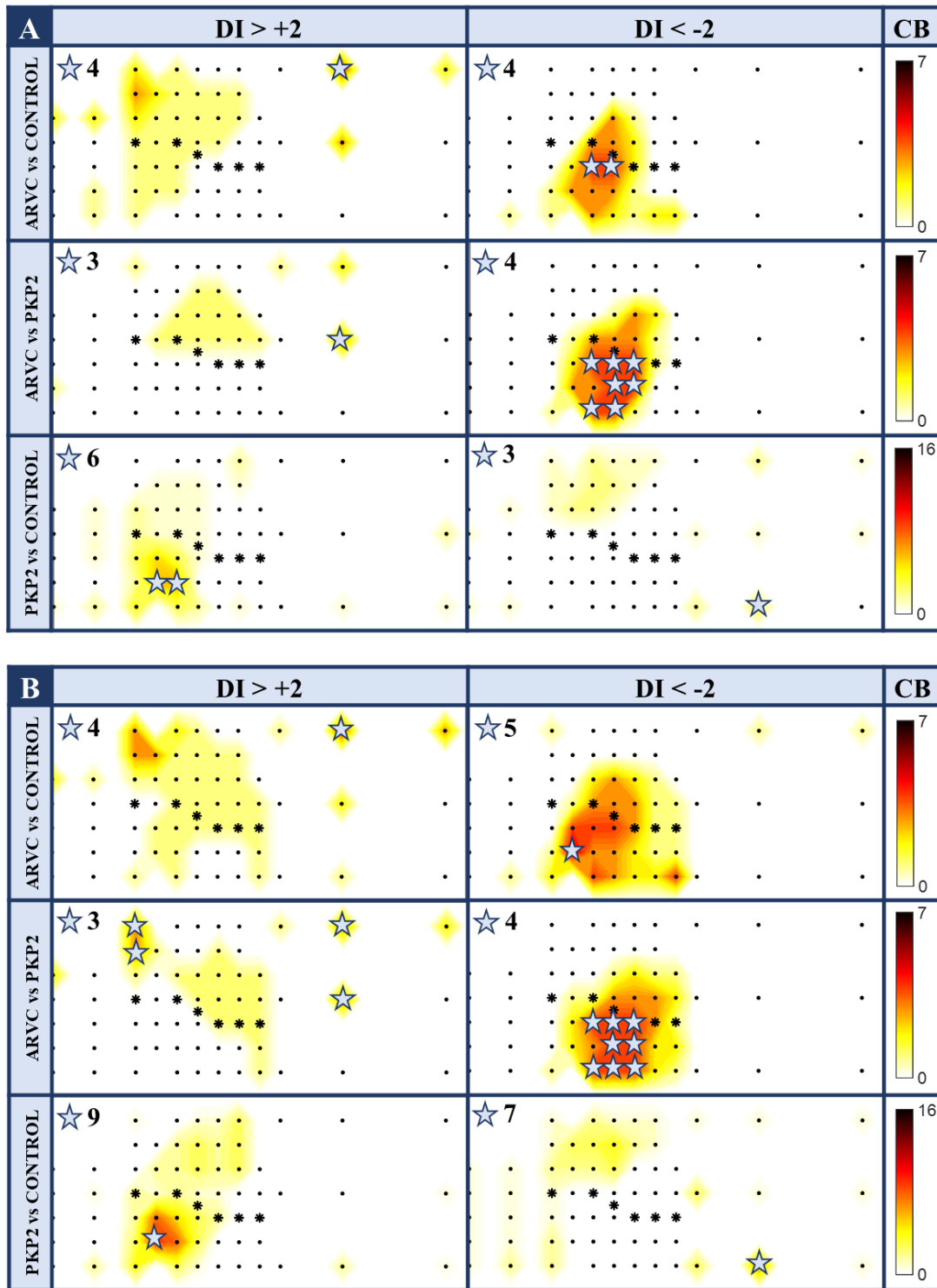


Figure 5.5: Summed individual departure maps for (A) STT-integrals and (B) terminal STT-integrals. Filled contour map that visualizes the summation of body surface leads that show (left) significant higher ($DI > +2.0$) and (right) significant lower ($DI < -2.0$) integrals. Each row refers to the groups that were compared with each other. White dots represent BSPM lead locations and red dots represent conventional 12-lead ECG positions. V1-2 and V4-6 of the 12-lead ECG were measured within the BSPM. Values in left-upper corner represent maximum summation of leads that show significant difference within the contour map. CB = Colorbar; DI = departure index.

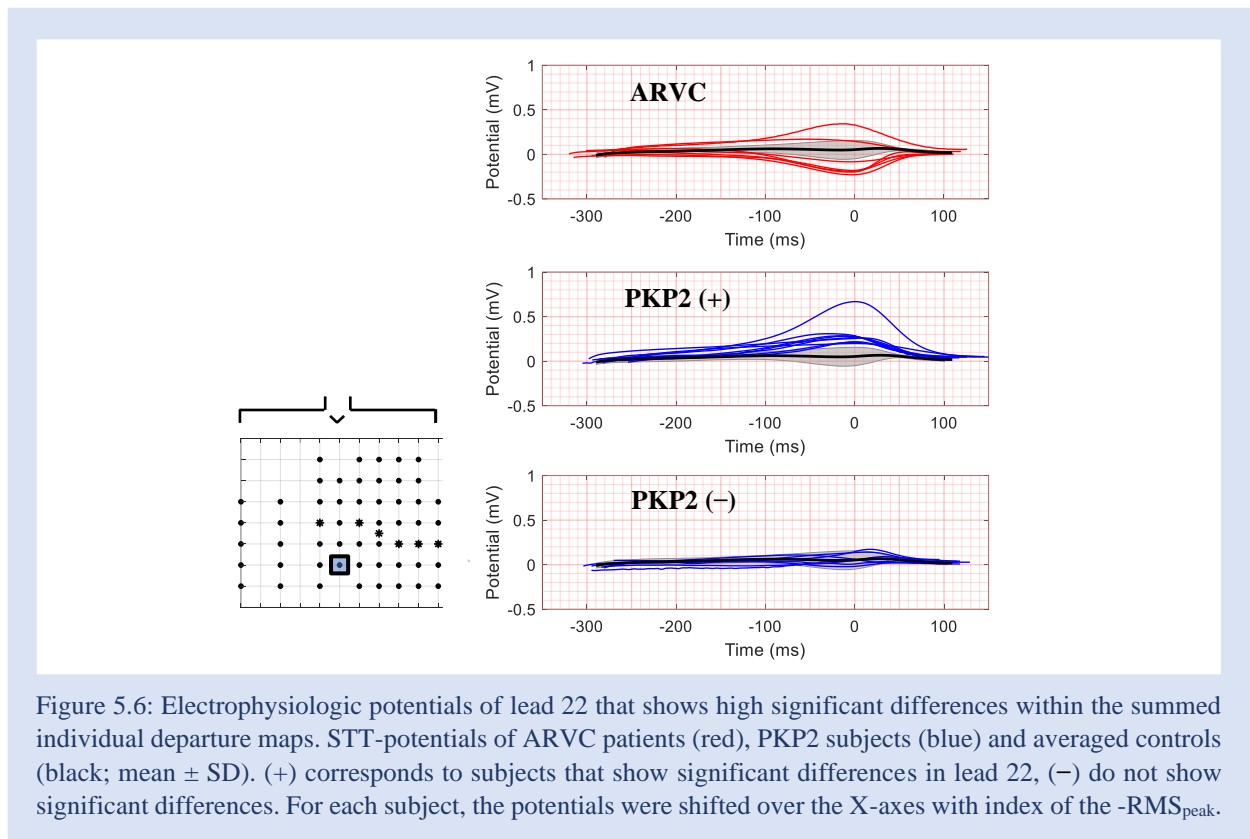


Figure 5.6: Electrophysiologic potentials of lead 22 that shows high significant differences within the summed individual departure maps. STT-potentials of ARVC patients (red), PKP2 subjects (blue) and averaged controls (black; mean \pm SD). (+) corresponds to subjects that show significant differences in lead 22, (-) do not show significant differences. For each subject, the potentials were shifted over the X-axis with index of the $-RMS_{peak}$.

Differences in simulated ECG signals based on similar TMP changes might be explained by the difference in distance between affected cardiac region to lead position on the torso model. Based on study results and ECG modeling, it was hypothesized that additional lead 40 might increase early detection of depolarization changes.

STT-segment

Significantly decreased terminal STT-integrals were found in five ARVC patients inferior of conventional leads V2-V4 (**Figure 5.5B**). This corresponds with the amount of ARVC patients that show major (4 patients) or minor (1 patient) repolarization abnormalities according to the TFC for ARVC. Two ARVC subjects do not show repolarization abnormalities yet, which can be explained by early stage of the disease. Both subjects were diagnosed with ARVC at day of BSPM measurement. Significant decreased STT-integrals suggests to arise in later stage in ARVC compared to significant increased QRS-integrals (**Table 5.3**). The departure maps suggest that detection of repolarization abnormalities could be improved with measurement of lead 22 (inferior of conventional lead V1-V2). This finding corresponds

with Samol *et al.* who investigated T-wave integrals in ARVC patients using 120-lead BSPM data.⁴⁹

Where 71% (5/7) of the ARVC patients show significantly decreased terminal STT-integrals in lead 22 compared to controls, 56% (9/16) PKP2 gene carriers show significant increased terminal STT-integrals in lead 22 (**Figure 5.5B and 5.6**). Where it is known that T-wave amplitudes were related to age, gender, and BMI,^{50,51} the amplitudes might also increase at shortening of refractory period in a local epicardial region or prolongation of the refractory period in a local endocardial region (**Figure 5.8; bottom row**). Opposite changes in transmembrane potentials will lead to T-wave inversions (**Figure 5.8; upper row**). The increase in terminal STT-integrals might be a reflection of early disease manifestation. These changes might be declared by defects in cell-cell adhesion, caused by the presence of PKP2 pathogenic gene variants in desmosomal proteins. However, not much is known about the fundamental progression of PKP2 pathogenic gene variants that eventually lead to ARVC. Long-term monitoring of pathogenic variant carriers might improve knowledge about early repolarization changes related to initial disease manifestation.

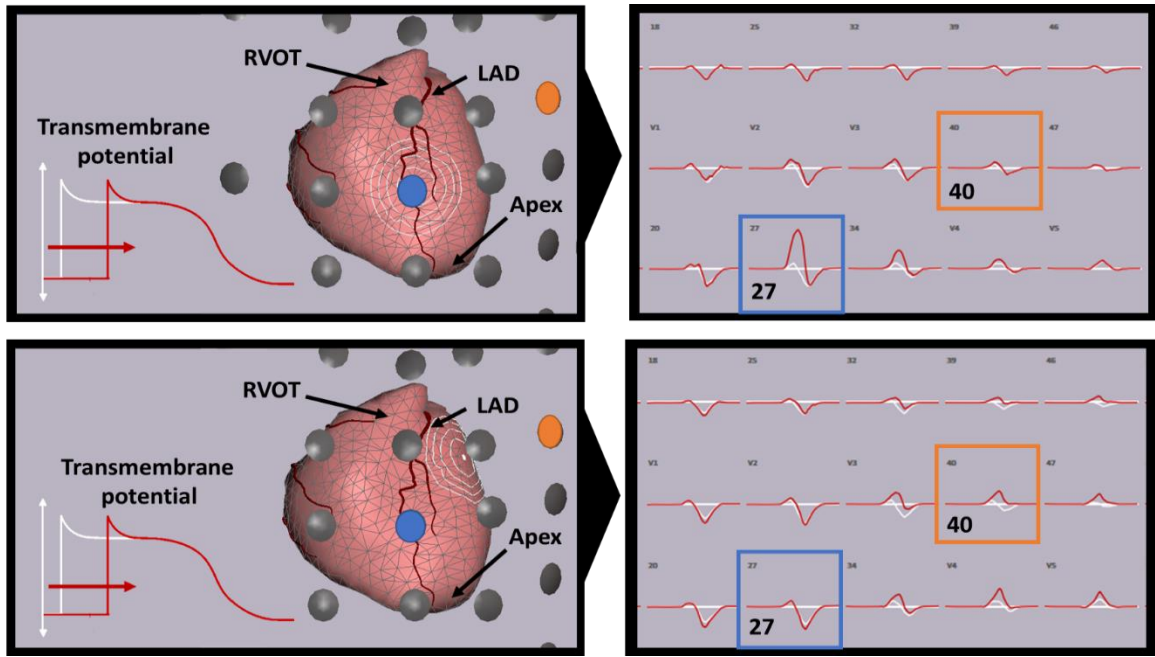


Figure 5.7: ECGsim modeling of depolarization abnormalities. Local transmembrane potentials (TMP) were altered by delayed depolarization (red) in one distinct cardiac region (white circles). Cardiac region was positioned at (upper row) right ventricular anterior-septal region on left anterior coronary (LAD), and at (bottom row) left ventricular mid-lateral wall. Electrocardiographic (ECG) signals were simulated based on the TMP, where normal ECG is white and the affected situation is black. Lead 27 and 40 were colored blue and orange, respectively.

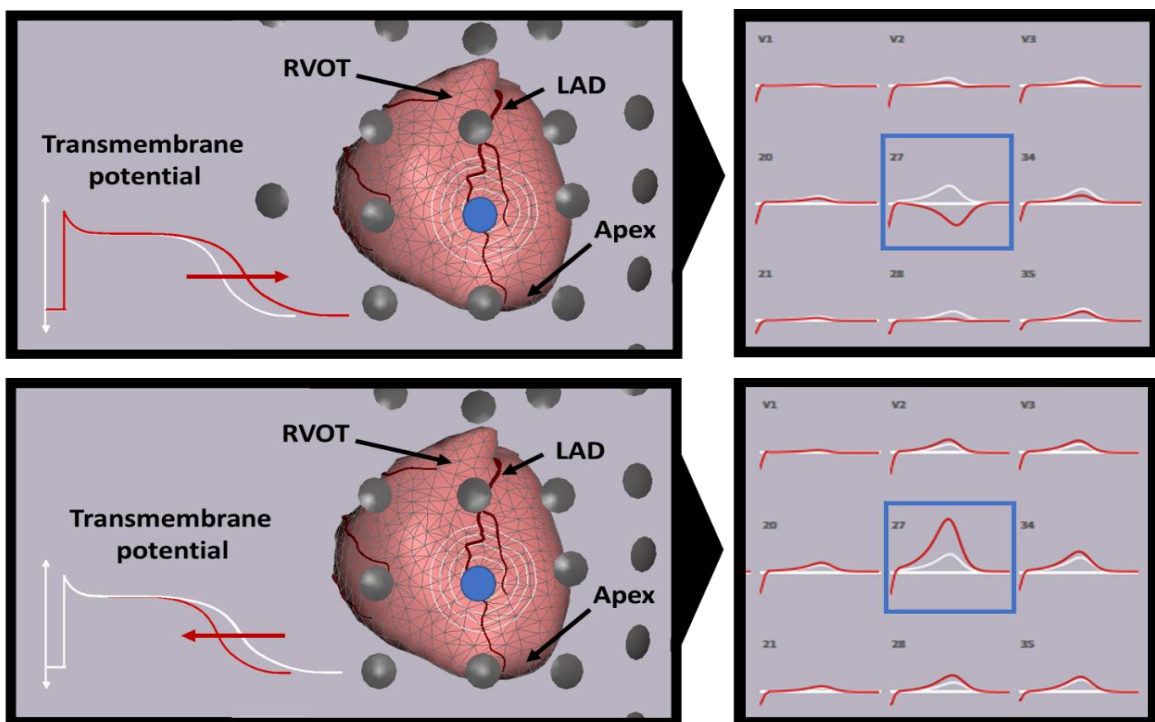


Figure 5.8: ECGsim modeling of repolarization abnormalities. Local transmembrane potentials (TMP) were altered in one distinct epicardial cardiac region (white circles). Refractory period in TMP was prolonged (upper row) or shortened (bottom row). Electrocardiographic (ECG) signals were simulated based on the TMP, where normal ECG is white and the affected situation is black. Lead 27 was colored blue.

Study limitations

The summed individual departure maps were visualized, representing the number of individuals that showed significant difference within the departure map. However, in the summed individual departure maps two individual significant areas that are near each other were merged and cannot be differentiated from each other in the summed individual departure maps. In other words, heterogeneity of the disease might have led to underestimation of the number of individuals that showed significant difference within the departure map. Besides, some measured leads were removed because of the presence of noise, that underestimated leads in the departure maps. No ECG potentials in both lead 22 and 40 have been removed in all subjects. Therefore, underestimation of the results in these leads can be excluded.

The results could be biased due to the small sample sizes that were used. However, the consistency in the departure maps and the substantiation with ECG modeling suggest that the results are likely applicable in larger sample sizes. Furthermore, a future clinical validation has to be performed in healthy subjects without RVOT VES, as due to the occurrence of RVOT VES the absence of an underlying pathological process cannot be guaranteed.

Future research

For clinical use, the additional ECG criteria and lead positions for the QRS- and STT-segment require clinical validation. Alterations of electrical changes that were observed in PKP2 pathogenic variant carriers require long-term monitoring to relate electrical abnormalities to early disease progression of ARVC. Furthermore, future research will focus on the analysis of the spatial distribution of disease specific parameters.

Conclusion

The departure mapping technique revealed additional lead positions beside conventional 12-lead ECG positions in which electrical changes were observed that may be used to identify first disease manifestation in pathogenic variant carriers. Additional information about the spatial distribution of electrical changes were observed in both the QRS- and STT-segment. Detection of the local electrophysiologic depolarization abnormalities suggest to improve by using an additional lead position located superior of conventional lead V4. Besides, placement of the right precordial leads in an inferior position might improve early detection of abnormalities in STT-segment.

CHAPTER 6

PART II

Body surface distribution of conventional diagnostic electrocardiographic criteria

Toward a disease-specific lead configuration for arrhythmogenic right ventricular cardiomyopathy

Introduction

Arrhythmogenic right ventricular cardiomyopathy (ARVC) is a complex disease due to clinical heterogeneity of the disease.² The disease is characterized by replacement of fibrofatty tissue that may lead to sudden cardiac death (SCD), ventricular arrhythmias or heart failure. Genetic defects in desmosomal proteins, with plakophilin-2 (PKP2) being the most frequently affected gene, contribute to disease development.

Nowadays, diagnosis of ARVC is based on the presence of major and minor criteria in different diagnostic tools. Diagnostic electrocardiographic (ECG) criteria according to the Task Force Criteria (TFC) of ARVC that can be observed in the conventional 12-lead ECG include T-wave inversions (TWI), prolonged terminal activation duration (TAD), and epsilon waves.⁹ TWI are an early and sensitive ECG marker for diagnosis of ARVC and are more common in patients with advanced right ventricular (RV) dysfunction.⁹ Prolonged TAD reflects RV activation delay and epsilon waves are electrical potentials of small amplitude at the end of the QRS-complex that reflect ventricular late potentials.^{3,15} Previous studies, published in the period of 2005-2020, reported a pooled sensitivity of 65% (62 - 67%) for TWI, 41% (38 - 44%) for prolonged TAD, and 16% (14 - 17%) for epsilon waves in ARVC patients (**Appendix A1**).

ARVC shows similarities with Brugada Syndrome, like predominant RV involvement and predisposition to arrhythmia and SCD.

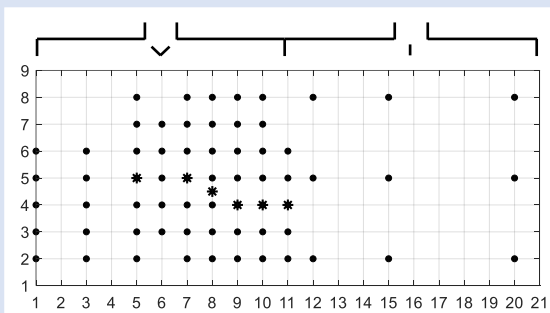


Figure 6.1: Visualization of 9x21 matrix that was determined to visualize the body surface map results. Column 1-11 and 11-21 correspond to the anterior and posterior body surface, respectively. Black dots refer to 64 torso lead locations of the body surface potential map. Black stars refer to the conventional 12-lead ECG positions, where V1-V2 and V4-V6 were included in the 64 torso leads.

Nevertheless, diagnosis of Brugada syndrome already strongly recommends a disease-specific lead configuration.^{4,52} The current ECG TFC for ARVC focus on detecting electrical RV abnormalities by observing ECG changes in the right precordial leads (V1 through V3). In this study, 64-lead body surface potential maps (BSPM) were used to display the spatial distribution of the diagnostic ECG TFC for ARVC in ARVC patients, PKP2 pathogenic variant carriers and control subjects. The study aims to identify the most properly lead positions for the current TFC for ARVC, for early detection of ARVC in pathogenic variant carriers.

Method

Study population

The study population consisted of 23 PKP2 pathogenic variant carriers and nine control subjects with symptomatic ventricular extrasystoles originating in the right ventricular outflow tract (RVOT VES). Patients without right bundle branch block (QRS width <120ms) and no other structural diseases that affect ECG morphology apart from ARVC symptoms were included in this study. Subjects with RVOT VES were considered to be control subjects, where subjects without signs of heart failure were included in the study (QRS width <120ms, LV ejection fraction (EF) >45%, RVEF >45%, RV end-diastolic volume index <110ml/m²).

The study was approved by the Medical Ethics Committee of University Medical Center Utrecht (17/907) and informed consent was obtained from each subject before enrolment.

Body surface potential mapping

67-lead BSPM were obtained in each subject, consisting of 64 torso and 3 limb leads. A 2D visualization of the 64 precordial lead positions can be observed in **Figure 6.1**, where column 1-11 corresponds to the anterior body surface and column 11-21 corresponds to the posterior body surface. The anterior body surface includes 55 leads, that were placed in nine vertical strips with strip 4 located at the sternum. Electrodes were separated 4cm in the vertical strip from each other. Strip 3 and 5-9 are located at same sagittal axis as the conventional precordial ECG leads. The posterior body surface includes 9 leads, that were placed in three vertical columns.

Body surface potentials were recorded (Biosemi, Amsterdam, The Netherlands) simultaneously with Wilson's central terminal as reference. BSPM

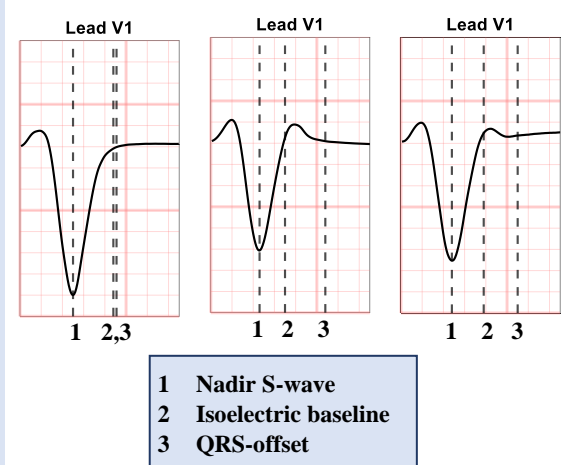


Figure 6.2: Visualization of three computational determined terminal activation duration (TAD) and S-wave upstroke measurements in lead V1. TAD (ms) corresponds to duration between line 1 to 3, and S-wave upstroke (ms) corresponds to the duration between line 1 to line 2. Dotted lines (1, 2 and 3) correspond to nadir of the S-wave, isoelectric baseline and QRS offset, respectively. Paper speed: 50mm/s; Voltage: 10mm/mV.

recordings were digitized using a 24-bit AD-converter and sampling rate of 2048Hz per channel. BSPMs were down-sampled to 1000Hz and were filtered with a moving average low-pass filter (window size 0.02s) and high-pass filter (window size 10s). Per subject, ten consecutive sinus beats obtained during resting respiration were averaged. Leads with noise were removed. QRS-onset, QRS-offset, T-wave apex and end T-wave were manually annotated using the root mean square (RMS) of all leads. QRS-complexes and STT-segments were segmented from the BSPM for all subjects. It was hypothesized that the STT-segment might be affected by heart rate, therefore the STT-segments were normalized to equal lengths of 400 samples. Extensive details about the signal preprocessing steps can be found in **Chapter 3**.

Data analysis

For each subject, T-wave integrals and TAD measurements were determined in each lead. T-wave integral (mVms) was defined as the signed area of the region between QRS-offset and T-wave end bounded by its graph, i.e. the summation of potentials in the interval between QRS-offset to T-wave end. Locations of the minimum and maximum T-wave integrals on the body surface were determined. Separate analysis of ARVC patients

with major repolarization abnormalities (ARVC TWI+) and without major repolarization abnormalities (ARVC TWI-) was performed.

In this study, the TAD measurement was computationally determined as the time duration of the nadir of the S-wave to the QRS-offset (**Figure 6.2**). The nadir of the S-wave was computationally determined if the amplitude of the S-wave exceeded 0.1mV. Otherwise, the TAD measurement in the corresponding lead was classified as non-existent. In case multiple S-wave peaks were found, the TAD was determined from the highest S-wave amplitude. Separate analysis of ARVC patients with prolonged TAD according to TFC (TAD+) and ARVC patients without prolonged TAD (TAD-) was performed.

Furthermore, the spatial distribution of S-wave upstroke and S-wave amplitude were assessed. S-wave upstroke (ms) was determined as the duration from the nadir of the S-wave to the isoelectric baseline (**Figure 6.2**) and therefore does not include late depolarization abnormalities, epsilon waves or R' wave. Nadir of the S-wave was determined similar as in the TAD measurement. The average of the first 20ms of the ST-segment was used as isoelectric baseline reference. S-wave amplitude was defined as the amplitude difference between the nadir of the S-wave and the isoelectric baseline.

Table 6.1: Patient group characteristics

Group	ARVC n=7	PKP2 n=16	CONTROL n=9
Male	4	5	3
Age (y)	36 ± 18	38 ± 17	34 ± 13
TFC (#)	6.6 ± 2.4	2.2 ± 0.4	-
Onset diagnosis (y)	3.7 ± 3.8	-	-
QRS width (ms)	103 ± 8	106 ± 6	105 ± 9
Heart rate (bpm)	61 ± 10	61 ± 11	63 ± 9
LV EDVI (ml/m ²)	93 ± 15	94 ± 11	95 ± 17
LV EF (%)	59 ± 5	55 ± 4	54 ± 5
RV EDVI (ml/m ²)	129 ± 40	92 ± 13	92 ± 14
RV EF (%)	41 ± 13	56 ± 6	53 ± 6

Abbreviations: ARVC = Arrhythmogenic Right Ventricular Cardiomyopathy; PKP2 = Plakophilin-2; TFC = Task Force Criteria; LV = left ventricle; EDVI = end diastolic volume index; EF = ejection fraction; RV = right ventricle.

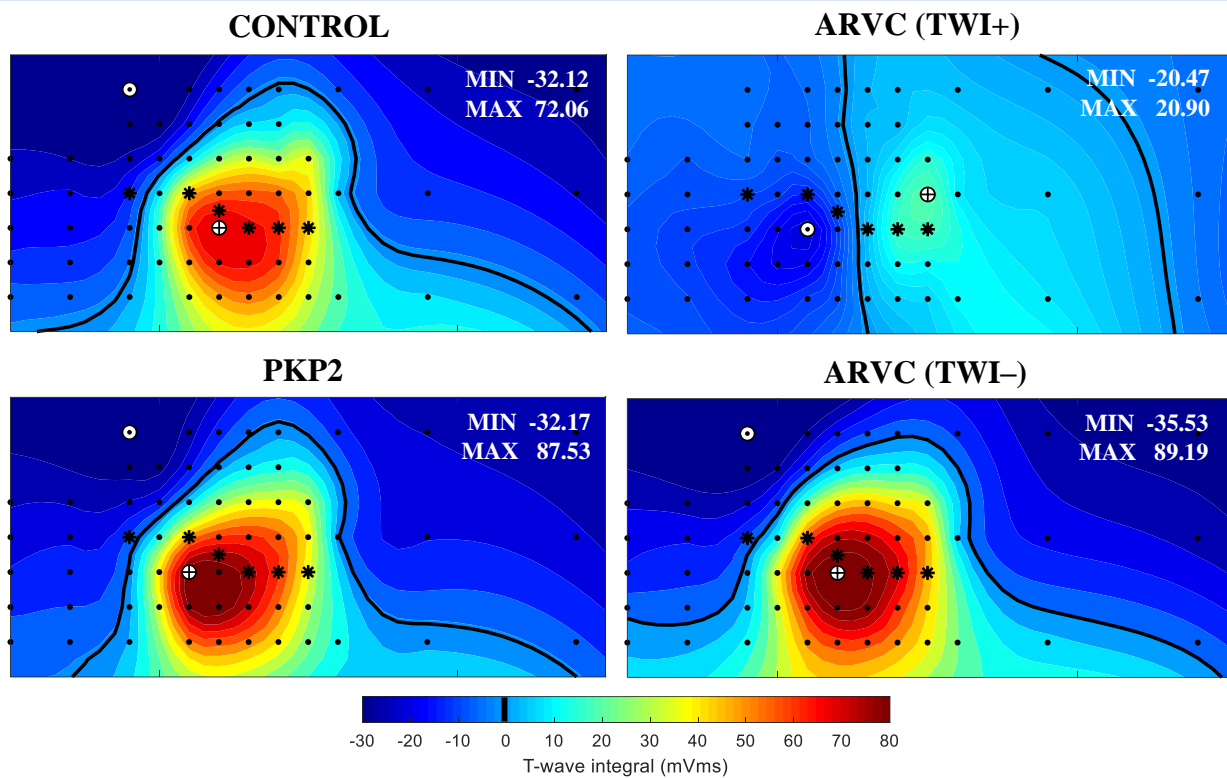


Figure 6.3: Spatial distribution of averaged T-wave integrals. The colorbar ranges between -30 and 80mVms for all plots, with black isopotential line corresponding to the T-wave integral equal to 0mVms. MIN and MAX T-wave integrals, displayed in right-upper corner, correspond to \ominus and \oplus positions in the 2D map, respectively. Both anterior and posterior body surface is visualized. ARVC (TWI+) and ARVC (TWI-) corresponds to ARVC patients with and without major repolarization abnormalities, respectively.

Data visualization

Two-dimensional (2D) isopotential maps were constructed to visualize the spatial distribution of ECG criteria over the body surface (Figure 6.1). For T-wave integrals, the spatial distribution over both the anterior and posterior body surface was visualized. The spatial distribution of TAD was only determined over the anterior body surface, as S-waves were not present in the posterior body surface. The location of both the minimal and maximal TAD measurement and T-wave integrals were displayed for all groups in a 2D anterior body surface map.

Statistical analysis

Continuous variables, expressed as mean \pm SD, were compared using Student's *t* test for normally distributed continuous variables. Categorical variables, expressed as frequency (%), were compared using χ^2 or Fisher's exact test. A *p*-value of 0.05 or less was considered statistically significant.

Results

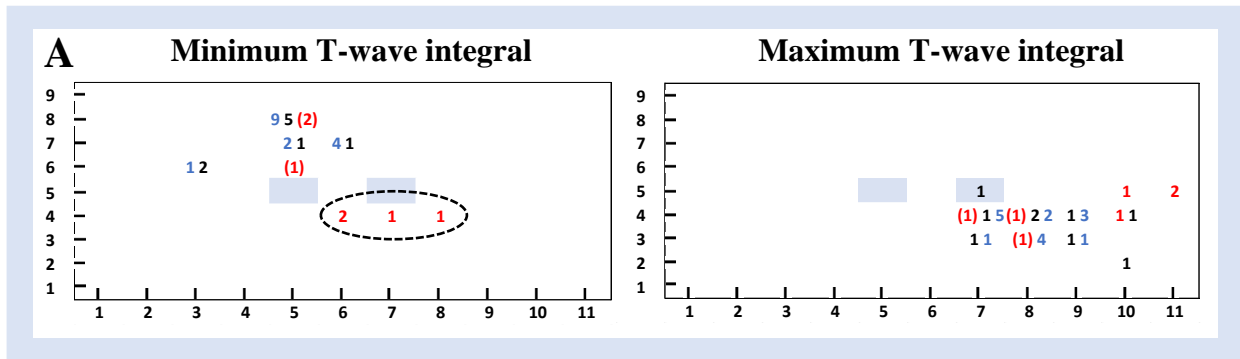
From all PKP2 pathogenic variant carriers, seven subjects met the TFC for ARVC. Four ARVC patients showed T-wave inversions through V3 (major criteria) and three patients showed prolonged TAD (minor criteria) according to patient files. Patient characteristics are stated in Table 6.1.

T-wave inversion

The averaged T-wave integral plots for ARVC (TWI+), ARVC (TWI-), PKP2 pathogenic variant carriers and controls are displayed in Figure 6.3. Both minimum and maximum T-wave integral positions were determined per group (Figure 6.4A) and T-wave integral measurements of conventional lead V1-V3 and positions of maximum T-wave inversions in ARVC(TWI+) patients (dotted circle) were determined (Figure 6.4B).

Terminal activation duration

The averaged TAD plots for ARVC (TAD+), ARVC (TAD-), PKP2 pathogenic variant carriers and



B	CONTROL n=9	PKP2 n=16	ARVC (TWI-) n=3	ARVC (TWI+) n=4
Minimum	-33.0 ± 13.0	-33.7 ± 15.7	-38.0 ± 7.0	-28.7 ± 12.0
Maximum	82.4 ± 33.7	99.7 ± 36.4	98.1 ± 28.1	22.7 ± 6.9
Lead V1	-12.0 ± 11.7	-6.28 ± 15.3	-5.8 ± 15.7	-8.6 ± 9.5
Lead V2	48.8 ± 28.1	52.7 ± 30.8	61.3 ± 43.1	-12.7 ± 6.8
Lead V3	65.5 ± 26.1	75.0 ± 25.4	83.1 ± 29.7	-7.5 ± 13.3
Lead 21	20.9 ± 14.6	43.5 ± 30.2	41.3 ± 35.1	-18.0 ± 10.5
Lead 27	65.3 ± 27.6	87.5 ± 39.4	82.7 ± 33.8	-20.5 ± 15.4
Lead 34	72.1 ± 28.0	86.7 ± 28.2	89.2 ± 24.1	-10.3 ± 16.2

Figure 6.4: (A) Location of (left) the minimum T-wave integral (TWI), i.e. maximum T-wave inversion on the body surface, and (right) the maximum T-wave integral in 7 ARVC patients (red), 16 PKP2 carriers (blue) and 7 controls (black). Only anterior chest is visualized, with lead V1 and V2 in light-blue. ARVC patients that not met the major Task Force Criteria for T-wave inversions were marked with (. Dotted oval corresponds to (from left to right) lead 21, 27 and 34.(B) Averaged T-wave integral values (mean ± SD) of different lead positions in ARVC patients, PKP2 carriers and controls.

controls are displayed in **Figure 6.5**. In **Appendix C.1**, the percentages of non-existent TAD measurements per lead are shown per group.

Other parameters

The spatial distribution of S-wave upstroke and S-wave amplitude can be observed in **Appendix C.2** and **C.3**, respectively.

Discussion

The current study reexamined the ECG TFC for ARVC in BSPM data to identify most optimal lead positioning for the early detection of ARVC. The spatial distributions of TWI and TAD over the body surface were investigated and minimum and maximum lead positions of the variables were determined. As epsilon waves are barely observed in clinical setting and were hard to detect in 12-lead

ECG, this study chose not to investigate body surface distribution of epsilon waves.

In ARVC (TWI+) patients, maximum TWI was observed inferior of conventional lead V2 (**Figure 6.4A**). Lead 27 showed most difference in T-wave integrals compared to PKP2 pathogenic variant carriers, which suggests early detection of repolarization abnormalities using an alternative lead placement in lead 27 (**Figure 6.4B**). Spatial distributions of TAD show gradually increase from left to right precordial leads, where lead placement shows to influence meeting this minor TFC for ARVC.

T-wave inversions

Apart from ARVC (TWI+) patients, all averaged T-wave integral plots show similar distributions, with similar positions of the minimum and maximum T-

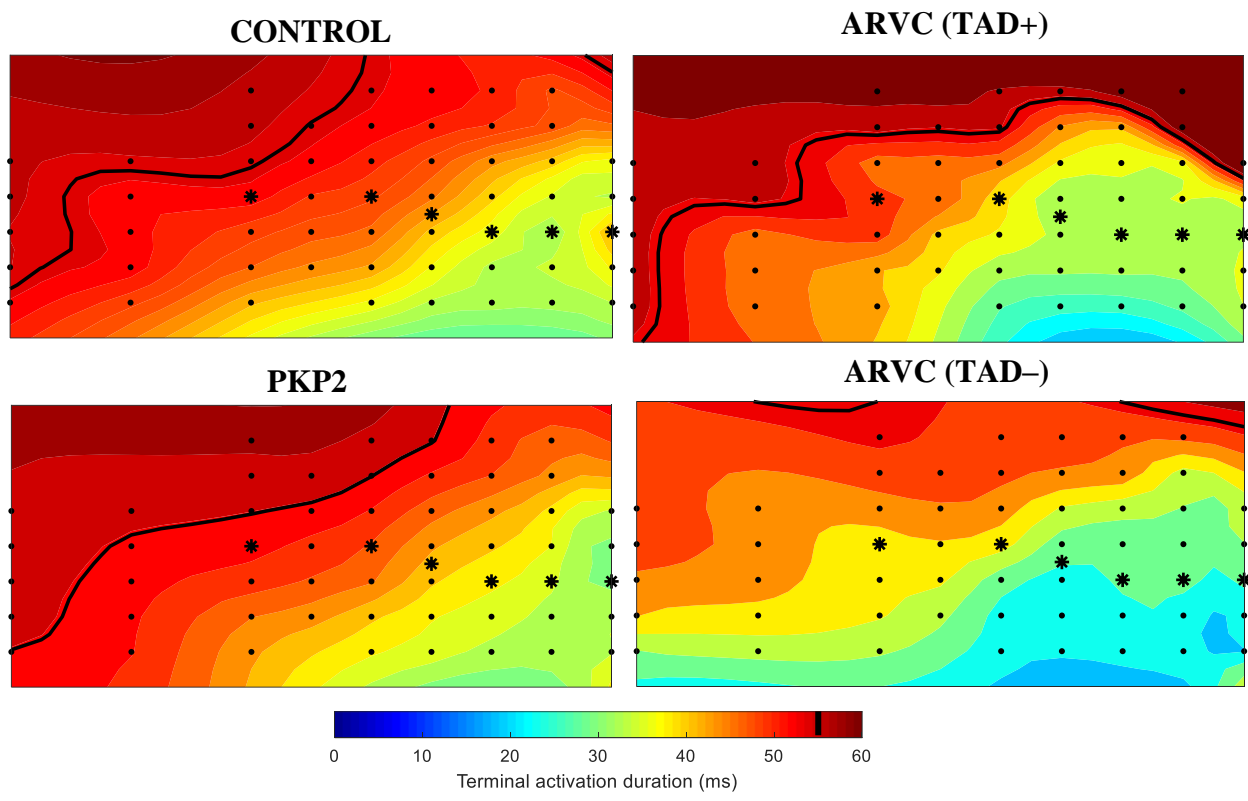


Figure 6.5: Spatial distribution of averaged terminal activation duration (TAD) measurements. The colorbar ranges between 0 and 60ms for all plots, with black isopotential line corresponding to the TAD equal to 55ms. Anterior body surface is visualized. ARVC (TAD+) and ARVC (TAD-) corresponds to ARVC patients with and without prolonged TAD, respectively.

wave integral. T-wave integrals in ARVC (TWI+) patients showed different spatial distribution over the body surface, with different minimum and maximum positions (**Figure 6.3** and **6.4A**). Minimum T-wave integral positions for all subjects without major repolarization abnormalities were mostly observed superior of conventional lead V1, where ARVC (TWI+) showed minimum T-wave integral positions in the area below lead V2. No significant difference in minimum T-wave integral values was observed between groups. ARVC (TWI+) patients showed decreased maximum T-wave integrals compared to all other groups. Maximum T-wave integral positions for all subjects without major repolarization abnormalities were located in the area inferior of conventional lead V2 toward V4/V5. ARVC (TWI+) showed a shift in maximum T-wave integral positions toward left precordial leads V5 and above V6 (**Figure 6.4A**).

Other than an increased maximum T-wave integral inferior of conventional lead V2, no differences were found in ARVC(TWI-) and PKP2

gene carriers compared to controls. No early progression in T-wave inversion distribution was observed. Where lead 21, 27 and 34 all showed maximum T-wave inversions within ARVC (TWI+) patients, largest difference between PKP2 and ARVC (TWI+) patients was found in lead 27 (**Figure 6.4B**). It was hypothesized that the lead position with maximum T-wave inversion is located nearest to the cardiac region with largest disease manifestation. Therefore, it was assumed that additional ECG measurements at lead 27 might improve early detection of T-wave inversions.

Spatial distribution of ventricular repolarization in ARVC patients was investigated before and showed similar distribution patterns.^{49,53,54} According to Heidi *et al.*, change in positions of minimum and maximum T-wave directions (**Figure 6.4A**), and thus the abnormal T-wave inversions at right anterior and inferior body surface, may reflect regionally delayed repolarization of the underlying structurally altered myocardium.⁵³ Samol *et al.* observed different T-wave integral distributions in

Table 6.3: Terminal activation duration (TAD) measurements of different lead locations of control, plakophilin-2 (PKP2) and arrhythmogenic right ventricular cardiomyopathy (ARVC) subjects. ARVC subjects with prolonged TAD according to TFC (TAD+) were separated with ARVC subjects without prolonged TAD (TAD-). TAD measurements were noted as mean \pm standard deviation.

	CONTROL n=7	PKP2 n=16	ARVC (TAD-) n=4	ARVC (TAD+) n=3
MINIMUM	29.9 \pm 7.0	30.0 \pm 4.5	26.3 \pm 10.8	29.0 \pm 2.6
MAXIMUM	59.3 \pm 10.3	60.9 \pm 7.8	55.3 \pm 8.1	67.0 \pm 4.4
Lead V1	53.4 \pm 10.3	53.1 \pm 6.3	41.5 \pm 10.6	50.3 \pm 14.0
Lead V2	49.1 \pm 7.6	49.1 \pm 5.9	40.5 \pm 9.3	40.5 \pm 2.1
Lead V3	43.1 \pm 7.1	42.5 \pm 7.8	28.3 \pm 9.0	33.8 \pm 2.5

PKP2-positive ARVC patients and PKP2-negative ARVC patients, which indicates differences in underlying structurally altered myocardium between pathogenic gene variants.⁴⁹

As mentioned before, T-wave inversions were found in approximately 65% of all ARVC patients (**Appendix A.1**). We hypothesize that this finding is related to the heterogeneous aspect of ARVC. The ECGsim software package, available from www.ecgsim.org and free of charge, was used to simulate T-wave inversions with maximum T-wave inversions below conventional lead V2 (**Figure 6.6**). The repolarization phase of transmembrane potentials (TMP) was adjusted in the region of the left anterior descending (LAD) artery in three different heart layers: (1) endocardial, (2) epicardial, and (3) transmural. It is hypothesized that the increased T-wave integrals observed in PKP2 pathogenic variant carriers and ARVC (TWI-) patients might be caused by an endocardial diseased region (**Figure 6.6; left**), where T-wave inversions were observed in both an epicardial and transmural diseased region (**Figure 6.6; mid and right**). In that case, we hypothesize that the progressive aspect of ARVC will always result in the presence of T-wave inversions, when disease characteristics distribute from endocardial to transmural regions.

Terminal activation duration

This is the first study that reported information about the spatial distribution of TAD over the body surface. The spatial distributions of TAD show increasing values from left to right precordial leads (**Figure 6.5** and **Table 6.3**). No local maximum or minimum was observed in the spatial distribution

plots. Therefore, individual positions of all subjects were not investigated in minimum and maximum distribution plots. Previous studies, including Cox *et al.*^{15,55} who proposed the criteria, only reported highest TAD measurement in V1 through V3. The results suggest conventional lead V1 shows highest TAD measurements and therefore lead placement of V1 has greatest influence on meeting the TFC for ARVC.

Besides, insight about the spatial distribution of TAD in controls, distribution maps of ARVC patients show unexpected results. The TAD measurements were expected to be prolonged (>55ms) in conventional lead V1, V2 or V3 in ARVC (TAD+) patients. Instead the results show lower TAD measurements in V1-V3 (**Table 6.3**) and an increased amount of non-existent TAD measurements around lead V3-V6 compared to controls (**Appendix C.1**). These findings might be explained by the results that were found in **Part I**, where prolonged R-wave apex durations and decreased S-wave amplitudes were observed in ARVC patients. Depending on the size of these ECG abnormalities, these observations might explain a decrease and eventually non-existent measurement in TAD.

The reproducibility of determining the TAD in ARVC patients was reassessed, because ARVC (TAD+) patients did not show prolonged TAD in V1-V3 compared to the PKP2 and control group. In this study, the interobserver variability of TAD measurements was higher compared to the variability that was determined by Cox *et al.*¹⁵ (**Appendix C.4**). A larger variation substantiates the suggestion that precordial lead placement might

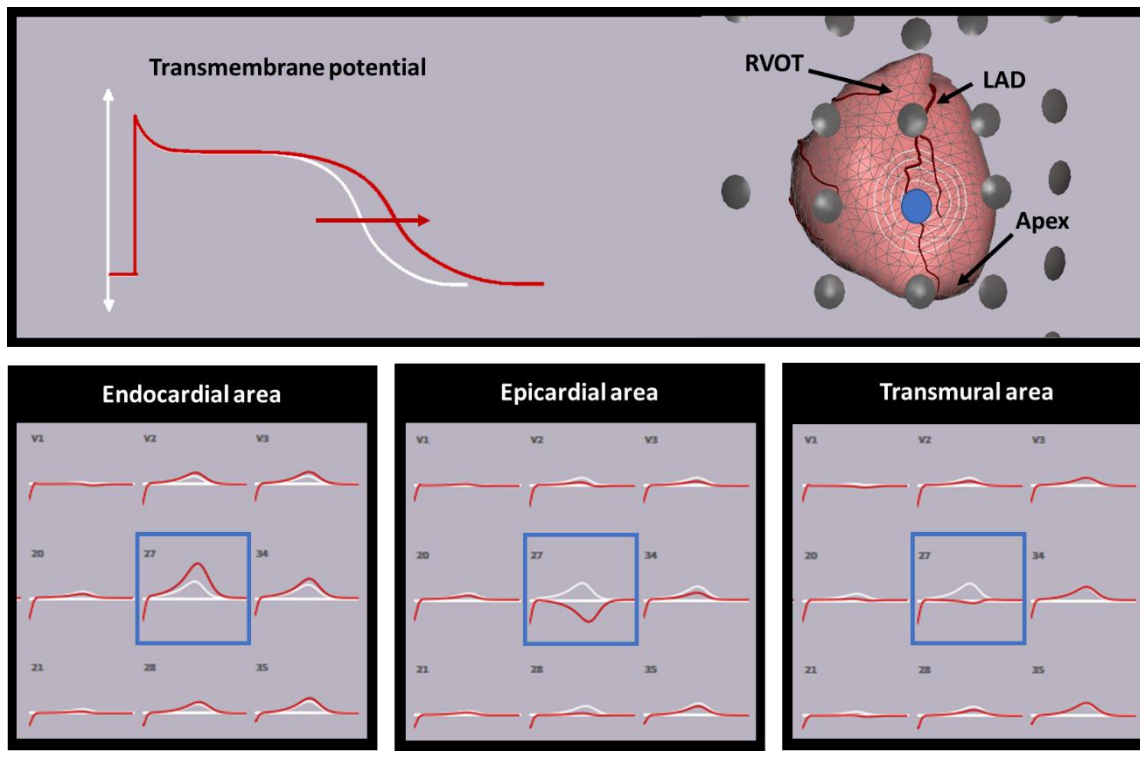


Figure 6.6: ECGsim modeling of repolarization abnormalities. Local transmembrane potentials (TMP) were prolonged in three distinct cardiac regions (white circles): endocardial, epicardial and transmural. Electrocardiographic (ECG) signals were simulated based on the TMP, where normal ECG is white and the affected situation is black. Lead 27 was colored blue. RVOT = right ventricular outflow tract. LAD = left anterior descending artery.

affect TAD measurement. Therefore, subsequent 12-lead ECG's should be precisely repositioned to adequately assess changes in TAD measurements.

In **Figure 6.7**, the depolarization phase of transmembrane potentials (TMP) was delayed in the region of the left anterior descending (LAD) artery in three different heart layers: (1) endocardial, (2) epicardial, and (3) transmural. The TMP in these cardiac regions were adjusted by decreasing the propagation velocities up to 25% of the normal (0.7m/s) propagation velocities. The decreased propagation velocities might be declared by defects in intercellular channels, i.e. gap junctions, caused by the presence of PKP2 pathogenic variants in desmosomal proteins.⁵⁶ Gap junctions play a critical role in the propagation of action potentials and defects in gap junctions might reduce cell-to-cell coupling and therefore influence propagation velocities. In case only endocardial myocytes in this same area were manually adjusted, a prolonged TAD was observed in lead 27 due to an increased S-wave amplitude and decreased R-wave amplitude

(**Figure 6.7; left**). An epicardial or transmural diseased region therefore corresponds to increased R-wave amplitudes and might decrease TAD (**Figure 6.7; mid and right**). This suggests that the progressive aspect of ARVC will result in ECG transition from prolonged TAD to decreased TAD, when characteristics distribute from endocardial to transmural. This hypothesizes suggests that the low prevalence of prolonged TAD (**Appendix A.1**) might be caused by detection of solely endocardial diseased regions in ARVC patients. Long-term monitoring in pathogenic variant carriers is required to investigate this hypothesis.

Other parameters

According to the results in **Part I** and TAD measurements, the S-wave showed important changes in ARVC patients. Therefore, apart from the conventional ECG criteria, the spatial distribution of the S-wave upstroke and S-wave amplitude have been investigated (**Appendix C.2** and **C.3**). The S-wave upstroke was determined in

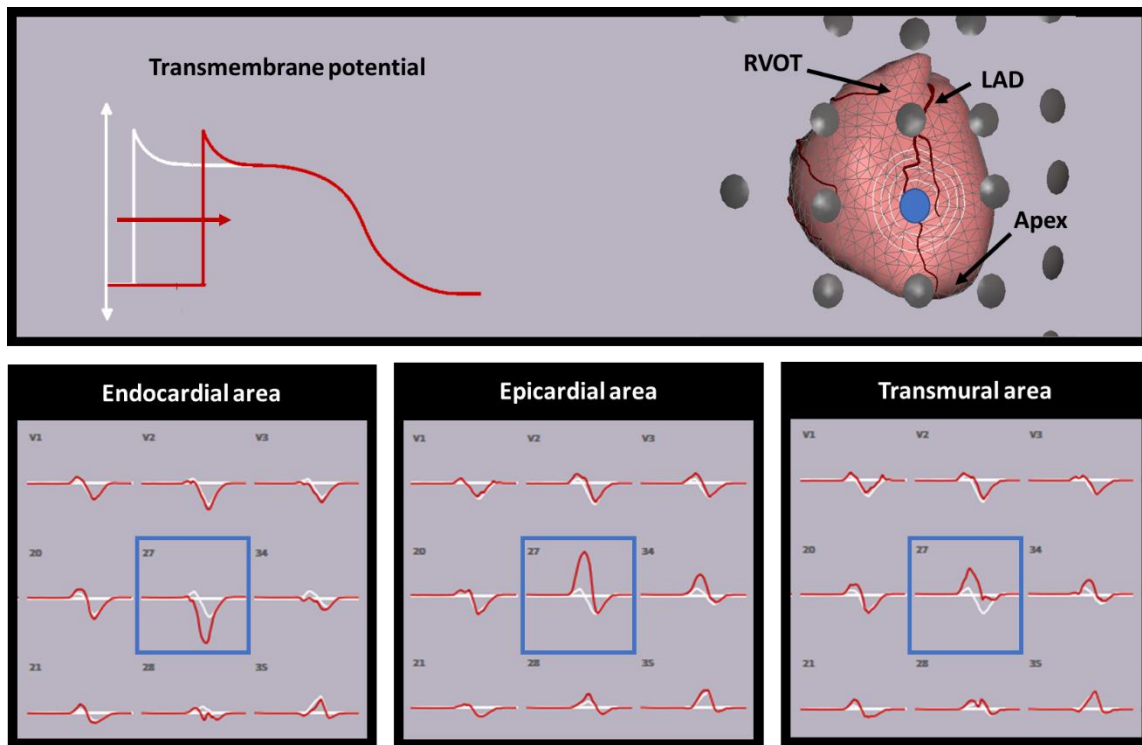


Figure 6.7: ECGsim modeling of depolarization abnormalities. Local transmembrane potentials (TMP) were prolonged in three distinct cardiac regions (white circles): endocardial, epicardial and transmural. Electrocardiographic (ECG) signals were simulated based on the TMP, where normal ECG is white and the affected situation is black. Lead 27 was colored blue. RVOT = right ventricular outflow tract. LAD = left anterior descending artery.

this study, as the TAD criteria was based on S-wave upstroke. Unlike the spatial distributions of TAD, the spatial distributions of S-wave upstroke in controls and PKP2 gene variant carriers show an averaged local maximum below lead V2 (**Appendix C.2; Figure C.2**). Similar to TAD spatial distributions, the S-wave upstroke gradually increases from conventional lead V6 toward V2. Where TAD increased from conventional lead V1 toward right precordial leads (**Figure 6.5**), S-wave upstroke gradually decreases. This can be explained by the difference in definition. In comparison with TAD, S-wave upstroke measurements do not include R' waves, which were present in healthy subjects from lead V1 and further right precordial (**Figure 6.2**).⁵⁷

In healthy subjects, the S-wave is deepest in the right precordial leads, usually in conventional lead V2.⁵⁷ This corresponds with the spatial distributions observed in this study (**Appendix C.3; Figure C.3**). Both PKP2 and control subjects show maximum S-wave amplitude in lead 27, inferior of conventional

lead V2. Significantly smaller S-wave amplitudes were observed in ARVC patients ($0.62 \pm 0.15\text{mV}$) compared to both PKP2 ($1.50 \pm 0.52\text{mV}$; $p=0.01$) and controls ($1.32 \pm 0.33\text{mV}$; $p=0.006$).

Limitations

In this study, current TFC for ARVC were computationally determined in a 64-lead BSPM. For the use of a computational algorithm, some assumptions have been made. First, the clinical definition of TAD was measured from the nadir of the S-wave to the end of all depolarizations, where the computational algorithm measured TAD from the nadir of the S-wave to QRS-offset. QRS-offset was manually determined in RMS of all leads and was therefore similar in all leads, where the clinical definition also includes local late depolarization potentials.

Besides, the ECG criteria could not be determined in all 64 leads, because of the fact that for example S-wave amplitudes were not present in all leads. We chose to not include leads with non-

existent criteria within the averaged isopotential plots, to prevent biased averaged leads when leads with non-existent criteria were set to zero. However, not including the non-existent criteria also biased the results, because in left-precordial body surface leads large number of non-existent criteria were observed.

Future research

This study hypothesized that the heterogeneous characteristics of ARVC might influence the prevalence of the current ECG criteria, as was substantiated with ECG simulations. Future research requires long-term monitoring of ECG criteria in PKP2 pathogenic variant carriers and ARVC patients to investigate ECG changes over time.

This study substantiated that early disease progression cannot be observed in the BSPM data within the repolarization segment. Besides, clinical depolarization criteria were questioned, where this study highlighted the need of clinical usable depolarization criteria for early detection of ARVC. The difficulty in detection of early disease abnormalities in PKP2 pathogenic variant carriers in

BSPM data was emphasized. Future research will further focus on the subtle electrical abnormalities, that cannot be recognized in the conventional 12-lead ECG yet, by investigating mean cardiac activation trajectories related to cardiac anatomy.

Conclusion

The current study showed that the presence of T-wave inversions, observed inferior of conventional lead V2, is an adequate ECG criterium for the diagnosis of ARVC. However, yet no early disease manifestation can be observed in the BSPM data within repolarization abnormalities. High variability was observed in TAD measurements in which V1 lead positioning has greatest influence on meeting the minor TFC for ARVC. Detection of decreased S-wave amplitudes inferior of conventional lead V2 suggest to improve ARVC diagnosis. To investigate the hypothesis that the progressive aspect of ARVC might result in transition of ECG changes over time, future research requires long-term ECG monitoring in pathogenic variant carriers.

CHAPTER 7

PART III

Novel CineECG method to relate mean cardiac activation patterns to cardiac anatomy

Toward a disease-specific lead configuration for arrhythmogenic right ventricular cardiomyopathy

Introduction

Arrhythmogenic right ventricular cardiomyopathy (ARVC) is a complex disease due to clinical heterogeneity of the disease.² The disease is characterized by replacement of fibrofatty tissue that may lead to sudden cardiac death (SCD), ventricular arrhythmias or heart failure. Genetic defects in desmosomal proteins, with plakophilin-2 (PKP2) being the most frequently affected gene, contribute to disease development. Symptom-free pathogenic variant carriers are potentially at risk because of the progressive character of the disease and therefore life-long clinical assessment for pathogenic variant carriers is needed.

Nowadays, diagnosis of ARVC is based on the presence of major and minor criteria in different diagnostic tools, like magnetic resonance imaging (MRI), echocardiography (ECHO), and 12-lead electrocardiography (ECG). Mast *et al.* showed that structural right ventricular (RV) disease progression was associated with prior depolarization abnormalities.⁸ This strengthens the need to early detect electrical changes in pathogenic variant carriers. Current depolarization and repolarization Task Force Criteria (TFC) for ARVC can be detected in the conventional 12-lead ECG. However, sensitivity of the current depolarization criteria is low and interpretation and detection of subtle electrical abnormalities remains complex.

Cortez *et al.* already showed that pathogenic variant carriers with ECG-negative ARVC bear early electrical abnormalities that can be detected using novel right precordial-adjusted vectorcardiogram (VCG) markers.⁵⁸ Van Dam *et al.* utilized a novel CineECG method that computes the mean temporo-spatial isochrone (mTSI) trajectory from ECG data, which represents the mean position of activation through the heart.^{32,37} mTSI, estimated from VCG, combines ECG data with a patient-specific cardiac-torso model. This novel technique showed that differences in mTSI trajectories were already present in patients who developed type-1 Brugada pattern in 12-lead ECG during Ajmaline infusion.³⁷ These results substantiates that subtle electrical abnormalities might be present in the conventional 12-lead ECG, but cannot be recognized yet. The goal of this study is to investigate mean cardiac activation trajectories related to cardiac anatomy in PKP2 pathogenic variant carriers that met the TFC for RVC, PKP2 pathogenic variant carriers and controls. The study aims to early detect electrical changes in PKP2

pathogenic variant carriers for early diagnosis of disease manifestation of ARVC.

Method

Subjects

The study population consisted of 23 PKP2 pathogenic variant carriers and nine control subjects with symptomatic ventricular extrasystoles originating in the right ventricular outflow tract (RVOT VES). Patients without right bundle branch block (QRS width <120ms) and no other structural diseases that affect ECG morphology apart from ARVC symptoms were included in this study. Subjects with RVOT VES were considered to be control subjects, where subjects without signs of heart failure were included in the study (QRS width <120ms, LV ejection fraction (EF) >45%, RVEF >45%, RV end-diastolic volume index <110ml/m²).

The study was approved by the Medical Ethics Committee of University Medical Center Utrecht (17/907) and informed consent was obtained from each subject before enrolment.

Body surface potential mapping

67-lead BSPM were obtained in each subject, consisting of 64 torso and 3 limb leads. The anterior body surface includes 55 leads, that were placed in nine vertical strips with strip 4 located at the sternum. The posterior body surface includes 9 leads, that were placed in three vertical columns. Lead positions 14, 26, 33-34, 41, 48, 53 correspond to conventional 12-lead ECG positions V1-V6 (**Figure 7.1; black stars**), respectively.

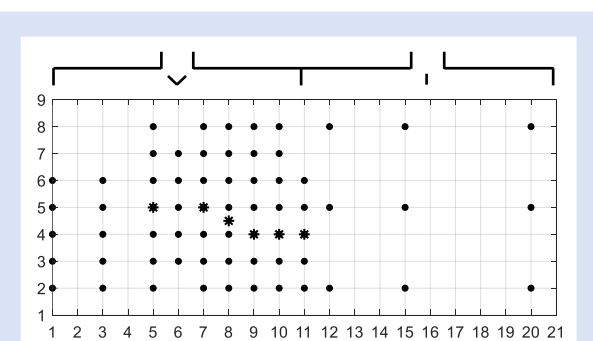


Figure 7.1: Visualization of the 64 torso lead positions of the body surface potential maps (BSPM). Column 1-11 and 11-21 correspond to the anterior and posterior body surface, respectively. Black dots refer to the 64 torso lead locations of the BSPM measurement. Black stars refer to the conventional 12-lead ECG positions, where V1-V2 and V4-V6 were included in the 64 torso leads.

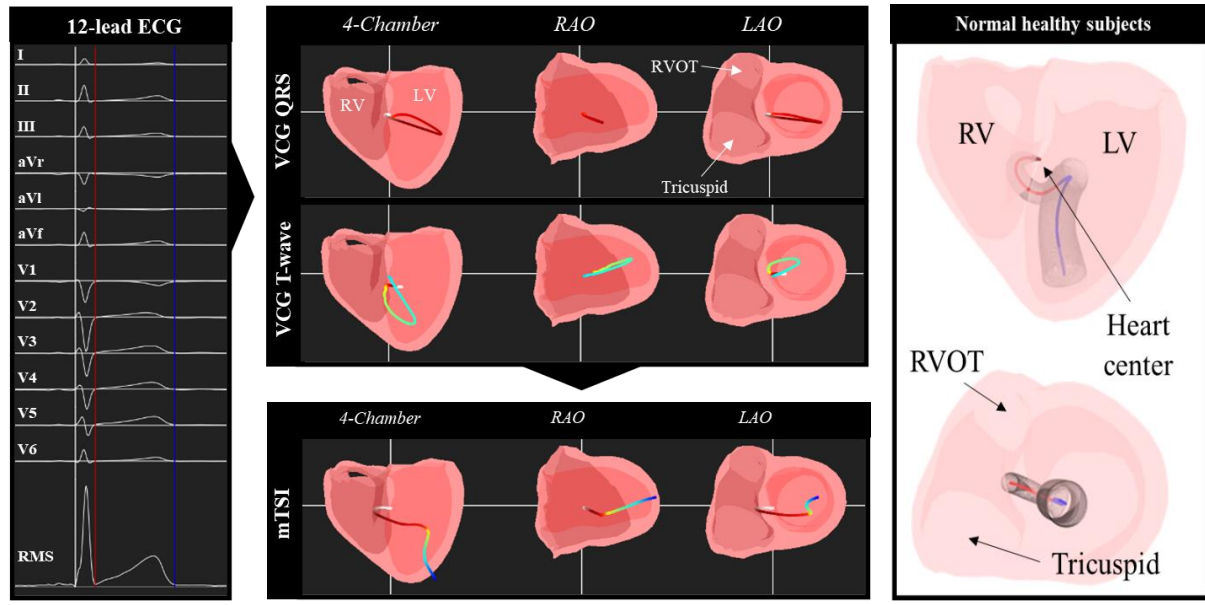


Figure 7.2: (Left) Visualization of computation of mean temporal spatial isochrone (mTSI) trajectory in CineECG. 12-lead ECG was converted to vectorcardiogram (VCG). mTSI trajectory was constructed from VCG using different propagation velocities in the QRS- and STT-segment. mTSI was colored from white to red (QRS-onset to QRS-offset) and red to blue (QRS-offset to end T-wave). VCG and mTSI were visualized in 4 chamber view, right anterior oblique (RAO) view, and left anterior oblique (LAO) view. (Right) Averaged mTSI trajectory of 42 healthy controls through the cardiac anatomy, with the ventricular depolarization in red and ventricular repolarization in blue. Transparent black circle plane corresponds to one standard deviation. RVOT = right ventricular outflow tract; LV = left ventricle; RV = right ventricle; RMS = root-mean-square;

Body surface potentials were recorded (Biosemi, Amsterdam, The Netherlands) simultaneously with Wilson's central terminal as reference. BSPM recordings were digitized using a 24-bit AD-converter and sampling rate of 2048Hz per channel. BSPMs were down-sampled to 1000Hz and were filtered with a moving average low-pass filter (window size 0.02s) and high-pass filter (window size 10s). Per subject, ten consecutive sinus beats were obtained during resting respiration. Ventricular extrasystoles were excluded and leads with noise were removed. Details about the signal preprocessing steps can be found in **Chapter 3**.

CineECG method

For each subject, data from conventional 12-lead positions were extracted from the 67-lead BSPM data. Conventional lead V3 was not directly measured within the BSPM data and was determined by the average of lead 33 (above conventional lead V3) and lead 34 (below conventional lead V3). The conventional 12-lead ECG data and standardized heart-torso model was used to compute the mTSI. mTSI was estimated from VCG signal, with VCG

signal computed from the 12-lead ECG data (**Figure 7.2**) taking the electrode positions on the torso into account:

$$\overline{VCG}(t) = \sum_{el=1}^9 \alpha_{el} ecg_{el}(t) \cdot \frac{|\vec{r}_{el} - \vec{r}_{ref}|}{\|\vec{r}_{el} - \vec{r}_{ref}\|} \quad (7.1)$$

where $\frac{|\vec{r}_{el} - \vec{r}_{ref}|}{\|\vec{r}_{el} - \vec{r}_{ref}\|}$ is the normalized vector between a reference position and electrode position on the thorax. Center of myocardial mass was used as reference position. For the unaugmented extremity leads (VR, VL, VF), α_{el} was set to 2 for the Y and Z directions and 0 for the X direction to correct for distance. For all precordial leads (V1-V6), α_{el} was set to 1 for all directions. mTSI was computed from the VCG signal:

$$\overline{mTSI}(t) = \overline{mTSI}(t-1) + v \cdot \frac{\overline{VCG}(t)}{\|\overline{VCG}(t)\|} \quad (7.2)$$

where the movement of mTSI is defined by the direction of VCG, previous position of mTSI and propagation velocity (v). In the QRS-segment, a propagation velocity of 0.7 m/s was used.^{33,34} Velocities at ST-segment and 50ms prior to end T-wave (terminal T-wave) were set initially to 0.2 m/s

and 0.35 m/s, respectively.³⁵ In case the mTSI trajectory propagated outside the cardiac model, the propagation velocity in ST-segment and T-wave were stepwise decreased. Normal His-Purkinje activation was assumed in all subjects, using the mid left septal region as start point from the mTSI. Furthermore, a standardized heart- and torso- model was used in all subjects.

Data analysis

Per subject, the averaged mTSI trajectory was calculated from five sinus beats, where QRS-onset, QRS-offset and end T-wave were manually annotated in the root mean square (RMS) curve from all leads. Per time instance, the average 3-dimensional (3D) mTSI trajectory was calculated.

mTSI parameters

To quantify differences in mTSI trajectories between groups, the following mTSI positions within the QRS-segment (and initial STT-segment) were determined for all subjects:

- **QRS₂₀:** mTSI trajectory propagation distance (mm) at 20ms after QRS-onset, using QRS-onset as reference position.
- **QRS₅₀:** mTSI trajectory propagation distance (mm) at 50ms after QRS-onset, using 20ms after QRS-onset as reference position.
- **QRS₈₀:** mTSI trajectory propagation distance (mm) at 80ms after QRS-onset, using 50ms after QRS-onset as reference position.
- **QRS₁₁₀:** mTSI trajectory propagation distance (mm) at 110ms after QRS-onset, using 80ms after QRS-onset as reference position.

Furthermore, the following mTSI parameters were investigated:

- **TCR:** Trans-cardiac ratio; ratio between the Euclidian distance between QRS-onset and QRS-offset divided by the length of the mean QRS-axis inside the heart model, to correct for inter-individual differences in heart size.
- **TCR_{min}:** Minimal trans-cardiac ratio; ratio between the Euclidian distance between QRS-onset and closest point of mTSI trajectory after 60% of QRS duration. Distance is divided by the length of the mean QRS-axis inside the heart model, to correct for inter-individual differences in heart size.
- **QRS-STT-angle:** 3D angle between mTSI vector of the last 10ms of the QRS-segment and the first 10ms of the STT-segment.

- **RV_{max}:** Transverse distance between location of mTSI at QRS-onset and farthest point of mTSI trajectory in the first 50ms of QRS duration.

Data visualization

All mTSI trajectories were visualized in both standard 4-chamber view and left anterior oblique view (LAO), where per group the averaged mTSI trajectory was calculated. The standard deviation (SD) per group was calculated as the mean Euclidian distance between the average mTSI trajectory and the individual mTSI trajectories per group. Depolarization and repolarization trajectories were visualized in red and blue respectively (**Figure 7.2; right**).

Results

From all PKP2 pathogenic variant carriers, seven subjects met the TFC for ARVC. Patient characteristics are stated in **Table 7.1**.

The mTSI trajectories of QRS-segment and STT-segments were computed for all subjects. The averaged mTSI trajectory per group was visualized (**Figure 7.3**) and mTSI parameters were determined (**Table 7.2**). In ARVC patients, differences in mTSI trajectory positions were observed up to 80ms after

Table 7.1: Patient group characteristics

Group	ARVC N=7	PKP2 N=16	CONTROL N=9
Male	4	5	3
Age (y)	36 ± 18	38 ± 17	34 ± 13
TFC (#)	6.6 ± 2.4	2.2 ± 0.4	-
Onset diagnosis (y)	3.7 ± 3.8	-	-
QRS width (ms)	90 ± 11	93 ± 9	94 ± 11
STT width (ms)	406 ± 20	389 ± 15	392 ± 13
Heart rate (bpm)	61 ± 10	61 ± 11	63 ± 9
LV EDVI (ml/m ²)	93 ± 15	94 ± 11	95 ± 17
LV EF (%)	59 ± 5	55 ± 4	54 ± 5
RV EDVI (ml/m ²)	129 ± 40	92 ± 13	92 ± 14
RV EF (%)	41 ± 13	56 ± 6	53 ± 6

Abbreviations: ARVC = Arrhythmogenic Right Ventricular Cardiomyopathy; PKP2 = Plakophilin-2; TFC = Task Force Criteria; LV = left ventricle; EDVI = end diastolic volume index; EF = ejection fraction; RV = right ventricle.

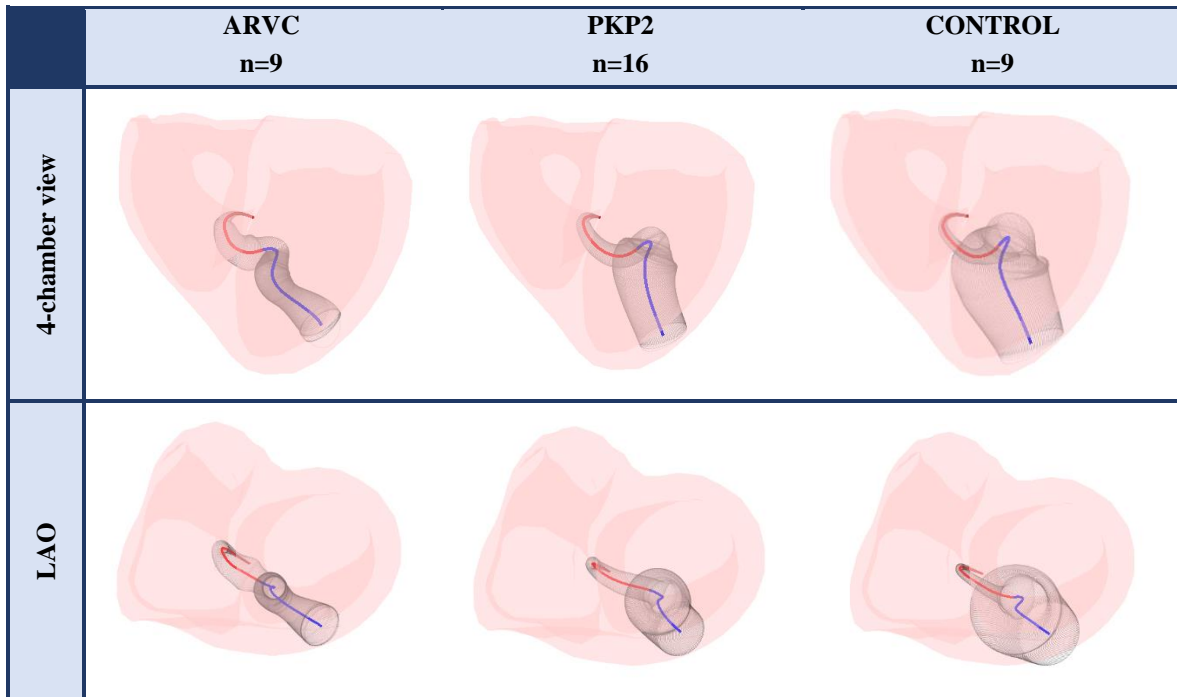


Figure 7.3: Visualization of mTSI trajectories of ARVC patients (n=7), PKP2 gene variant carriers (n=16), and controls (n=9). Ventricular depolarization was shown in red and ventricular repolarization in blue. Transparent black circle plane corresponds to one standard deviation.

QRS-onset compared to controls (**Table 7.2; blue**). From QRS₂₀ to QRS₈₀, the averaged mTSI trajectory of ARVC patients was propagated (1, QRS₂₀) more apical, (2, QRS₅₀) less toward the left ventricles, and (3, QRS₈₀) more apical compared to controls. No visual differences were observed in TCR, TCRmin, QRS-STT-angle and RVmax.

The mTSI trajectories of ARVC patients with T-wave inversions and normal T-waves were compared with each other (**Figure 7.4**). Direction of T-wave were investigated for pathophysiological explanation of cardiac substrate. The effect of T-wave inversions in ARVC patients can be observed in the averaged mTSI trajectories, where T-wave inversions result in a visual difference in mTSI trajectory direction in the STT-segment.

Discussion

The current study aims to investigate mean cardiac activation trajectories related to the cardiac anatomy, to early detect subtle electrical changes that could not be detected in the conventional 12-lead ECG. The main results show differences in initial QRS trajectories up to 80ms after QRS-onset (**Table 7.2; marked blue**).

QRS-segment

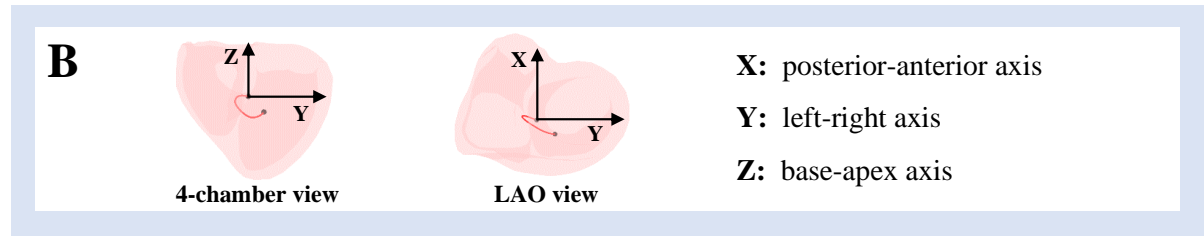
The mTSI parameters used in this study focused on terminal QRS and initial ST trajectory, because in

this range a marker of activation delay of ARVC was suspected. However, differences in mTSI trajectory positions were already observed at 20ms and 50ms after QRS-onset in ARVC patients compared to controls (**Table 7.2**). The mTSI trajectory position at 20ms after QRS-onset was located more basal in ARVC patients. Besides, a decreased propagation in mTSI position at 50ms after QRS-onset was observed from right toward left ventricle. No visual differences were observed in TCR, TCRmin, QRS-STT-angle and RVmax, which suggests normal cardiac activation trajectories related to cardiac anatomy.

The hypothesis was that ARVC could be observed in the terminal QRS-segment. However, visual differences in QRS trajectory positions were found in the initial and mid QRS-segment (up to 80ms after QRS onset), which corresponds with the results from **Part I** in this thesis. The results might suggest electrical changes in the septal-apical ventricular region, where it was assumed to observe late electrical activation in the RV basal region. These results might be explained by the fact that this study only included subjects without prolonged QRS duration (>120ms) and thus no substantially late stage of disease progression. In **Appendix D**, a second study population subdivided by QRS-duration showed terminal QRS trajectory positions visual deviated at prolonged QRS duration. The

Table 7.2: mTSI parameters determined in the ARVC, PKP2 and control group (A), including a 2D visualization of the X, Y and Z axes within the cardiac anatomy (B). Different mTSI positions of ARVC compared to PKP2 or CONTROL are marked blue. See text for definitions of all mTSI parameters.

A	ARVC			PKP2			CONTROL		
	X	Y	Z	X	Y	Z	X	Y	Z
QRS ₂₀ (mm)	4 (3)	-11 (1)	1 (5)	3 (5)	-7 (4)	-2 (5)	2 (4)	-10 (3)	-3 (2)
QRS ₅₀ (mm)	-1 (4)	5 (9)	-13 (6)	-1 (5)	13 (5)	-13 (3)	-2 (4)	13 (3)	-12 (3)
QRS ₈₀ (mm)	-6 (3)	14 (3)	-3 (10)	-4 (7)	14 (4)	4 (8)	-4 (5)	13 (6)	4 (7)
QRS ₁₁₀ (mm)	0 (5)	4 (6)	1 (5)	-1 (5)	4 (6)	1 (7)	-1 (2)	2 (7)	3 (10)
TCR (%)	22 (11)			27 (10)			23 (11)		
TCRmin (%)	20 (14)			26 (12)			22 (11)		
QRS-STT-angle (°)	54 (34)			35 (30)			43 (38)		
RVmax (mm)	14 (5)			8 (4)			10 (3)		



terminal QRS trajectories of ARVC patients with prolonged QRS duration showed that the terminal mTSI trajectory changed toward the right ventricular base. This might suggest late right ventricular activation in ARVC patients. The decreased QRS-STT-angle show that mTSI trajectory at the transition from depolarization to repolarization change less abrupt, which might support the possible existence of late right ventricular activations or the presence of overlap between the depolarization and repolarization phase.

STT-segment

In all groups, the mTSI trajectories within the STT-segments were directed toward the posterior left ventricular apex (**Figure 7.3**). Subdividing the ARVC group in the presence or absence of T-wave inversions showed visual differences in mTSI trajectories (**Figure 7.4**). In ARVC patients with T-wave inversions, the terminal T-wave trajectories were directed toward the left ventricular mid-posterior wall. In healthy subjects, the T-wave mTSI trajectory always is directed toward the apical region along the septal wall immediately after the QRS mTSI (**Figure 7.1**). This can be explained by the knowledge that the last cells to depolarize are the first to repolarize and therefore the repolarization

phase occurs at the same time in both ventricles from base toward apex. ARVC patients with T-wave inversions show T-wave mTSI trajectories directed toward left ventricular mid-posterior wall, hypothesizing that the right ventricle is last to depolarize and first to repolarize. This finding correlates with the direction from minimum toward maximum T-wave integrals in **Part II** of this thesis (**Figure 6.2; ARVC (TWI+)**).

Limitations

In the current study, both QRS-onset and QRS-offset were detected computationally in CineECG, but could manually be adjusted. Beat annotations (QRS-onset, QRS-offset and T-wave end) in CineECG therefore differed compared to BSPM data that were used in previous parts of this thesis. Small annotation errors of especially the QRS-offset might have resulted in different trajectory positions in the ventricular anatomy, as the propagation velocity in the QRS-segment is higher compared to the initial ST-segment.

Furthermore, the propagation velocities were set to 0.7, 0.2 and 0.35ms for QRS-segment, ST-segment and terminal T-wave, respectively. It is known that repolarization patterns propagate with smaller velocity compared to depolarization

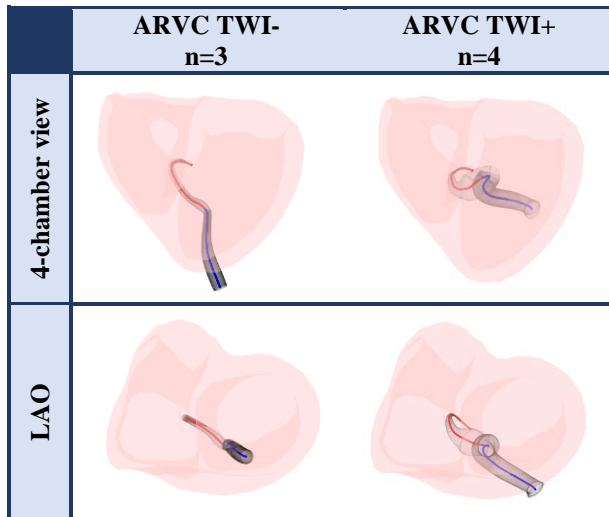


Figure 7.4: Four-chamber visualization of T-wave mTSI trajectories in all seven individual ARVC patients, with origin of all trajectories located in center of cardiac mass. Left: ARVC patients without T-wave inversions (TWI-) and right: ARVC patients with T-wave inversions (TWI+).

activity. However, the specific value is unknown. The current propagation settings were based on a physiological aspect of propagation patterns, where the repolarization phase arises from local source points. The repolarization phase propagates faster when these local regions repolarize more and more neighbor myocytes. Therefore, initial and terminal T-wave were set to 0.2 and 0.35ms, respectively. Future studies have to investigate the appropriate propagation settings.

Future studies

This study used the novel CineECG method to localize early disease progression in PKP2 pathogenic variant carriers. The CineECG method is still in their infancy,^{59,37} therefore the proof-of-concept needs to be confirmed in further studies.

In some patients, the propagation velocities within the STT-segment were gradually decreased to prevent the mTSI to propagate outside the cardiac model. Future studies have to investigate the appropriate propagation settings, where a decrease of propagation velocity might indicate difference in cardiac anatomy and/or orientation. Furthermore, this study used a standardized heart and torso model for all subjects, which might affect mTSI results. Therefore, the effect of the use of patient-specific heart models derived from MRI or CT should be tested in future studies.

Conclusion

For detection of early ECG changes caused by initial disease manifestation in PKP2 pathogenic variant carriers, the results suggest to focus on the initial and mid QRS-segment, instead of the terminal QRS-segment. In a further stage of disease progression, changes in the terminal QRS-segments can be observed. Future research requires investigation of the effect of disease progression on mTSI trajectories, to fully understand every stage of disease progression of ARVC.

CHAPTER 8

Validation study

**Toward a disease-specific lead configuration for arrhythmogenic
right ventricular cardiomyopathy**

Introduction

Arrhythmogenic right ventricular cardiomyopathy (ARVC) is a complex disease due to clinical heterogeneity of the disease.² The disease is characterized by replacement of fibrofatty tissue that may lead to sudden cardiac death (SCD), ventricular arrhythmias or heart failure. Genetic defects in desmosomal proteins, with plakophilin-2 (PKP2) being the most frequently affected gene, contribute to disease development. Symptom-free carriers are potentially at risk because of the progressive character of the disease and therefore life-long clinical assessment for pathogenic variant carriers is needed.

The amount of information obtained with conventional 12-lead electrocardiography (ECG) suffices for most clinical applications. However, in some applications the use of extra ECG leads or other lead locations on the chest has proven to increase the detection rate of ECG abnormalities.

In previous parts of this research thesis, 67-lead body surface potential maps (BSPM) data was investigated and the current ECG criteria were reexamined for lead placement. Lead 27 and 40 showed large differentiation for ARVC in both S-wave amplitudes, T-wave inversions and QRS-integrals. A visualization of positions of lead 27 and 40 can be observed in **Figure 8.1**. Additional lead positions and new ECG criteria were found by computational research, but the usability of the new criteria and lead positions have to be validated in a clinical context. This validation study aims to investigate (1) the diagnostic value, i.e. sensitivity (SE) and specificity (SP), of additional ECG criteria in PKP2-positive ARVC patients and (2) whether additional lead positions show a higher diagnostic

value compared to the conventional 12-lead ECG positions.

Method

Study subjects

The study population consisted of 23 PKP2 pathogenic variant carriers and nine control subjects with symptomatic ventricular extrasystoles originating in the right ventricular outflow tract (RVOT VES). Patients without right bundle branch block (QRS width <120ms) and no other structural diseases that affect ECG morphology apart from ARVC symptoms were included in this study. Subjects with RVOT VES were considered to be control subjects, where subjects without signs of heart failure were included in the study (QRS width <120ms, LV ejection fraction (EF) >45%, RVEF >45%, RV end-diastolic volume index <110ml/m²).

The study was approved by the Medical Ethics Committee of University Medical Center Utrecht (17/907) and informed consent was obtained from each subject before enrolment.

ECG recording

67-lead BSPM were obtained in each subject, consisting of 64 torso and 3 limb leads. The anterior body surface includes 55 leads, that were placed in nine vertical strips with strip 4 located at the sternum. The posterior body surface includes 9 leads, that were placed in three vertical columns. Lead positions 14, 26, 33-34, 41, 48, 53 correspond to conventional 12-lead ECG positions V1-V6 (**Figure 8.1; blue dots**), respectively.

Body surface potentials were recorded (Biosemi, Amsterdam, The Netherlands) simultaneously with Wilson's central terminal as reference. BSPM recordings were digitized using a 24-bit AD-converter and sampling rate of 2048Hz per channel. BSPMs were down-sampled to 1000Hz and were filtered with a moving average low-pass filter (window size 0.02s) and high-pass filter (window size 10s). Per subject, ten consecutive sinus beats were obtained during resting respiration. Ventricular extrasystoles were excluded and leads with noise were removed. Details about the signal preprocessing steps can be found in **Chapter 3**.

For all subjects, the conventional 12-lead ECG positions within the 67-lead BSPM data and two additional lead positions (lead 27 and 40) were collected (**Figure 8.1; orange and yellow dot**). Conventional and additional lead positions were reconstructed to conventional ECG recordings settings, using paper speed of 25 mm/s and sampling frequency of 500Hz.

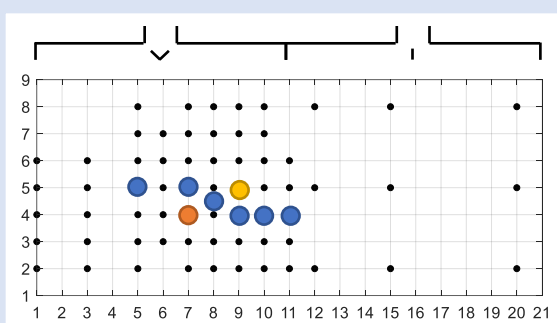
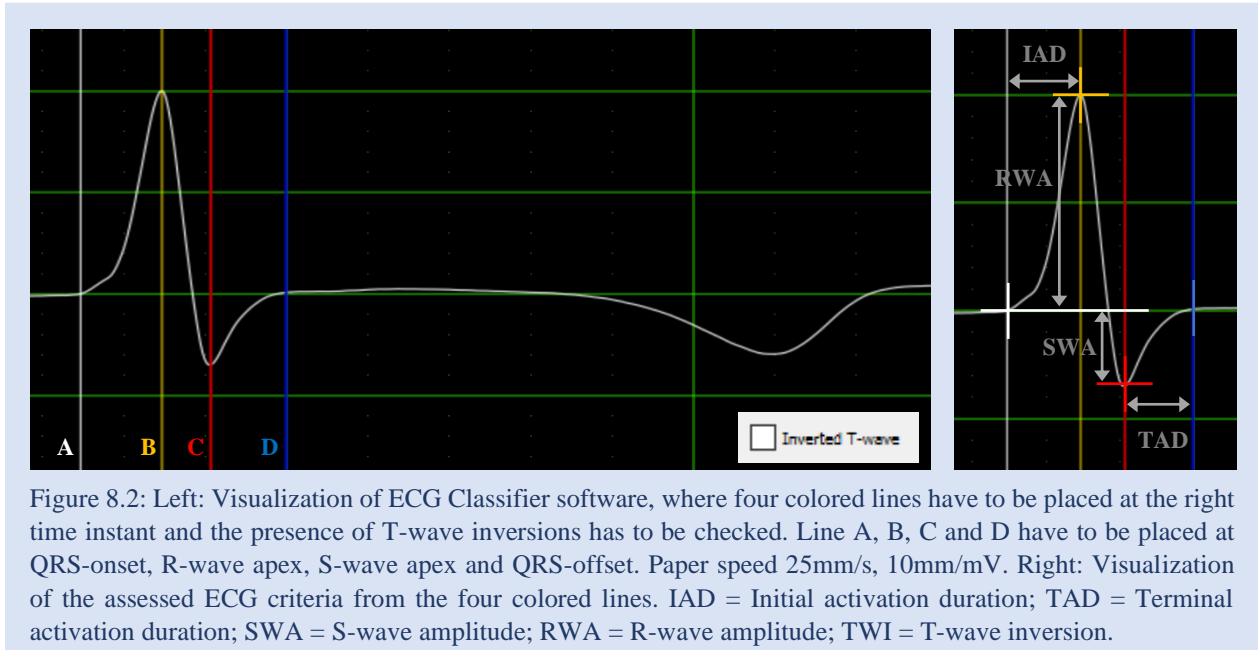


Figure 8.1: Overview of 64-lead body surface potential map positions (black dots) on the anterior (column 1-11) and posterior (column 11-21) body surface. Blue dots refer to the conventional 12-lead ECG positions (V1-V6). Orange and yellow dot correspond to lead 27 and 40, respectively.



ECG classification

ECG analysis was performed manually by two physicians, using the ECG Classifier software (ECG Excellence BV). The physicians were instructed to manually set four colored lines at the right time instant within an individual lead measurement: QRS-onset, R-wave apex, S-wave apex, and QRS-offset (**Figure 8.2, left**). Moreover, the presence of T-wave inversion was examined. QRS-onset and QRS-offset were defined as the earliest onset of the QRS-complex and end of all depolarization deflections, respectively. Both individual lead measurements (V1-V6, L27 and L40) and subjects (ARVC, PKP2 and controls) were randomized and physicians were blinded for all other patient information. In case no R-wave amplitude or S-wave amplitude was present within the lead measurement, the physicians were instructed to place the current line between the neighbored lines.

Data analysis

From the ECG classifier software, the following six ECG criteria related to depolarization and repolarization abnormalities were examined:

- **Terminal activation duration (TAD):** time duration (ms) from the nadir of the S-wave to the end of all depolarization deflections.
- **Initial activation duration (IAD):*** Time duration (ms) from QRS-onset to R-wave apex.
- **S-wave amplitude (SWA):*** Amplitude (mV) from the isoelectric baseline (at QRS-onset) to the nadir of the S-wave.

- **R-wave amplitude (RWA):*** Amplitude (mV) from the isoelectric baseline (at QRS-onset) to the nadir of the R-wave.
- **R to S ratio (RSr):*** Ratio between amplitude of the R-wave and (absolute) amplitude of the S-wave.
- **T-wave inversion (TWI):** T-wave negativity.

ECG criteria marked with * correspond to additional ECG criteria for early detection of ARVC. RWA and SWA were present at amplitudes outside the interval of -0.05 to 0.05mV. Systematically, nonexistent RWA and SWA result in nonexistent TAD or IAD measurements. Parameters that could not be determined were set to 0. RSr was calculated as:

$$RSr = \frac{RWA - SWA}{RWA + SWA} \quad (8.1)$$

where RSr equal to -1.0 corresponds to absent RWA and 1.0 corresponds to absent SWA. RSr of 0 indicates that R-wave and S-wave have equal amplitudes.

Statistical analysis

Receiver Operating Characteristic (ROC) curves were used to define optimal threshold value for classification of ARVC. The optimal threshold value was defined using the maximum Youden index (SE + SP - 1), which corresponds with the maximum potential effectiveness of a biomarker. In ARVC patients, the best cut-off value per parameter per lead for ARVC diagnosis was determined. Next, sensitivity (SE), specificity (SP) and area under the

ROC curve (AUC) were determined to investigate the diagnostic value of the ECG parameters in ARVC patients, PKP2 pathogenic variant carriers and controls. The three highest values of AUC for detection of ARVC were chosen to eventually compare the conventional 12-lead positions with the new lead positions.

The repeatability coefficient (RPC) between the two physicians was determined for both QRS-onset and QRS-offset, defined as $1.96 \times SD$. Besides, the deviation in QRS-onset and QRS-offset within different lead positions was investigated.

Results

From all PKP2 pathogenic variant carriers, seven subjects met the TFC for ARVC. Patient characteristics are stated in **Table 8.1**. From all 32 subjects, eight individual lead measurements were manually examined by two physicians, resulting in 256 examined lead measurements per physician.

IAD, TAD, RWA, SWA, RSr and QRS duration were computed from the time annotations of both physicians and visualized per group per lead position (**Figure 8.2**). The diagnostic values (SE, SP and AUC) of ARVC disease were determined per parameter per lead, from which the three leads with highest diagnostic value are shown in **Table 8.2**. The diagnostic values were also determined in PKP2 pathogenic variant carriers, using same cut-off values for ARVC differentiation.

The repeatability coefficient was determined for both the QRS-onset and QRS-offset. At the QRS-onset, the RPC ranged from 4.7 to 17ms in all leads, where the RPC at the QRS-offset ranged from 12 to 20ms.

Discussion

This study aimed to investigate (1) the diagnostic value of additional ECG criteria in ARVC patients and PKP2 pathogenic variant carriers and (2) whether additional lead positions show a higher diagnostic value compared to the conventional 12-lead ECG positions. Two physicians assessed the QRS-onset, maximum R-wave amplitude, maximum S-wave amplitude, QRS-offset and T-wave inversion within blinded, randomized single-lead ECG recordings. From these results, six (including four additional) ECG parameters were determined: IAD, TAD, RWA, SWA, RSr and TWI. The results showed additional leads (L27 and L40) were highly sensitive for the differentiation of ARVC (**Table 8.2**). However, parameters that were based on time intervals showed to be more sensitive for deviation errors (**Figure 8.3**), compared to parameters that were based on amplitudes. From all

Table 8.1: Patient group characteristics

Group	ARVC N=7	PKP2 N=16	CONTROL N=9
Male	4	5	3
Age (y)	36 ± 18	38 ± 17	34 ± 13
TFC (#)	6.6 ± 2.4	2.2 ± 0.4	-
Onset diagnosis (y)	3.7 ± 3.8	-	-
Heart rate (bpm)	61 ± 10	61 ± 11	63 ± 9
LV EDVI (ml/m ²)	93 ± 15	94 ± 11	95 ± 17
LV EF (%)	59 ± 5	55 ± 4	54 ± 5
RV EDVI (ml/m ²)	129 ± 40	92 ± 13	92 ± 14
RV EF (%)	41 ± 13	56 ± 6	53 ± 6

Abbreviations: ARVC = Arrhythmogenic Right Ventricular Cardiomyopathy; PKP2 = Plakophilin-2; TFC = Task Force Criteria; LV = left ventricle; EDVI = end diastolic volume index; EF = ejection fraction; RV = right ventricle.

lead positions, conventional leads V3-4, lead 27 and 40 showed highest diagnostic values in all ECG parameters except at TWI.

The distribution of IAD showed an increase in measurement values from V1 to V6, where TAD shows a decrease in duration (**Figure 8.1**). High standard deviations were observed in all leads. IAD, also referred to as R-wave-peak-time, ventricular activation time, or intrinsicoid deflection, represents the early phase of ventricular depolarization, and reflects the electrical activation duration from the endocardium to the epicardium.⁶⁰ The normal conditions of IAD in V1-V2 (<35ms) and V5-V6 (<45ms) agree with the IAD measurements in PKP2 pathogenic variant carriers and controls (**Figure 8.3**).⁶⁰ Large prolongation of IAD in lead V3, 27 and 40 was observed in ARVC patients, that suggests a delay in the electrical activation duration from the endocardium to the epicardium in these lead regions.

TAD reflects the RV activation duration and is assumed to be prolonged in right precordial leads V1-V3 when exceeding 55ms.⁵⁵ Despite RV dysfunction in the ARVC group (**Table 8.1**), PKP2 pathogenic variant carriers and controls showed prolonged TAD in V1-V2, where lower TAD measurements were observed in ARVC patients.

RWA increased from V1 to V6, where the S-wave showed a decrease in amplitude. The tallest RWA is most commonly observed in lead V4, followed by V5, where SWA is deepest in the right precordial leads, usually in lead V2.⁵⁷

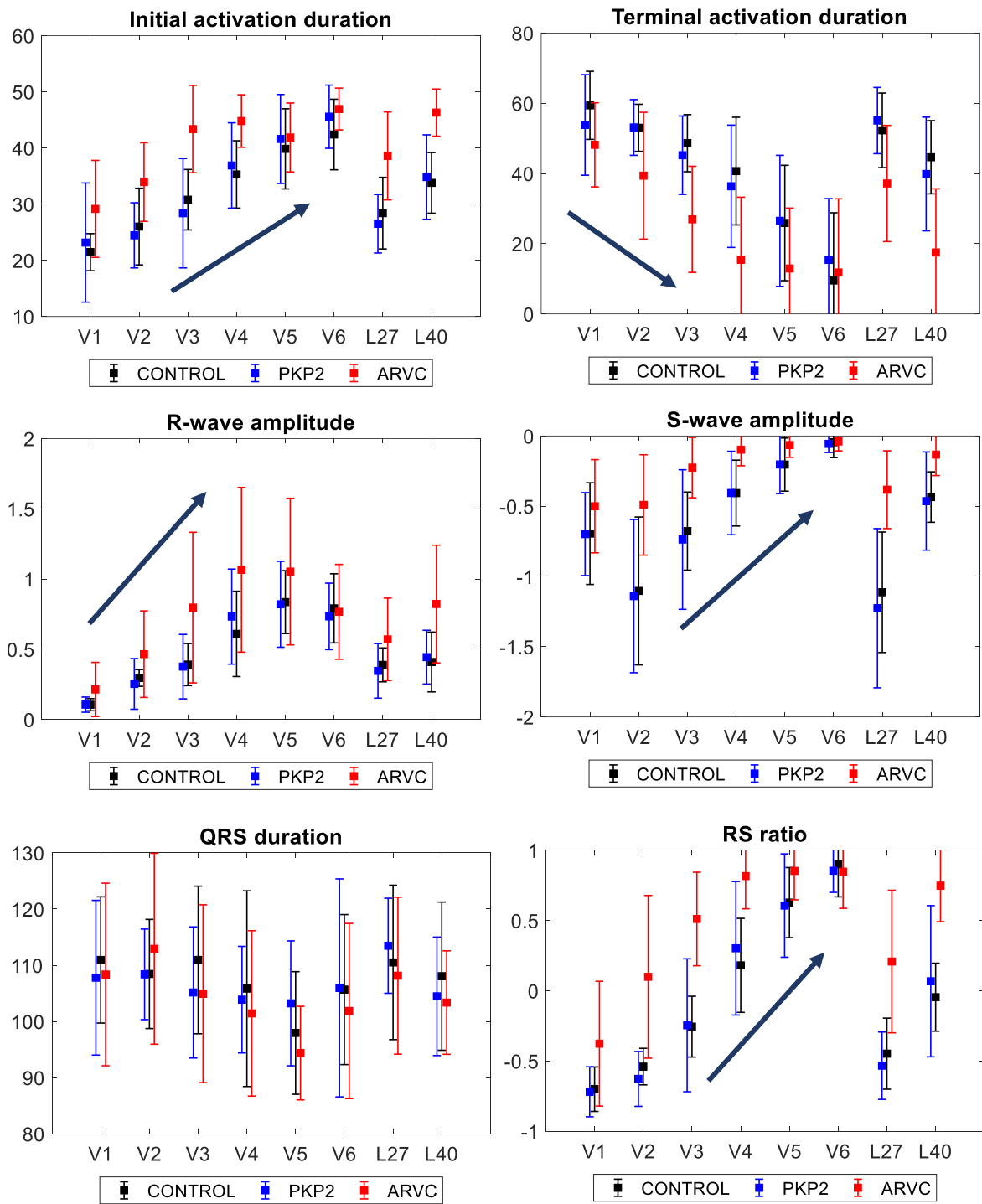


Figure 8.3: Depolarization parameters measurements (mean \pm standard deviation) of ARVC (red), PKP2 (blue) and CONTROL patients (black). Each parameter is determined in eight different lead positions (V1-V6, L27 and L40). Blue arrows display an increase or decrease of parameter measurements over conventional lead V1-V6.

This corresponds with the RWA and SWA measurements in this study. In ARVC patients, largest RWA and SWA difference with controls was observed in conventional leads V2-V4, lead 27 and 40. As RS ratio is defined as the ratio between SWA and RWA, ARVC patients showed even larger differences in RS ratio compared to controls in these lead positions.

Per parameter, the diagnostic values of the best three lead positions were noted based on AUC (Table 8.2). Highest diagnostic values of ARVC was observed in IAD (L40 and V4), SWA (L27), and RSr (V3, V4 and L40). Highest sensitivity and specificity for the differentiation of ARVC was observed in IAD (SE 86-100%, SP 79-100%), SWA (SE 86-100%, SP 78-89%) and RSr (SE 100%, SP 78-100%). Nevertheless, other ECG parameters also showed high sensitivity and specificity values.

Within this study, six different parameters had to be determined by physicians within 256 single-leads potentials. Due to the large dataset and therefore a highly time-consuming activity, this study chose to

let physicians manually point four different time instants within each single-lead potential. Based on these four instants, all six different parameters could computationally be determined. Despite the use of the easy to use ECG classifier software to clinical validate ECG parameters, a large difference in both QRS-onset (10-16ms) and QRS-offset (20-23ms) was observed within subjects (Figure 8.3A). Large difference at onset of the QRS-complex was observed (Figure 8.3.B) using lead V1 as reference onset. All other lead positions were annotated at a later QRS-onset. QRS-offset therefore showed a more diffused difference at time of offset over all leads. The measurement errors within QRS-onset and QRS-offset were observed over all precordial leads V1-V6.

Limitations

A general limitation in studies including ARVC patients is classification of definite ARVC, as other diseases can show similarities with ARVC. The current TFC for ARVC is the best available clinical

Table 8.2: Diagnostic values (SE, SP and AUC) of ARVC disease for six different parameters. Three leads with highest diagnostic values over the full decision range (AUC) were noted. Parameters with highest diagnostic values were marked blue.

ECG criteria	Lead position	Cutoff value	ARVC			PKP2		
			SE (%)	SP (%)	AUC (%)	SE (%)	SP (%)	AUC (%)
IAD (ms)	L40	> 41.9ms	86	100	97	13	100	59
	V4	> 39.9ms	100	78	90	31	78	55
	V3	> 41.9ms	86	100	89	0	100	48
TAD (ms)	V3	< 41.5ms	86	89	93	31	89	58
	L40	< 27.5ms	71	100	90	13	100	58
	V4	< 27.5ms	71	89	84	19	89	57
RWA (mV)	L40	> 0.38mV	100	67	84	63	56	60
	V3	> 0.47mV	71	78	79	31	78	47
	V4	> 0.80mV	71	78	76	31	78	61
SWA (mV)	L27	> -0.86mV	100	89	97	31	78	47
	L40	> -0.33mV	86	78	94	38	67	51
	V3	> -0.51mV	86	89	93	38	67	52
RSr	L40	> 0.31	100	100	100	25	100	57
	V3	> 0.05	100	89	99	25	89	47
	V4	> 0.34	100	78	94	56	78	61
TWI	V1	-	100	11	-	81	11	-
	V2	-	57	100	-	6	100	-
	L27	-	57	100	-	0	100	-

Abbreviations: IAD = initial activation duration; TAD = terminal activation duration; RWA = R-wave amplitude; SWA = S-wave amplitude; RSr = RS ratio; TWI = T-wave inversions; SE = sensitivity; SP = specificity; AUC = area under curve.

gold standard for diagnosis of ARVC under reasonable conditions. In this study, we assumed definite ARVC diagnosis in PKP2 gene variant carriers that met the TFC for ARVC.

The current clinical validation study was performed in the same patient population that was used before in this research thesis. No different dataset was available to validate additional lead positions and ECG criteria. Therefore, overestimation of the presented diagnostic values has to be taken into account.

Future perspectives

As was noted before, the usability of additional ECG criteria and lead positions has to be performed on a new validation dataset. Future clinical validation should also investigate diagnostic values (SE and SP) with pathological conditions simulating ARVC, such as myocarditis and sarcoidosis.⁶¹

Conclusion

This study investigated current and additional ECG criteria and additional lead positions for the differentiation of ARVC in PKP2 pathogenic variant carriers. ECG parameters that were based on time-intervals showed large errors, which emphasizes the importance of implementation of properly defined ECG criteria. The overall results showed highest diagnostic values in IAD (lead 40), SWA (lead 27) and RSr (leads V3, V4 and 40), but clinical validation performed in a new larger dataset has to confirm this finding.

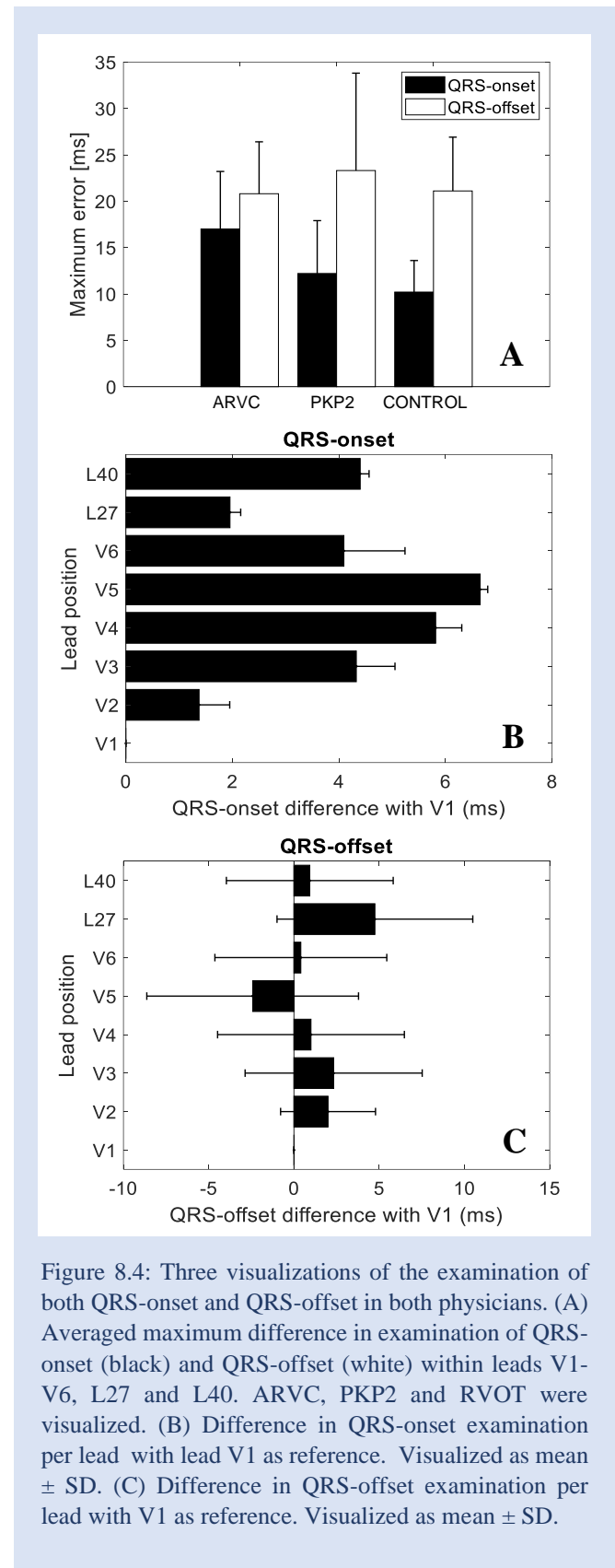


Figure 8.4: Three visualizations of the examination of both QRS-onset and QRS-offset in both physicians. (A) Averaged maximum difference in examination of QRS-onset (black) and QRS-offset (white) within leads V1-V6, L27 and L40. ARVC, PKP2 and RVOT were visualized. (B) Difference in QRS-onset examination per lead with lead V1 as reference. Visualized as mean \pm SD. (C) Difference in QRS-offset examination per lead with V1 as reference. Visualized as mean \pm SD.

CHAPTER 9

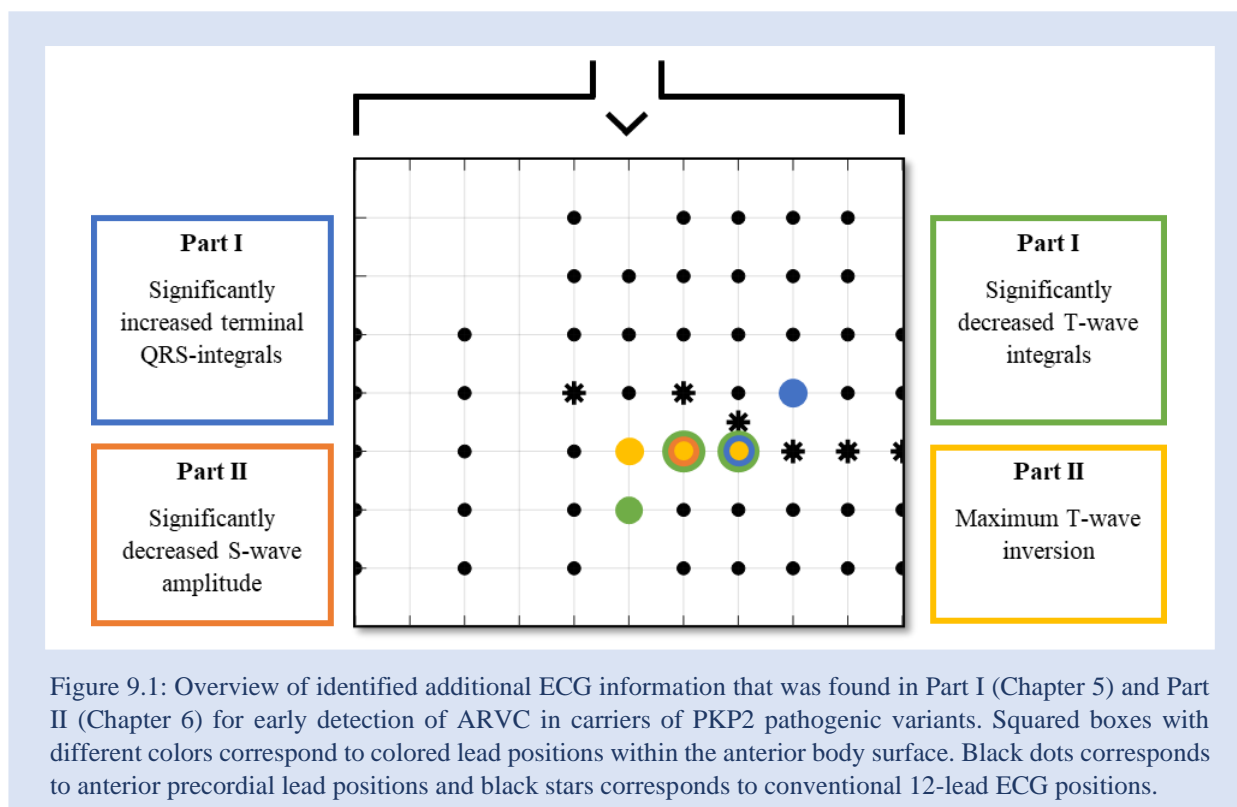
General discussion

GENERAL DISCUSSION

Additional ECG lead locations and ECG parameters have shown to be a potential benefit in the early detection of ARVC in PKP2 pathogenic variant carriers (**Chapter 8**). In the current TFC for ARVC, a major criterium for the identification of ARVC patients is the presence of T-waves inversions. In this study, PKP2 pathogenic variant carriers that met the TFC for ARVC, asymptomatic PKP2 pathogenic variant carriers and controls could be solely identified on depolarization characteristics (**Chapter 5 and 6**). The repolarization phase did not provide additional information to aid the early detection of disease manifestation. This emphasizes the importance of accurate monitoring of depolarization changes in PKP2 pathogenic variant carriers.

In lead 34 and 40 of the body surface potential map, the integral difference between ARVC subjects and controls was the highest (**Figure 9.1: blue dots and Chapter 5**). In these lead positions, increased terminal QRS-integrals were observed in all ARVC patients and up to 25% of all PKP2 pathogenic variant carriers (**Chapter 5**). Furthermore, S-wave amplitude in lead 27 was significantly decreased in ARVC subjects compared to controls (**Figure 9.1: orange dot and Chapter 6**). Maximum T-wave inversions in ARVC patients were observed in leads located inferior of conventional lead V2, whereby additional lead positioning suggests better detection of T-wave inversions (**Figure 9.1: yellow and green dots; Chapters 5 and 6**). However, T-wave inversions suggests not to be useful as a marker for initial disease manifestation, as no repolarization abnormalities have been observed in ARVC patients without T-wave inversions (**Chapter 6**).

T-wave inversions in ARVC patients were investigated before in multi-lead systems,^{49,53,54} but this is the first study that also focused on depolarization abnormalities in PKP2 pathogenic variant carriers that met the TFC for ARVC, asymptomatic PKP2 pathogenic variant carriers and controls. The departure mapping technique (**Chapter**



5) observed changes in the initial depolarization phase in local ventricular regions, where the novel CineECG method (**Chapter 7**) showed differences in the initial and mid depolarization mTSI trajectory through the ventricular anatomy. Where all current depolarization TFC for ARVC focus on the terminal depolarization phase, additional information about disease manifestation might be observed in the initial depolarization phase.

Additional ECG parameters (S-wave amplitude, R to S ratio, and initial activation duration) have shown to be a highly sensitive marker in the early detection of ARVC in PKP2 pathogenic variant carriers (**Chapter 8**). Two additional lead positions, located inferior of conventional lead V2 and superior of conventional lead V4, showed potential benefit in the detection rate of these additional ECG parameters. This thesis is a first step toward a disease-specific lead configuration that might improve the screening process for early detection of ARVC in PKP2 pathogenic variant carriers.

CLINICAL IMPLICATIONS

Early detection of disease manifestation in pathogenic variant carriers is clinically relevant for risk-stratification of ventricular arrhythmic events or SCD. Besides, early ECG-based diagnosis of ARVC might aid the screening process in both the hospital ‘financial & time’ aspect and reduce the screening load for pathogenic variant carriers. Screening procedures for PKP2 pathogenic variant carriers might be improved by using additional or changed lead positions for detection of subtle depolarization changes. Therefore, the current TFC for ARVC might need revision and requires additional ECG criteria that focus on the initial depolarization phase.

STUDY LIMITATIONS

A general limitation in studies including ARVC patients is the classification of ARVC, as other diseases can show similarities with ARVC. The current TFC for ARVC is the best available clinical gold standard for diagnosis of ARVC under reasonable conditions. The best diagnostic approach might be an invasive myocardial biopsy to determine whether there is fibrofatty tissue present in the right ventricle. However, a biopsy is rarely performed because it is invasive and shows poor sensitivity and specificity due to the diffuse characteristics of ARVC.⁶² In this study, definite ARVC diagnosis was assumed when meeting the TFC for ARVC, but misclassification of ARVC has to be taken into account.

Variation in precordial lead positions in the BSPM, body build and heart orientation might have affected the BSPM waveforms. For example, in the conventional 12-lead ECG recordings, variation in precordial lead placement of as little as 2 cm can result in important diagnostic errors.^{63,64} In future, reexamination and exclusion of these variations that affect BSPM waveforms might be obtained by investigating patient-specific heart-torso models from MRI/CT images.

In this study, BSPM signals were filtered, because of a significant amount of mains noise in the recordings. Mechanical noise (breathing) and mains noise are known factors to affect the recorded ECG. Inadequate filter setting might negatively affect the ECG, thereby also possibly filtering out high frequent signals characterizing ventricular disease.⁶³ Therefore, in future studies a recording of the BSPM needs to be performed in an environment with limited noise.

Manual segmentation of BSPM data may have introduced a human error in beat annotations, as QRS-onset, QRS-offset and T-wave end. Therefore, an reliable algorithm that automatically detects QRS-onset, -offset and T-wave end is recommended.

The sample size in this study is small, due to a rare patient population fulfilling the inclusion criteria. Nevertheless, the sample size is comparable to other studies.^{49,53,54,65} The small sample sizes might have caused biased results, but the high prevalence in the small ARVC group and the pathophysiological substantiation of ECG simulations suggest that results should also be applicable in larger group of patients. However, therefore a study in a larger group of patients is required.

This thesis is divided into three research parts and a validation study to eventually design a disease-specific lead configuration that might improve the screening process of pathogenic variant carriers. In **Part I**, the definition of terminal integrals (defined as the integral between RMS_{apex} and QRS-offset) can be debated, because this is not a fixed time interval and may have caused different integral outcomes based on different time intervals. Furthermore, most optimal lead positions for R-wave apex duration and RS ratio were obtained from departure maps of terminal QRS-integrals. Departure mapping might be deployed for the investigation of most optimal lead positions using these specific ECG criteria as input. In **Part II**, the ARVC group was subdivided based on the presence of ECG criteria, which resulted in even smaller patients groups that were compared with each other. Larger sample sizes are needed for subdividing ARVC patients based on disease progression. In **Part III**, the mean cardiac activation pattern through the cardiac anatomy was performed using a standardized cardiac model. Reexamination in patient-specific torso-heart models might substantiate if changes in initial and mid depolarization phase were related to disease progression or differences in cardiac orientation within the heart- and torso model. At last, a **validation study** was performed on the same dataset that was used to identify additional ECG criteria and optimal lead positioning. In the future, a new validation dataset has to be used to give an unbiased estimate of the benefit of the additional ECG criteria and lead positions.

FUTURE RESEARCH

This study investigated additional lead positions and ECG criteria for early detection of ARVC solely in PKP2 pathogenic variant carriers. Samol *et al.* observed differences in spatial distributions of T-wave integrals between PKP2-positive ARVC patients and PKP2-negative ARVC patients, that substantiates the need of pathogenic specific lead positioning.⁴⁹ Research expansion toward other pathogenic variants is required to investigate the hypothesis that different pathogenic variants might need different optimal lead positions for early detection of ARVC. Future research should investigate whether the current TFC for ARVC can be revised toward a pathogenic-variant-specific ECG criteria.

From the thesis results and ECG simulations (**Chapter 6**) we hypothesize that the heterogeneous and progressive aspect of ARVC might require TFC for ARVC that are based on ECG changes during disease manifestation and progression, like in Brugada Syndrome or myocardial ischemia. It is already known that T-wave inversions are more common in patients with advanced RV dysfunction and T-wave inversions through V4 are related to LV involvement.^{18,19} ECG changes during initial disease manifestation must be investigated through long-term ECG monitoring in pathogenic variant carriers and correlation of additional ECG criteria with disease progression is required.

In ECG-based screening procedures with pathogenic variant carriers at risk for ARVC, it is major important to limit the variation in precordial lead placement in order to detect small ECG abnormalities. For future perspectives, lead placement variability might be reduced by registration of a 3D camera recording that visualizes precordial leads positions on a torso for repositioning.⁶⁶

Future clinical validation studies have to take into account that ARVC shows many similarities with other diseases like RVOT tachycardia, Brugada Syndrome, myocarditis and sarcoidosis.^{61,67} The lack of research in specificity of the current ECG criteria for ARVC highlights the need of differentiation of ARVC from diseases that mimic ARVC (**Appendix A.1**).

CONCLUSION

The current thesis showed that additional depolarization characteristics and lead positioning may improve the early detection of disease manifestation in PKP2-pathogenic variant carriers. The study results suggest that repolarization abnormalities are not a useful marker for detection of initial disease manifestation. Future research requires long-term monitoring of pathogenic variant carriers to relate newly identified depolarization criteria with onset of disease manifestation.

References

REFERENCES

1. Neto JE, Tonet J, Frank R, Fontaine G. Arrhythmogenic Right Ventricular Cardiomyopathy/Dysplasia (ARVC/D)-What We Have Learned after 40 Years of the Diagnosis of This Clinical Entity. *Soc Bras Cardiol.* 2018;112(1):91-103. doi:10.5935/abc.20180266
2. Quarta G, Elliott PM. Diagnostic criteria for arrhythmogenic right ventricular cardiomyopathy. *Rev Esp Cardiol.* 2012;65(7):599-605. doi:10.1016/j.recesp.2012.02.016
3. Basso C, Corrado D, Marcus FI, Nava A, Thiene G. Arrhythmogenic right ventricular cardiomyopathy. *Lancet.* 2009;373:1289-1300. doi:10.1016/S0140-6736(09)60256-7
4. Priori S, Blomstro C, Blom N, et al. 2015 ESC Guidelines for the management of patients with ventricular arrhythmias and the prevention of sudden cardiac death. *Eur Soc Cardiol.* 2015;17:1601-1687. doi:10.1093/europace/euv319
5. van der Harst P. Aritmogene rechterventrikelcardiomyopathie: verschillende uitingen als voorbode van mogelijk te voorkomen plotse hartdood. *Ned Tijdschr Geneesk.* 2004;2396-2402.
6. van der Zwaag PA, Cox MGPI, van der Werf C, et al. Recurrent and founder mutations in the Netherlands: Plakophilin-2 p.Arg79X mutation causing arrhythmogenic right ventricular cardiomyopathy/dysplasia. *Netherlands Hear J.* 2010;18(12):583-591. doi:10.1007/s12471-010-0839-5
7. Jacob KA, Noorman M, Cox MGPI, Groeneweg JA, Hauer RNW, van der Heyden MAG. Geographical distribution of plakophilin-2 mutation prevalence in patients with arrhythmogenic cardiomyopathy. *Netherlands Hear J.* 2012;20(5):234-239. doi:10.1007/s12471-012-0274-x
8. Mast TP, James CA, Calkins H, et al. Evaluation of structural progression in arrhythmogenic right ventricular dysplasia/cardiomyopathy. *JAMA Cardiol.* 2017;2(3):293-302. doi:10.1001/jamacardio.2016.5034
9. Marcus FI. Diagnosis of ARVC; proposed modification of the task force criteria. *Eur Heart J.* 2010;31(7):1533-1541. doi:10.1161/CIRCULATIONAHA.108.840827
10. Garrod D, Chidgey M. Desmosome structure, composition and function. *Biochim Biophys Acta - Biomembr.* 2008;1778(3):572-587. doi:10.1016/j.bbmem.2007.07.014
11. Ohno S. The genetic background of arrhythmogenic right ventricular cardiomyopathy. *J Arrhythmia.* 2016;32:398-403. doi:10.1016/j.joa.2016.01.006
12. Asimaki A, Kleber AG, Saffitz JE. Pathogenesis of Arrhythmogenic Cardiomyopathy. *Can J Cardiol.* 2015:1-22.
13. Bosman LP, Verstraelen TE, van Lint FHM, et al. The Netherlands Arrhythmogenic Cardiomyopathy Registry: design and status update. *Netherlands Hear J.* 2019;27(10):480-486. doi:10.1007/s12471-019-1270-1
14. Cox MGPI, van der Zwaag PA, van der Werf C, et al. Arrhythmogenic right ventricular dysplasia/cardiomyopathy: pathogenic desmosome mutations in index-patients predict outcome of family screening: Dutch arrhythmogenic right ventricular dysplasia/cardiomyopathy genotype-phenotype follow-up study. *Circulation.* 2011;123(23):2690-2700. doi:10.1161/CIRCULATIONAHA.110.988287
15. Cox MGPI, Nelen MR, Wilde AAM, et al. Activation delay and VT parameters in arrhythmogenic right ventricular dysplasia/cardiomyopathy: Toward improvement of diagnostic ECG criteria. *J Cardiovasc Electrophysiol.* 2008;19(8):775-781. doi:10.1111/j.1540-8167.2008.01140.x
16. Nasir K, Bomma C, Tandri H, et al. Electrocardiographic features of arrhythmogenic right ventricular dysplasia/cardiomyopathy according to disease severity: A need to broaden diagnostic criteria. *Circulation.* 2004;110(12):1527-1534. doi:10.1161/01.CIR.0000142293.60725.18
17. García-Niebla J, Baranchuk A, Bayés de Luna A. Epsilon Wave in the 12-Lead Electrocardiogram: Is Its Frequency Underestimated? *Rev Española Cardiol (English Ed).* 2016;69(4):438. doi:10.1016/j.rec.2015.09.012
18. Jain R, Dalal D, Daly A, et al. Electrocardiographic features of arrhythmogenic right ventricular dysplasia. *Circulation.* 2009;120(6):477-487. doi:10.1161/CIRCULATIONAHA.108.838821

19. Romero J, Mejia-Lopez E, Manrique C, Lucariello R. Arrhythmogenic right ventricular cardiomyopathy (ARVC/D): A systematic literature review. *Clin Med Insights Cardiol.* 2013;7:97-114. doi:10.4137/CMC.S10940
20. Zhang L, Liu L, Kowey PR, Fontaine GH. *Send Orders for Reprints to Reprints@benthamscience.Net The Electrocardiographic Manifestations of Arrhythmogenic Right Ventricular Dysplasia.* Vol 10.; 2014.
21. Bauce B, Frigo G, Marcus FI, et al. Comparison of Clinical Features of Arrhythmogenic Right Ventricular Cardiomyopathy in Men Versus Women. *Am J Cardiol.* 2008;102(9):1252-1257. doi:10.1016/j.amjcard.2008.06.054
22. Ruwald A-C, Marcus F, Mark NA, et al. Association of competitive and recreational sport participation with cardiac events in patients with arrhythmogenic right ventricular cardiomyopathy: results from the North American multidisciplinary study of arrhythmogenic right ventricular cardiomyopathy. *Eur Heart J.* 2015;36:1735-1743. doi:10.1093/eurheartj/ehv183
23. Sattar Y, Abdullah HM, Neisani Samani E, Myla M, Ullah W. Arrhythmogenic Right Ventricular Cardiomyopathy/Dysplasia: An Updated Review of Diagnosis and Management. *Cureus.* August 2019;11. doi:10.7759/cureus.5381
24. Barr RC, Spach MS. Construction and interpretation of body surface maps. *Prog Cardiovasc Dis.* 1983;26(1):33-42. doi:10.1016/0033-0620(83)90017-8
25. Lux RL. Body Surface Potential Mapping Techniques. In: *Comprehensive Electrocardiology.* Volume 1., ; 2010:2291.
26. Sridharan MR, Horan LG. History of Body Surface Electrocardiographic Mapping. In: *Body Surface Electrocardiographic Mapping.* Boston; 1998:21-27. doi:10.1007/978-1-4613-1769-2_2
27. Hoekema R. *The Interindividual Variability of the Electrocardiogram.* Utrecht; 1999.
28. MettingVanRijn AC, Peper A, Grimbergen CA. Amplifiers for bioelectric events: a design with minimal number of parts. *Med Biol Eng Comput.* 1994;32:305:310.
29. MettingVanRijn AC, Kuiper AP, Linnenbank AC, Grimbergen CA. Patient Isolation in Multichannel Bioelectric Recordings by Digital Transmission Through a Single Optical Fiber. *IEEE Trans Biomed Eng.* 1993;40(3):302-308. doi:10.1109/10.216416
30. Di Bernardo D, Langley P, Murray A. Effect of changes in heart rate and in action potential duration on the electrocardiogram T wave shape. *Physiol Meas.* 2002;23(2):355-364. doi:10.1088/0967-3334/23/2/311
31. Lee RJ, Liem LB, Cohen TJ, Franz MR. Relation between repolarization and refractoriness in the human ventricle: Cycle length dependence and effect of procainamide. *J Am Coll Cardiol.* 1992;19(3):614-618. doi:10.1016/S0735-1097(10)80281-5
32. van Dam PM. A new anatomical view on the vector cardiogram: The mean temporal-spatial isochrones. *J Electrocardiol.* 2017;50(6):732-738. doi:10.1016/j.jelectrocard.2017.08.010
33. Roberts DE, Hersh LT, Scher AM. Influence of cardiac fiber orientation on wavefront voltage, conduction velocity, and tissue resistivity in the dog. *Circ Res.* 1979;44(5):701-712. doi:10.1161/01.RES.44.5.701
34. Kleber AG, Janse MJ, Wilms-Schopman FJG. Changes in conduction velocity during acute ischemia in ventricular myocardium of the isolated porcine heart. *Circulation.* 1986;73(1):189-198. doi:10.1161/01.CIR.73.1.189
35. Cranefield PF, Hoffman BF. Propagated repolarization in heart muscle. *J Gen Physiol.* 1958;41(4):633-649.
36. Durrer D, van Dam RT, Freud GE, Janse MJ, Meijler FL, Arzbaecher RC. Total excitation of the isolated human heart. *Circulation.* 1970;41(6):899-912. doi:10.1161/01.CIR.41.6.899
37. van Dam PM, Locati ET, Ciconte G, et al. Novel CineECG Derived from Standard 12-Lead ECG Enables Right Ventricle Outflow Tract Localization of Electrical Substrate in Patients with Brugada Syndrome. *Circ Arrhythmia Electrophysiol.* 2020. doi:10.1161/circep.120.008524
38. Shimizu W, Takagi M, Aiba T, Taguchi A, Kurita T, Kamakura S. Body Surface Distribution and Response to Drugs of ST Segment Elevation in Brugada Syndrome: Clinical Implication of Eighty-Seven-Lead Body Surface Potential Mapping and Its Application to Twelve-Lead Electrocardiograms. *J*

- Cardiovasc Electrophysiol.* 2000;11(4):396-404.
39. Ibanez B, James S, Agewall S, et al. 2017 ESC Guidelines for the management of acute myocardial infarction in patients presenting with ST-segment elevation. *Eur Heart J.* 2018;39(2):119-177. doi:10.1093/eurheartj/ehx393
 40. Meregalli PG. UvA-DARE (Digital Academic Repository) Brugada syndrome: clinical and pathophysiological aspects Meregalli, P.G. 2009. <https://dare.uva.nl/search?identifier=72df5970-1041-4fa3-9cd9-56027283b153>.
 41. Hong K, Brugada J, Oliva A, et al. Value of electrocardiographic parameters and ajmaline test in the diagnosis of Brugada syndrome caused by SCN5A mutations. *Circulation.* 2004;110(19):3023-3027. doi:10.1161/01.CIR.0000144299.17008.07
 42. McCabe JM, Armstrong EJ, Ku I, et al. Physician accuracy in interpreting potential ST-segment elevation myocardial infarction electrocardiograms. *J Am Heart Assoc.* 2013;2(5):1-9. doi:10.1161/JAHA.113.000268
 43. Sadeghi R, Dabbagh VR, Tayyebi M, Zakavi SR, Ayati N. Diagnostic value of fragmented QRS complex in myocardial scar detection: Systematic review and meta-analysis of the literature. *Kardiol Pol.* 2016;74(4):331-337. doi:10.5603/KP.a2015.0193
 44. Buttà C, Zappia L, Laterra G, Roberto M. Diagnostic and prognostic role of electrocardiogram in acute myocarditis: A comprehensive review. *Ann Noninvasive Electrocardiol.* 2020;25(3):125-134. doi:10.1111/anec.12726
 45. Deluigi CC, Ong P, Hill S, et al. ECG findings in comparison to cardiovascular MR imaging in viral myocarditis. *Int J Cardiol.* 2013;165(1):100-106. doi:10.1016/j.ijcard.2011.07.090
 46. Sayah DM, Bradfield JS, Moriarty JM, Belperio JA, Lynch JP. *Cardiac Involvement in Sarcoidosis: Evolving Concepts in Diagnosis and Treatment.* Vol 38.; 2017. doi:10.1055/s-0037-1602381
 47. Ikeda K, Yamaki M, Honma K. Use of Body Surface Electrocardiographic Mapping to Localize the Asynergic Site in Previous Myocardial Infarction. *J El.* 1990;23(1):13-22.
 48. Hamid MS, Norman M, Quraishi A, et al. Prospective evaluation of relatives for familial arrhythmogenic right ventricular cardiomyopathy/dysplasia reveals a need to broaden diagnostic criteria. *J Am Coll Cardiol.* 2002;40(8):1445-1450. doi:10.1016/S0735-1097(02)02307-0
 49. Samol A, Wollmann C, Vahlhaus C, et al. T-wave integral : an electrocardiographic marker discriminating patients with arrhythmogenic right ventricular cardiomyopathy from patients with right ventricular outflow tract tachycardia. 2013:582-589. doi:10.1093/europace/eus311
 50. Gambill CL, Wilkins ML, Haisty WK, et al. T wave amplitudes in normal populations. Variation with ECG lead, sex, and age. *J Electrocardiol.* 1995;28(3):191-197. doi:10.1016/S0022-0736(05)80257-2
 51. Nasir JM, Rubal BJ, Jones SO, Shah AD. The effects of body mass index on surface electrocardiograms in young adults. *J Electrocardiol.* 2012;45(6):646-651. doi:10.1016/j.jelectrocard.2012.07.022
 52. Corrado D, Zorzi A, Cerrone M, et al. Relationship between arrhythmogenic right ventricular cardiomyopathy and brugada syndrome. *Circ Arrhythmia Electrophysiol.* 2016;9(4). doi:10.1161/CIRCEP.115.003631
 53. Heidi A.P. Peeters, Arne SippensGroenewegen, Bas A. Schoonderwoerd, Eric F.D. Wever, Cornelis A. Grimbergen, Richard N.W. Hauer and EOR de M. Body-Surface QRST Integral Mapping - Arrhythmogenic Right Ventricular Dysplasia Versus Idiopathic Right Ventricular Tachycardia. *Circulation.* 1997;95(12):2668-2676. doi:10.1161/01.CIR.95.12.2668
 54. Luigi De Ambroggi, Ezio Aimè, Carlo Ceriotti, Marina Rovida and SN. Mapping of Ventricular Repolarization Potentials in Patients With Arrhythmogenic Right Ventricular Dysplasia - Principal Component Analysis of the ST-T Waves. *Circulation.* 1997;96(12):4314-4318. doi:10.1161/01.CIR.96.12.4314
 55. Cox MG PJ, Van Der Smagt JJ, Wilde AAM, et al. New ECG criteria in arrhythmogenic right ventricular dysplasia/ cardiomyopathy. *Circ Arrhythmia Electrophysiol.* 2009;2(5):524-530. doi:10.1161/CIRCEP.108.832519
 56. King JH, Huang CLH, Fraser JA. Determinants of myocardial conduction velocity: Implications for arrhythmogenesis. *Front Physiol.* 2013;4 JUN(June):1-14. doi:10.3389/fphys.2013.00154

57. Gering LE, Surawicz B, Knilans TK, Tavel ME. *Chou's Electrocardiography in Clinical Practice*. 6th ed. Saunders Elsevier; 2008.
58. Cortez D, Svensson A, Carlson J, et al. Right precordial-directed electrocardiographical markers identify arrhythmogenic right ventricular cardiomyopathy in the absence of conventional depolarization or repolarization abnormalities. 2017;1-10. doi:10.1186/s12872-017-0696-x
59. Roudijk R, Loh P, Van Dam P. Mean Temporal Spatial Isochrones Direction as Marker for Activation Delay in Patients with Arrhythmogenic Cardiomyopathy. *Comput Cardiol (2010)*. 2018;45:1-4. doi:10.22489/CinC.2018.033
60. Pérez-Riera AR, De Abreu LC, Barbosa-Barros R, Nikus KC, Baranchuk A. R-Peak Time: An Electrocardiographic Parameter with Multiple Clinical Applications. *Ann Noninvasive Electrocardiol*. 2016;21(1):10-19. doi:10.1111/anec.12323
61. Avella A, D'Amati G, Pappalardo A, et al. Diagnostic value of endomyocardial biopsy guided by electroanatomic voltage mapping in arrhythmogenic right ventricular cardiomyopathy/dysplasia. *J Cardiovasc Electrophysiol*. 2008;19(11):1127-1134. doi:10.1111/j.1540-8167.2008.01228.x
62. Wang W, James CA, Calkins H. Diagnostic and therapeutic strategies for arrhythmogenic right ventricular dysplasia/cardiomyopathy patient. *Europace*. 2019;21(1):9-21. doi:10.1093/europace/euy063
63. Paul Kligfield, Leonard S. Gettes, James J. Bailey, Rory Childers, Barbara J. Deal, E. William Hancock, Gerard van Herpen, Jan A. Kors, Peter Macfarlane, David M. Mirvis, Olle Pahlm, Pentti Rautaharju and GSW. Recommendations for the Standardization and Interpretation of the Electrocardiogram. *Circulation*. 2007;115(10):1306-1324. doi:10.1161/CIRCULATIONAHA.106.180200
64. Kania M, Rix H, Fereniec M, et al. The effect of precordial lead displacement on ECG morphology. *Med Biol Eng Comput*. 2014;52(2):109-119. doi:10.1007/s11517-013-1115-9
65. Marcinkevics R, Neill JO, Law H, et al. Multichannel electrocardiogram diagnostics for the diagnosis of arrhythmogenic right ventricular dysplasia. 2018:13-19. doi:10.1093/europace/eux124
66. Van Dam P, Roudijk RW, Boonstra MJ. Feasibility study of a 3D camera to reduce electrode repositioning errors during longitudinal ECG acquisition. *Under Rev J Electrocardiol*. 2020.
67. Corrado D, van Tintelen PJ, McKenna WJ, et al. Arrhythmogenic right ventricular cardiomyopathy: evaluation of the current diagnostic criteria and differential diagnosis. *Eur Heart J*. 2020;41(14):1414-1429. doi:10.1093/eurheartj/ehz669

Appendix

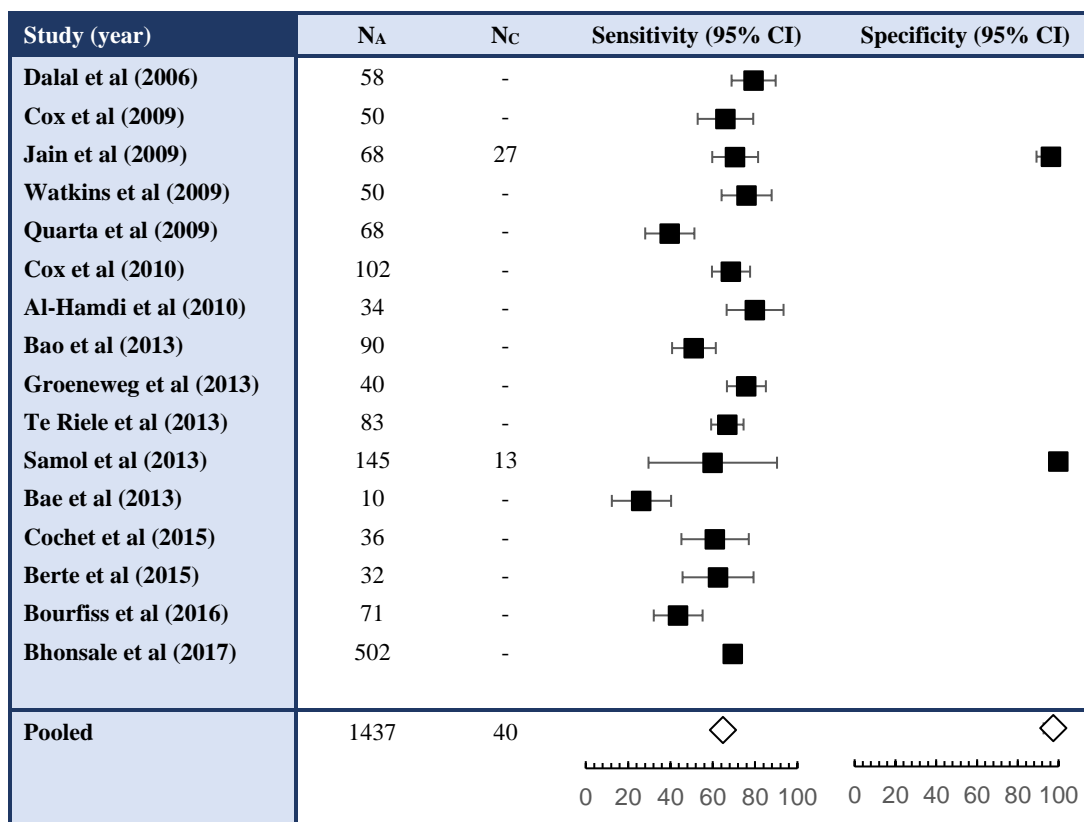
APPENDIX A - INTRODUCTION

A.1 PREVALENCE OF ECG TFC FOR ARVC

Many previous studies have investigated the presence of TFC in ARVC patients. Many different sensitivities were found and therefore, this small literature study was set up to view the prevalence of ECG TFC in ARVC patients. The current literature study focused on T-wave inversion from V1 through V3 in the absence of RBBB (major criteria), prolonged terminal activation delay in V1, V2 or V3 (minor criteria), and epsilon waves in V1, V2 or V3 (minor criteria).

Pubmed was queried using the following search terms and abbreviations: arrhythmogenic right ventricular cardiomyopathy/dysplasia, diagnosis, electrocardiography, PKP2[#], features*, criteria*. Only articles in English, published in the period of 2005-2020 were considered. The results showed [#]40 and *36 results, from which 19 studies showed relevant data. In **Table A.1**, **A.2**, and **A.3**, the sensitivities and specificities of the T-wave inversion, prolonged TAD and epsilon waves were displayed, respectively. As can be observed, not often the specificity was reported in the current 19 studies. Specificities were determined in control groups including healthy subjects with no history, symptoms or underlying cardiomyopathy.

Table A.1: Forest plot visualizing the sensitivity and specificity of T-wave inversion (through V3) in ARVC patients.



N_A = number of ARVC subjects; N_C = number of controls; CI = confidence interval

Table A.2: Forest plot visualizing the sensitivity and specificity of prolonged TAD in ARVC patients.

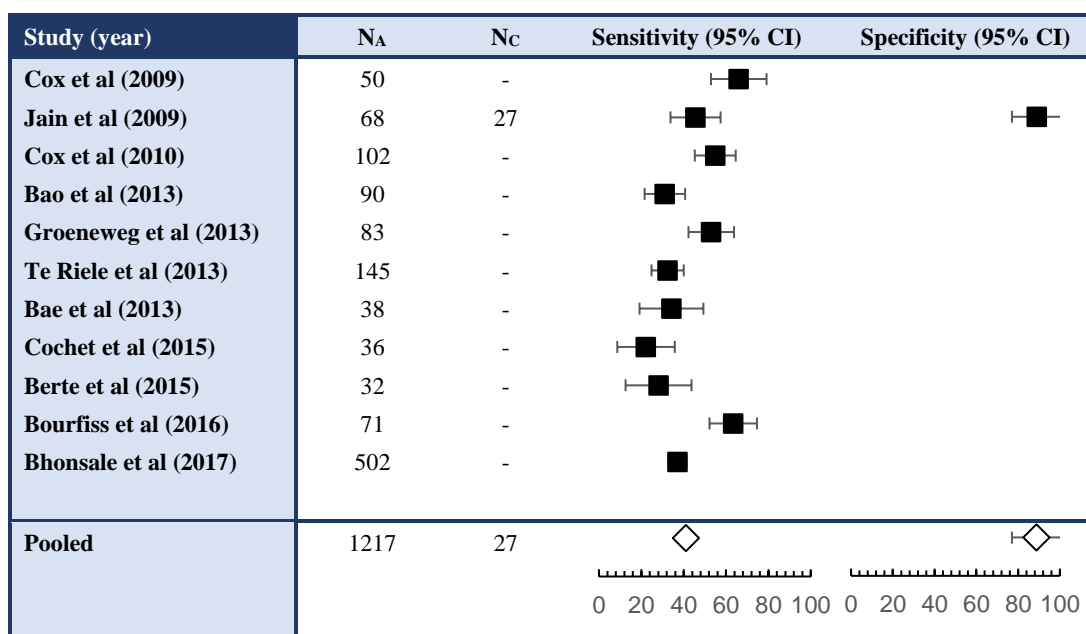
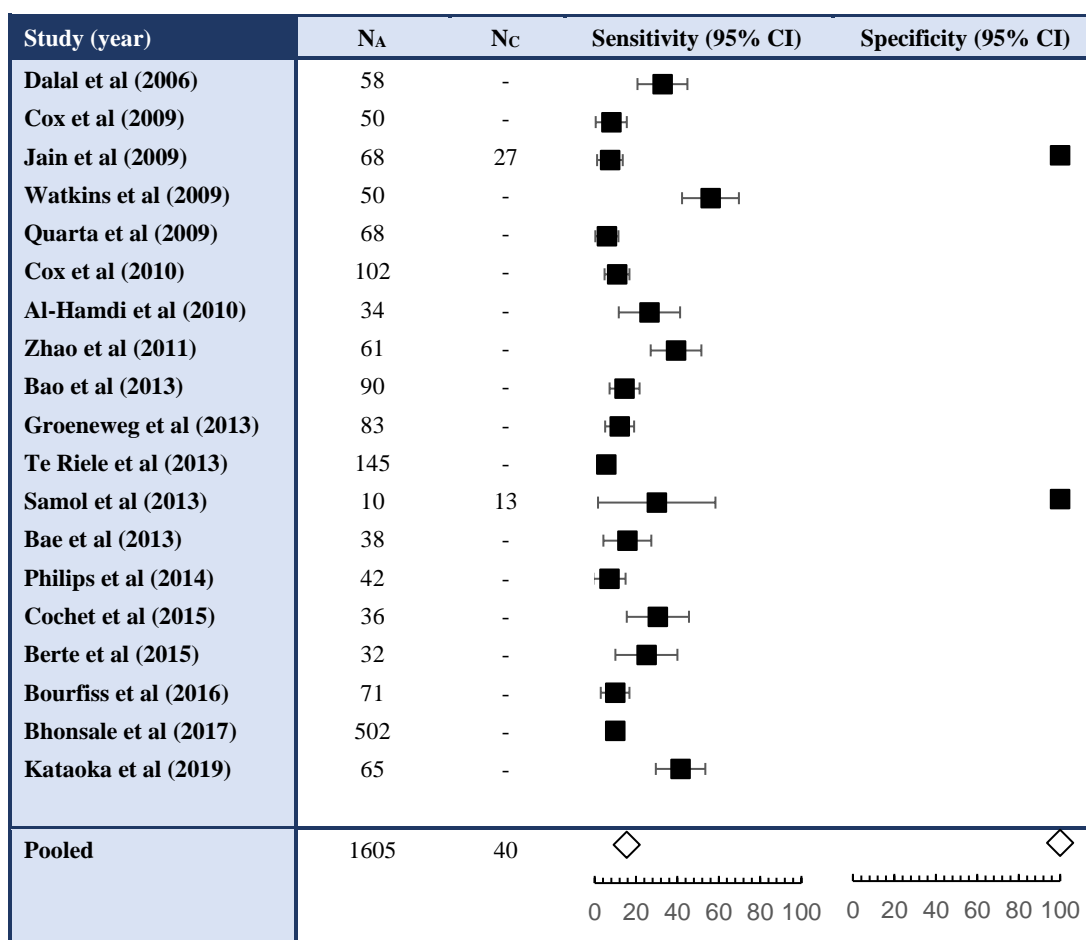


Table A.3: Forest plot visualizing the sensitivity and specificity of Epsilon waves in ARVC patients.



N_A = number of ARVC subjects; N_C = number of controls; CI = confidence interval

APPENDIX B – PART I

B.1 INTEGRALS MAPPING

The average QRS-integrals for all groups were determined and visualized in integral maps (**Figure B.1**). The minimum QRS-integral position was similar for each averaged group and located in lead 21 (marked with \ominus). In the ARVC group, the maximum QRS-integral position was positioned in lead 35, where the maximum position in PKP2 and CONTROL was positioned more toward the left precordial region (lead 42) (marked with \oplus).

ARVC subjects showed significant higher minimum averaged QRS-integrals ($-18.6 \pm 10.2\text{mVms}$) compared to PKP2 subjects ($-43.1 \pm 19.4\text{mVms}$; $p=0.005$) and controls ($-34.2 \pm 12.0\text{mVms}$; $p=0.016$). Maximum averaged QRS-integrals

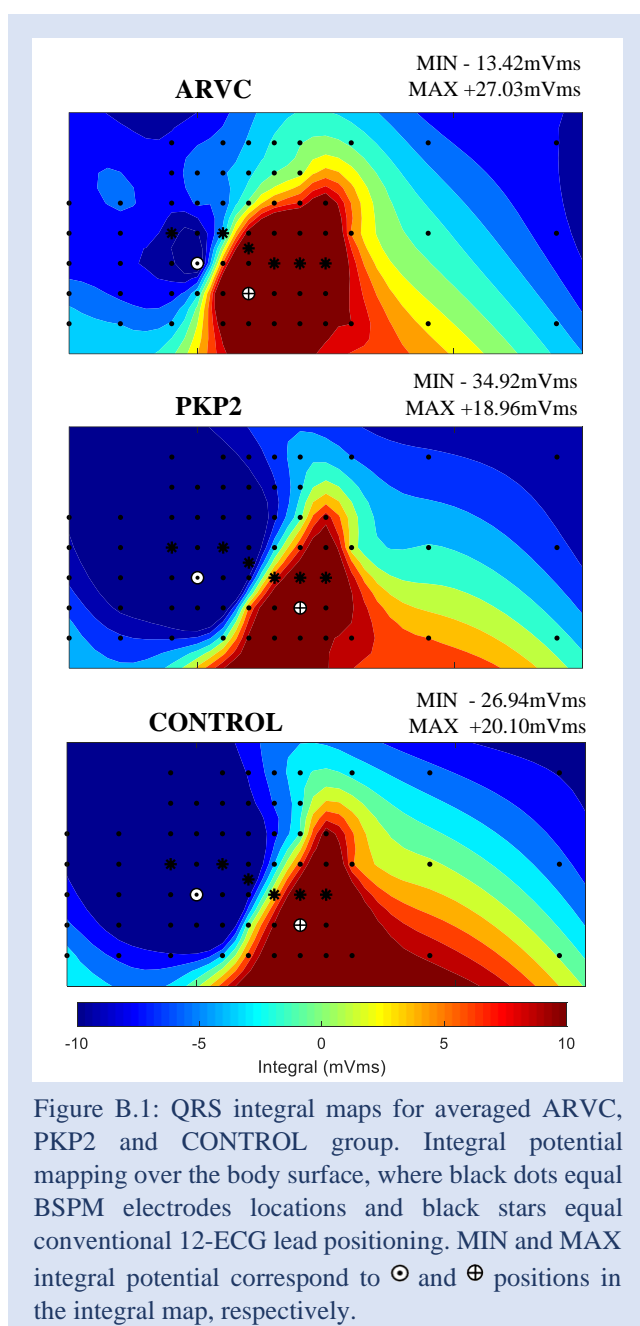


Figure B.1: QRS integral maps for averaged ARVC, PKP2 and CONTROL group. Integral potential mapping over the body surface, where black dots equal BSPM electrodes locations and black stars equal conventional 12-ECG lead positioning. MIN and MAX integral potential correspond to \ominus and \oplus positions in the integral map, respectively.

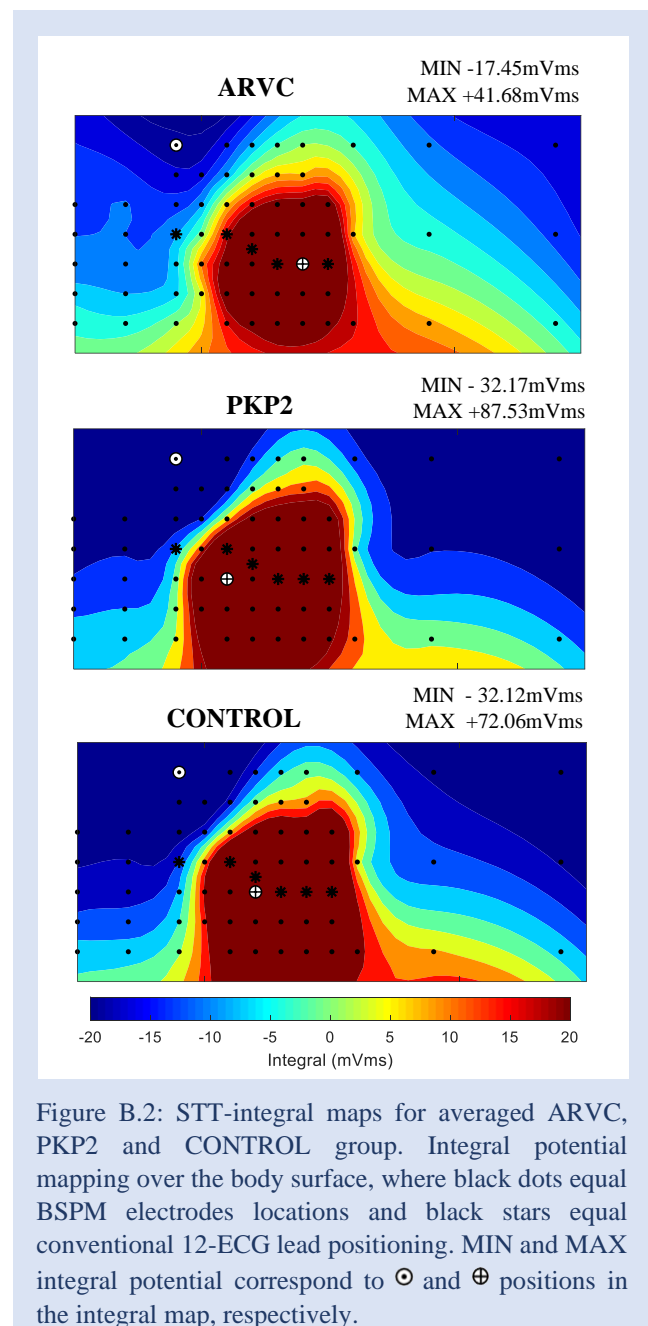


Figure B.2: STT-integral maps for averaged ARVC, PKP2 and CONTROL group. Integral potential mapping over the body surface, where black dots equal BSPM electrodes locations and black stars equal conventional 12-ECG lead positioning. MIN and MAX integral potential correspond to \ominus and \oplus positions in the integral map, respectively.

of ARVC subjects ($33.5 \pm 21.6\text{mVms}$) showed no differences compared to PKP2 subjects ($24.4 \pm 9.7 \text{ mVms}$; $p=0.17$) and controls ($23.7 \pm 10.0\text{mVms}$; $p=0.24$).

The average STT-integrals for all groups were determined and visualized in integral maps (**Figure B.2**). The minimum STT-integral position was similar for each averaged group and located in lead 11 (marked with \ominus). The maximum STT-integral position was observed in lead 48 in the ARVC group and in lead 27/34 in the PKP2/CONTROL group. Besides, the averaged ARVC group showed decreased maximum and increased minimum STT-integrals compared to PKP2 and CONTROLS.

B.2 DEPARTURE MAPPING

In Part I of this thesis, departure maps were determined for QRS-integrals, terminal QRS-integrals, STT-integrals and terminal STT-integrals. In **Figure B.3**, the departure maps of the QRS-integrals and STT-integrals for an individual ARVC patient were visualized. A filled 2D contour plot was used to visualize the isolines of departure indexes, using a colormap from [-4:1:4].

A region of significant increased QRS-integrals around the maximum marker (\oplus) was observed (**Figure B.3; left**). The maximum departure index was +3.12 and was observed in lead 47. **Figure B.3 (right)** visualizes the significant decreased STT-integrals in the area inferior of conventional lead V2. Here, the minimum departure index (\ominus) was observed in lead 22, and the maximum departure index (\oplus) was observed in the reciprocal lead 60.

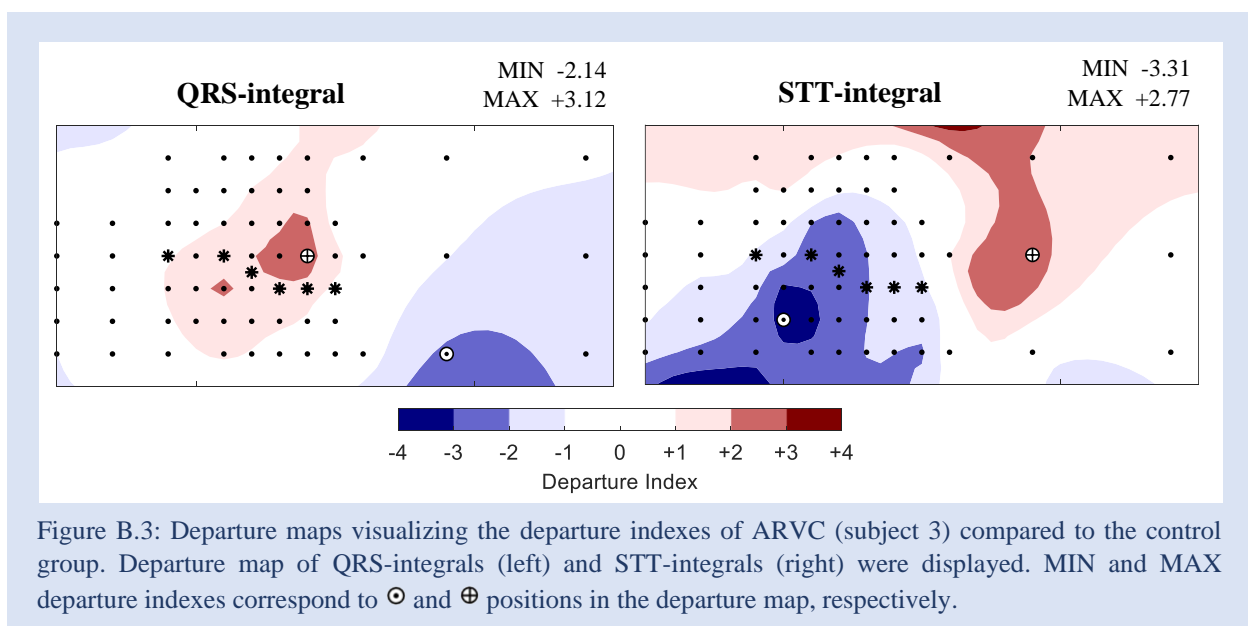
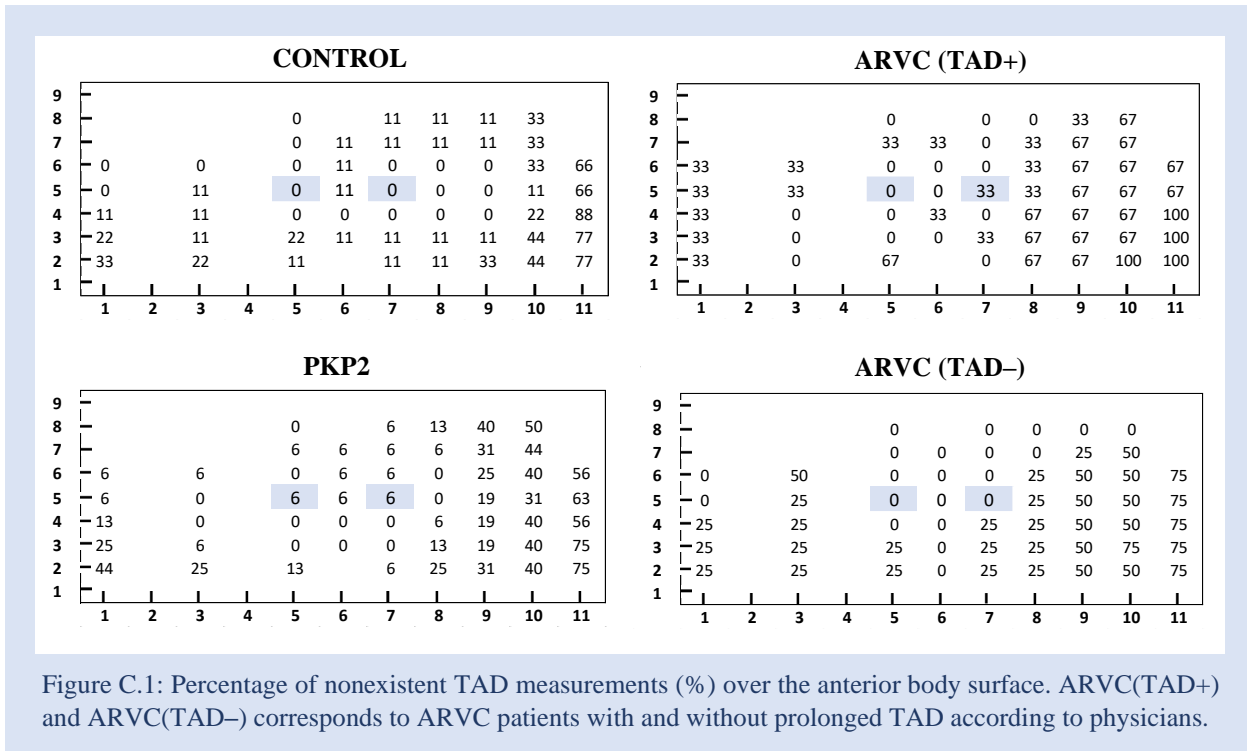


Figure B.3: Departure maps visualizing the departure indexes of ARVC (subject 3) compared to the control group. Departure map of QRS-integrals (left) and STT-integrals (right) were displayed. MIN and MAX departure indexes correspond to \ominus and \oplus positions in the departure map, respectively.

APPENDIX C – PART II

C.1. NON-EXISTENT TAD MEASUREMENTS

TAD measurements were defined non-existent when S-wave amplitudes were not present in a lead or when the lead potential was removed due to presence of noise. The percentages of non-existent TAD measurements over the anterior body surface were visualized, showing an increase in percentage toward left precordial leads (**Figure C.1**).



C.2. SPATIAL DISTRIBUTION OF S-WAVE UPSTROKE

S-wave upstroke, first described by Nasir *et al.*¹⁶, was defined as the time interval from nadir of the S-wave to the isoelectric baseline. The spatial distributions of the S-wave upstroke over the anterior body surface were determined and visualized (**Figure C.2**). The position of the maximum S-wave upstroke was investigated in all individual subjects (**Figure C.3**). Note that ARVC maximum position is defined above lead V6 (**Figure C.2**), but that S-waves were absent in five out of seven ARVC patients (**Figure C.1**). This resulted in a shift of maximum S-wave upstroke position. The local maximum S-wave upstroke in the averaged spatial distribution plot in lead 21 was 45.0ms and is decreased compared to PKP2 or CONTROLS.

C.3. SPATIAL DISTRIBUTION OF S-WAVE AMPLITUDE

Spatial distribution of S-wave amplitude was investigated in all groups. Averaged S-wave amplitude distributions were shown in **Figure C.4**, where the averaged maximum S-wave amplitude can be observed in the area of lead V2. Position and maximum S-wave amplitude were investigated in all individual subjects and were visualized (**Figure C.5**). ARVC patients showed smaller S-wave amplitudes ($0.9 \pm 0.43\text{mV}$) compared to PKP2 ($1.5 \pm 0.52\text{mV}$) and controls ($1.32 \pm 0.33\text{mV}$).

C.4. REPRODUCIBILITY OF TAD

Differences in TAD measurements between computational algorithm and clinical physician were investigated in all seven ARVC patients in both BSPM data and 12-lead ECG data from patient files. Clinical examination was performed in lead V1 to V3 by one physician from conventional 12-lead recording using paper speed of 25 mm/s, low-pass filter at 150Hz and sample frequency of 1000Hz.

Computational examination was performed based on the algorithm explained in the method of this study (**Chapter 6**). QRS-offset was manually determined in the root-mean-square (RMS) of all leads. In **Figure C.5**, an example of computational determination of TAD measurements in one ARVC patient can be observed for both BSPM data (black) and 12-ECG data (red). Both lead potentials (solid lines) and RMS (dotted lines) show large agreement between BSPM data and 12-ECG data.

The TAD measurements of both the computational algorithm and physician were determined and visualized (**Figure C.6** and **Table C.1**). The averaged number of days between recording of 12-lead ECG data and BSPM data was 6.3 ± 8.5 days. The results showed high variation between physician and computational algorithm, but also within physicians the computational algorithm.

TAD measurement between BSPM data and 12-lead ECG data by one physician showed variations of 13.6 ± 16.8 ms (range 0-25ms) in V1, 15.7 ± 14.6 ms (range 0-30ms) in V2, and 11.4 ± 10.8 ms (range 5-25ms) in V3. Cox *et al.* analyzed ECG data from 42 ARVC patients and 27 controls in a randomized setting and after blinding for other results.¹⁵ The results from Cox *et al.* show smaller variation (2.9 ± 3.5 ms; range 0-15ms) compared to the results in this study, but there can be debated that the 12-lead ECG positioning was not performed twice. According to the spatial distribution of TAD, precordial lead placement might affect TAD measurement and therefore might result in higher TAD variation in V1 to V3.

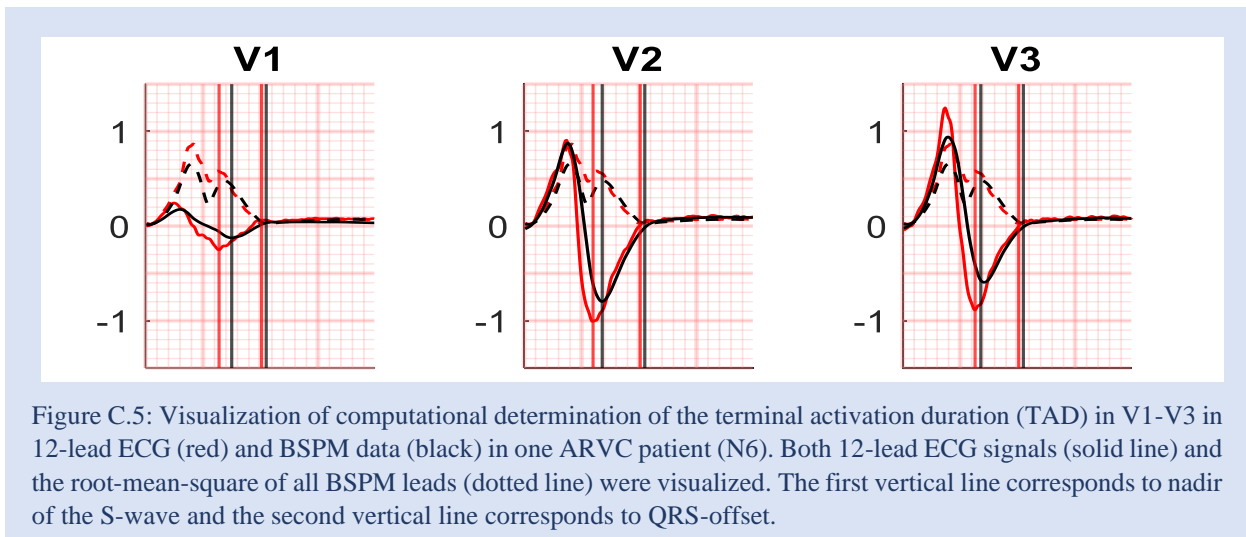


Table C.1: Terminal activation duration measurements by computer algorithm [A] and physician [B] in lead V1, V2 and V3. TAD measurements were noted in mean (standard deviation).

	V1			V2			V3		
	A	B	<i>p-value</i> *	A	B	<i>p-value</i> *	A	B	<i>p-value</i> *
BSPM	45.3 (12.0)	44.3 (13.0)	0.73	40.5 (7.3)	40.7 (12.1)	0.66	31.2 (7.0)	30.8 (7.4)	0.051
12-ECG	35.6 (7.0)	49.3 (13.0)	0.01	36.4 (5.7)	52.1 (11.9)	0.003	24.3 (8.8)	41.4 (12.8)	0.01
<i>p-value</i> #	0.07	0.46		0.30	0.08		0.19	0.046	

BSPM versus 12-ECG

* Computational algorithm versus physician

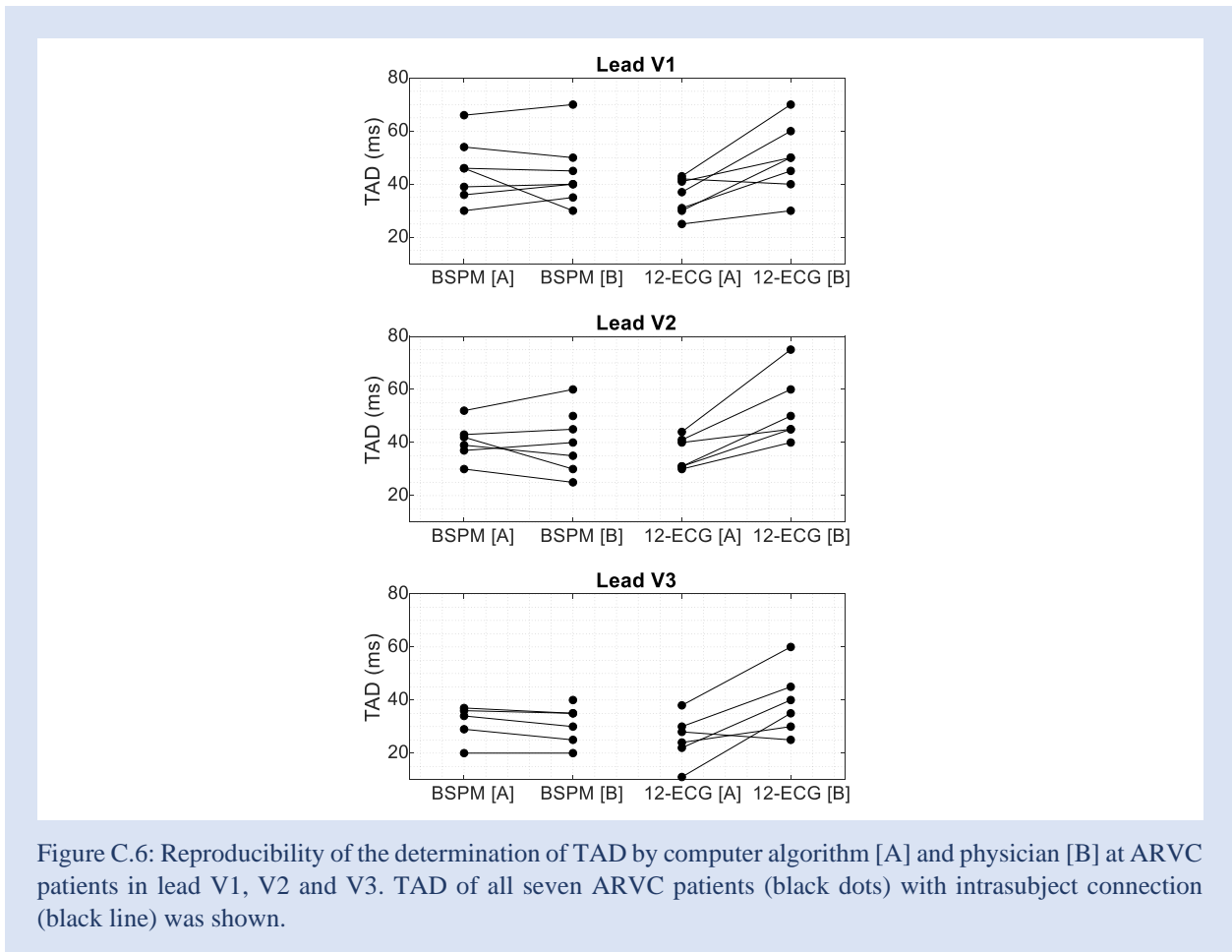


Figure C.6: Reproducibility of the determination of TAD by computer algorithm [A] and physician [B] at ARVC patients in lead V1, V2 and V3. TAD of all seven ARVC patients (black dots) with intrasubject connection (black line) was shown.

APPENDIX D – PART III

Table D.1: Group characteristics in mean (SD), for every patient group. Where ARVC (A), ARVC (B), and ARVC (C) correspond to QRS-width <90ms, 90-120ms, and >120ms, respectively.

Group	ARVC (A)	ARVC (B)	ARVC (C)
Number (#)	9	13	6
QRS segment (ms)	81 (5)	103 (9)	151 (21)
STT segment (ms)	311 (17)	307 (39)	330 (33)

D.1. OTHER ARVC POPULATION

A larger dataset including conventional 12-lead ECGs from 28 ARVC patients was used to visualize ARVC disease progression in subgroups. No subject characteristics were available from this group besides definite ARVC diagnosis. All ARVC patients were divided in three subgroups based on QRS-duration: <90ms (A), 90-120ms (B) and >120ms (C). ECG characteristics per group were shown in **Table D.1**.

The averaged mTSI trajectories of the QRS-segment (red) and STT-segment (blue) were visualized for three ARVC patient groups, subdivided by QRS-width (**Figure D.1**). Similar mTSI parameters were determined as in **Chapter 7 (Table D.2)**. ARVC (A) show compact QRS mTSI trajectory (TCR and minimal TCR of 16%) and initial ST-segment is directed towards the septal region immediately after QRS-offset (QRS-STT-angle of 81%). As was observed in ARVC patients in **Chapter 7**, QRS₂₀ was positioned more basal in ARVC(A) patients compared to controls (Z). At QRS₅₀, increase in QRS-duration results in a more posterior-basal position (X and Z) in the ventricular anatomy. At QRS₈₀, an increase in QRS-duration causes a decreased trajectory propagation toward the left ventricle (Y) and deviating toward the posterior wall (X). The delayed right ventricular activation, that results in a late ventricular activation pattern toward the right-basal ventricular wall, can be observed in ARVC (C) in QRS₁₁₀ (Z).

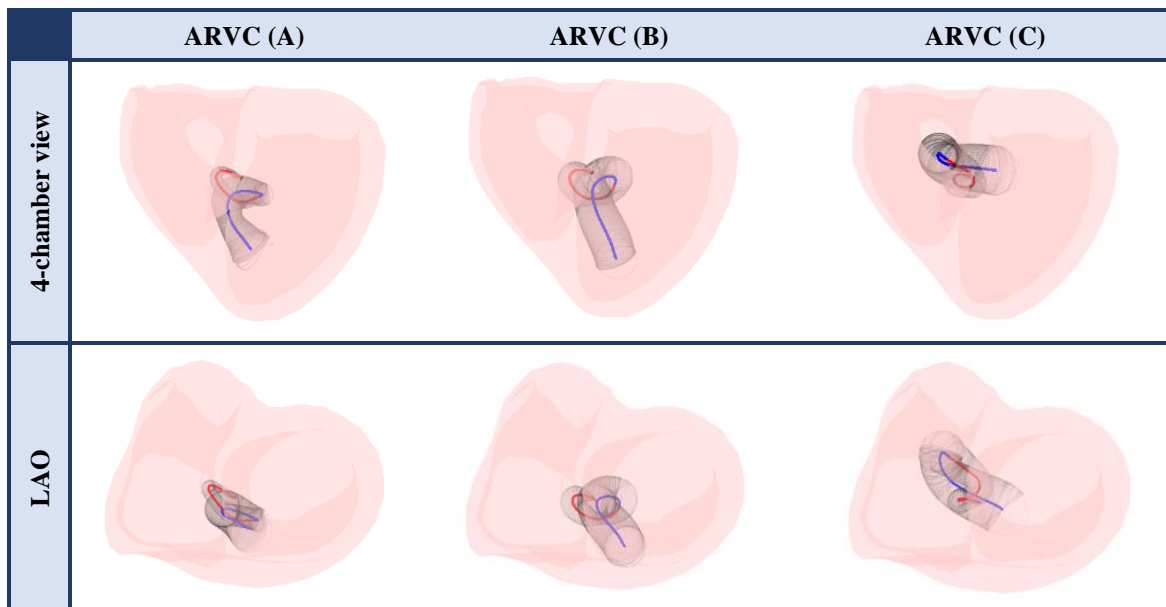
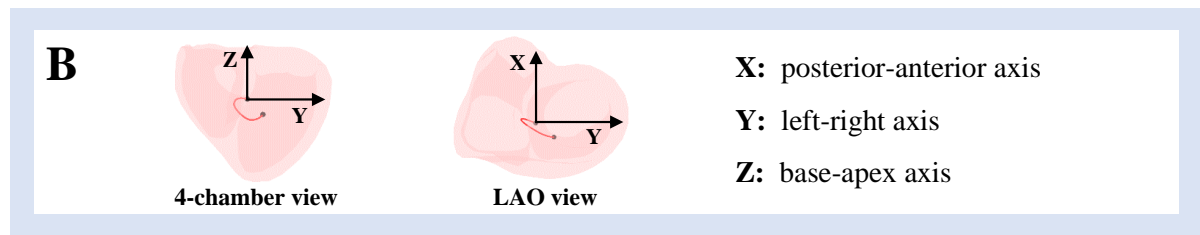


Figure D.1: Visualization of ARVC patients with (A) QRS-width <90ms (n=9), (B) 120ms > QRS-width >90ms (n=13), and (C) QRS-width > 120ms (n=6). Ventricular depolarization was shown in red and ventricular repolarization in blue. Transparent black circle plane corresponds to one standard deviation.

At increased QRS-durations, i.e. conduction disturbances, the mTSI trajectory differed from the normal mTSI trajectory in its terminal QRS-segment, but also differences were observed in the early QRS trajectory pattern (**Table D.2 and Figure D.1**). In ARVC (C), late ventricular activation caused large changes in QRS-end, with QRS trajectories positioned at right basal-posterior area. The transition from terminal QRS-segment toward initial ST-segment is more curved at increased QRS-duration (lower QRS-STT-angle), where terminal T-wave trajectories were directed toward left mid-posterior ventricular wall.

Table D.2: mTSI parameters determined in the ARVC (A), ARVC (B) and ARVC (C) group (A), including a 2D visualization of the X, Y and Z axes within the cardiac anatomy (B). Different mTSI parameters of ARVC (C) compared to ARVC (A) are marked blue. See text (Chapter 7) for definitions of all mTSI parameters.

A	ARVC (A)			ARVC (B)			ARVC (C)		
	X	Y	Z	X	Y	Z	X	Y	Z
QRS ₂₀ (mm)	3 (4)	-10 (1)	3 (2)	1 (5)	-8 (4)	0 (5)	-1 (3)	-7 (4)	0 (2)
QRS ₅₀ (mm)	-6 (2)	8 (4)	-14 (2)	-4 (2)	6 (7)	-12 (2)	0 (7)	1 (8)	-5 (9)
QRS ₈₀ (mm)	-3 (7)	14 (5)	3 (5)	1 (10)	12 (7)	4 (8)	6 (5)	4 (5)	7 (6)
QRS ₁₁₀ (mm)	1 (3)	-3 (2)	1 (2)	4 (5)	-1 (7)	8 (7)	4 (8)	-7 (7)	7 (6)
TCR (%)		16 (6)			20 (10)			46 (20)	
TCRmin (%)		16 (7)			14 (8)			19 (22)	
QRS-STT-angle (°)		79 (44)			48 (37)			34 (45)	
RVmax (mm)		12 (3)			11 (6)			11 (5)	



Disease-Specific Electrocardiographic Lead Positioning for Early Detection of Arrhythmogenic Right Ventricular Cardiomyopathy

Janna Ruisch^{1,2}, Machteld J Boonstra², Rob W Roudijk², Peter M van Dam², Cornelis H Slump¹, Peter Loh²

¹University of Twente, Enschede, The Netherlands

²University Medical Center Utrecht, Utrecht, The Netherlands

Abstract

Arrhythmogenic right ventricular cardiomyopathy (ARVC) is characterized by replacement of cardiomyocytes by fibrofatty tissue which can lead to ventricular arrhythmias, heart failure or sudden cardiac death. Genetic defects in desmosomal proteins, as plakophilin-2 (PKP2), are known to contribute to disease development. Current electrocardiographic (ECG) criteria for ARVC diagnosis only focus on right precordial leads, but sensitivity of current depolarization criteria is limited. This study aimed to identify additional depolarization criteria with most optimal lead configurations for early detection of ARVC in PKP2 pathogenic mutation carriers. In PKP2-positive ARVC patients (n=7), PKP2 pathogenic variant carriers (n=16) and control subjects without structural heart disease (n=9), 67-lead body surface potential maps (BSPM) were obtained. Terminal QRS-integrals were determined and quantitatively compared to controls using departure mapping. Significantly different terminal QRS-integrals were identified in lead 34 (conventional V3), 40 and 41 (conventional V4). To conclude, a clear distinction between ARVC patients, asymptomatic mutation carriers and healthy controls was observed.

1. Introduction

Arrhythmogenic right ventricular cardiomyopathy (ARVC) is characterized by replacement of cardiomyocytes by fibrofatty tissue that may lead to sudden cardiac death, ventricular arrhythmias or heart failure. Genetic defects in desmosomal proteins, with plakophilin-2 (PKP2) being the most frequently affected gene, contribute to disease development. The current 2010 Task Force Criteria (TFC) for diagnosis of ARVC are based on a set of major and minor criteria from different diagnostic modalities. However, diagnosis of ARVC is complex due to a heterogenous clinical presentation of the disease.¹⁻³

The association between structural and electrical progression in ARVC patients has been demonstrated.⁴ Significant structural right ventricular (RV) progression were associated with prior depolarization abnormalities. Therefore, accurate detection of electrical abnormalities is of utmost importance for early detection of ARVC. Current electrocardiographic (ECG) criteria of ARVC focus on the presence of abnormalities (e.g. epsilon waves, prolonged terminal activation duration (TAD) or negative T-waves) in right precordial leads V1-V3. However, only negative T-waves showed to be highly sensitive (79%) compared to prolonged TAD (40%) and epsilon waves (10%).^{1,5}

The amount of information obtained with conventional 12-lead ECG suffices for most clinical applications. However, in some applications the use of extra ECG leads or other lead locations has proven to increase the detection rate, like Brugada Syndrome or posterior or inferior myocardial infarction.⁶⁻⁸ This study aims to determine additional depolarization criteria and optimal lead positioning for early detection of ARVC in PKP2 pathogenic variant carriers.

2. Method

2.1. Study population

The study population consisted of PKP2 pathogenic variant carriers (n=23) and control subjects (n=9) with symptomatic ventricular extrasystoles originating in the right ventricular outflow tract (RVOT VES). Exclusion criteria were a right bundle branch block (QRS width > 120ms) and other structural diseases that affect ECG morphology apart from ARVC symptoms. Besides, controls that showed signs of heart failure were excluded in the study (LV or RV ejection fraction < 45%, RV end-diastolic volume index > 110ml/m²). PKP2 pathogenic variant carriers were tested to meet the TFC for ARVC and assigned to either the ARVC subgroup (TFC ≥ 4) or PKP2 subgroup. Informed consent was obtained from all subjects. The study was approved by the Medical Ethics Committee of University Medical Center Utrecht (17/907).

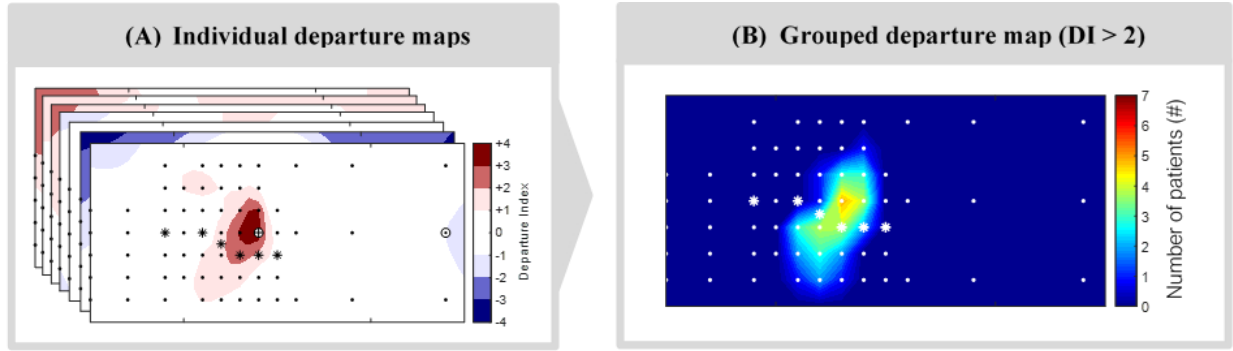


Figure 1. Overview that visualizes the combining process of all individual departure maps toward one single grouped departure map. (A) Seven individual departure maps (ARVC vs CONTROL) with the departure index (DI) per lead position. (B) Grouped departure map, where the value at each lead corresponds to the total ARVC subjects that show significantly different integrals ($DI > 2$) in the body surface potential map. The small dots indicate all BSPM electrodes and the stars refer to the conventional 12-lead electrode positions.

2.2. Body surface potential mapping

67-lead body surface potential map (BSPM) were obtained in each subject, consisting of 64 precordial and 3 limb leads (Figure 1, small dots). The anterior body surface includes 55 leads, that were placed in nine vertical strips. Within the vertical strips, leads were separated 4cm from each other. The posterior body surface includes 9 leads, that were placed in three vertical columns. BSPM were recorded (sampling frequency 2048Hz, 24bits/sample, Biosemi, Amsterdam, The Netherlands). Precordial leads were referenced to Wilson's central terminal. BSPMs were down-sampled to 1000Hz. Leads with noise were removed.

2.3. Data analysis

Per subject, ten consecutive sinus beats obtained during resting respiration were averaged. QRS-onset and QRS-end were manually annotated using the root mean square (RMS) of all leads. Early electrical depolarization abnormalities of ARVC disease in PKP2 pathogenic variant carriers were investigated by comparing integral maps from BSPM data. Integral maps were computed of the last 60ms of the QRS complex (terminal QRS integral), which indicates a mean potential direction over this interval.

2.4. Departure mapping technique

The departure index (DI) was used to determine the extent of integral deviation from the normal range in the control group. The DI was calculated by:

$$DI = \frac{I_N - \mu_{control}}{\sigma_{control}} \quad (1)$$

where I_N equals the integral of an individual subject N , $\mu_{control}$ is the mean integral of control group and $\sigma_{control}$ is the standard deviation of the integrals in control group.

Both ARVC subjects and PKP2 pathogenic variant carriers were compared with the control group. DI was calculated for each integral per lead and integrals significantly differing (> 2 SD) from the control data were classified as abnormal. Per subgroup, individual departure maps were summed to identify significant differences per group (Figure 1).

Receiver Operating Characteristic (ROC) curves were used to define optimal cut-off values for ARVC classification. The diagnostic values of ARVC of additional ECG parameters and lead positions were determined by calculating the sensitivity (SE) and specificity (SP).

3. Results

From all PKP2 pathogenic variant carriers, seven subjects met the TFC for ARVC. Patient characteristics are stated in Table 1.

Table 1: Patient characteristics

Variables	ARVC (n = 7)	PKP2 (n = 16)	CONTROL (n = 9)
Male	4	5	3
Age (y)	36 ± 18	38 ± 17	34 ± 13
TFC (#)	6.6 ± 2.4	2.2 ± 0.4	-
Onset diagnosis (y)	3.7 ± 3.8	-	-
QRS width (ms)	103 ± 8	106 ± 6	105 ± 9
Heart rate (bpm)	61 ± 10	61 ± 11	63 ± 9
LV EDVI (ml/m ²)	93 ± 15	94 ± 11	95 ± 17
LV EF (%)	59 ± 5	55 ± 4	54 ± 5
RV EDVI (ml/m ²)	129 ± 40	92 ± 13	92 ± 14
RV EF (%)	41 ± 13	56 ± 6	53 ± 6

Abbreviations: LV = left ventricle. EDVI = end-diastolic volume index. EF = ejection fraction. RV = right ventricle. TFC = Task Force Criteria.

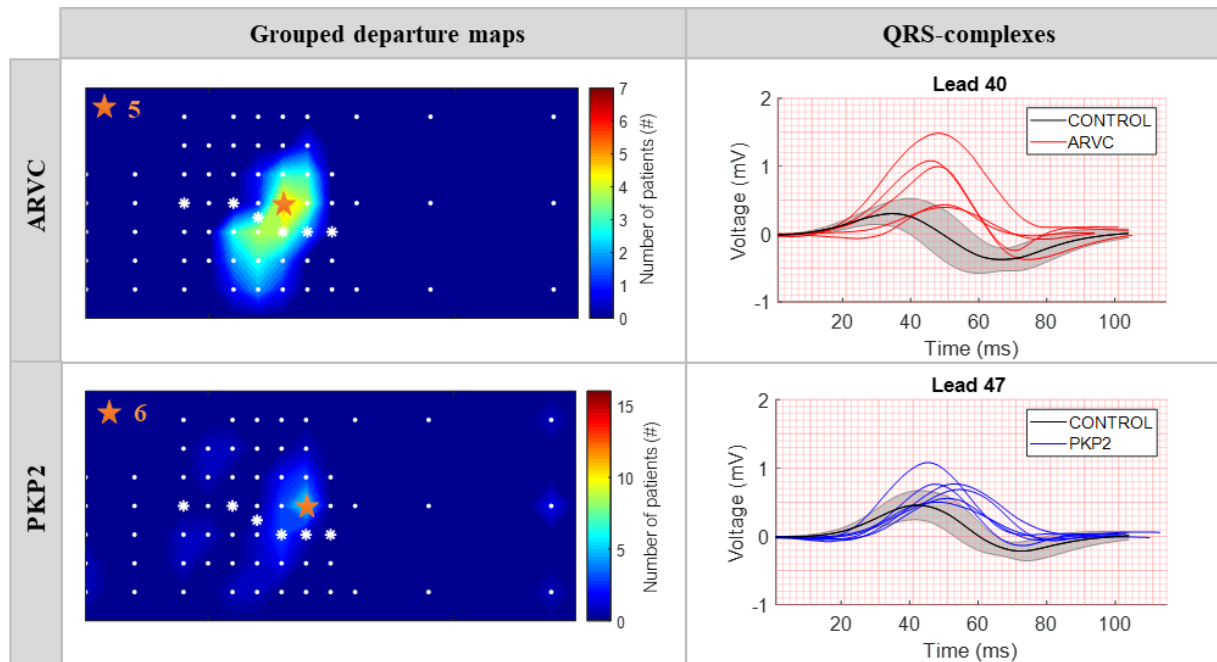


Figure 2. Grouped departure maps ($DI > 2$) of terminal QRS-integrals (left) and QRS-complexes of orange starred lead positions (right). The grouped departure maps and QRS-potentials of ARVC vs CONTROL (upper row) and PKP2 vs CONTROL (bottom row) were visualized. Orange stars correspond to leads where most subjects showed significantly different integrals. Maximum was noted in left-upper corner of the grouped departure map.

Lead 40 is significantly different in five out of seven ARVC patients (Figure 2, orange star). Six out of 16 PKP2 pathogenic variant carriers showed different terminal QRS-integrals in lead 47. The QRS-complexes of five ARVC subjects in lead 40 and six PKP2 pathogenic variant carriers in lead 47 were visualized in Figure 2.

The difference in both terminal QRS-integrals and R-wave apex duration were determined in conventional 12-lead positions, lead 40 and 47 (Table 2) for both groups.

4. Discussion

The purpose of this study was to identify additional depolarization parameters and optimal lead placement for the early detection of ARVC in PKP2 pathogenic variant carriers. Significant differences were found in terminal QRS-integrals compared to the control group. The results indicate that depolarization abnormalities can be observed in other leads beyond conventional 12-lead ECG positions V1-V3. From the grouped departure map, lead 40 (above lead 41 which corresponds to conventional V4) showed significant increased terminal QRS-integrals ($DI > 2$) in five out of seven ARVC patients. In PKP2 pathogenic variant carriers, lead 47 (above lead 48 which position corresponds to conventional V5) showed significantly different integrals.

Significantly higher terminal QRS-integrals in both ARVC and PKP2 pathogenic variant carriers, can be

explained by increased R-wave amplitudes (mV), delayed R-wave apex (ms), and decreased S-wave amplitude (mV) in QRS-complexes (Figure 2). These changes might be declared by defects in cell-cell adhesion, caused by the presence of PKP2 pathogenic gene variants in desmosomal proteins. Desmosomes are essential to withstand mechanical stresses caused by the contractile function of the heart. Segments with largest mechanical stress during the cardiac cycle were most commonly structural affected in ARVC, like the inflow tract, outflow tract or apex of the RV. This study observed electrical changes in ARVC patients are not only present in the RV, but can appear in LV. PKP2 is known to be a right ventricular dominant disease, but based on results in this study the right-sided phenotype might only be valid for structural abnormalities. This hypothesizes that the area of electrical abnormalities does not have to agree with the area of structural abnormalities, which substantiates the need of revision of the current ECG TFC for ARVC.

Despite the known heterogenous clinical presentation of ARVC, terminal QRS-integrals and R-wave apex duration showed to be a highly sensitive ($>86\%$) and specific ($>89\%$) criteria in lead V3, V4 and 40 for all subjects. Using these cut-off values in PKP2 pathogenic variant carriers, up to 44% were classified with electrical abnormalities that were found in ARVC patients.

This study excluded patients with prolonged QRS-duration ($QRS > 120\text{ms}$) to focus on initial

Table 2. Differentiation of ARVC subjects (n=7) and PKP2 pathogenic variant carriers (n=16) from control subjects (n=9) for both conventional 12-lead ECG positions and new lead positions found with the departure mapping technique.

Lead	Terminal QRS-integral (mVms)					R-wave apex duration (ms)				
	CO (mVms)	ARVC		PKP2		CO (ms)	ARVC		PKP2	
		SE (%)	SP (%)	SE (%)	SP (%)		SE (%)	SP (%)	SE (%)	SP (%)
14 (V1)	-2.9	29	100	6	100	10	71	78	25	78
26 (V2)	-13.9	57	89	13	89	15	86	78	56	78
*33-34 (V3)	-11.9	100	89	44	89	28	86	89	25	89
41 (V4)	-1.7	100	89	44	89	37	86	100	25	100
48 (V5)	16.6	57	89	13	89	37	86	67	50	67
53 (V6)	18.2	43	78	13	78	38	57	67	50	67
40	-1.9	100	100	31	100	32	100	89	38	89
47	4.3	86	89	38	89	40	43	89	19	89

Abbreviations: CO = cut-off value. SE = sensitivity. SP = specificity.

* The average of lead 33 and 34 corresponds with conventional V3 position.

depolarization abnormalities as we assumed that first electrical changes caused by disease progression do not directly result in increased QRS-duration. Besides, RVOT VES patients were used as controls. A future clinical validation has to be performed in healthy subjects without RVOT VES, as due to the occurrence of RVOT VES the absence of an underlying pathological process cannot be guaranteed. Electrical abnormalities in RVOT VES subjects might affect the results found with the departure mapping technique. Furthermore, a clinical validation of these additional parameters is required to relate electrical changes with early disease progression. Alterations of electrical abnormalities that were also observed in PKP2 pathogenic variant carriers require longer follow-up to relate electrical abnormalities to early disease progression of ARVC.

5. Conclusion

This study revealed additional lead positions beside conventional 12-lead ECG positions in which electrical changes were observed that may be used to identify the onset of disease in pathogenic mutation carriers. Similar depolarization changes in both ARVC patients and PKP2 pathogenic variant carriers were shown. The additional lead positions in combination with the newly identified depolarization criteria, are likely to improve detection of the early onset of disease in PKP2 pathogenic variant carriers.

Acknowledgments

This work was supported by the Netherlands Cardiovascular Research Initiative, an initiative with support of the Dutch Heart Foundation (grant numbers CVON2015-12 eDETECT and QRS-Vision 2018B007).

References

- [1] Marcus FI. Diagnosis of ARVC; proposed modification of the task force criteria. *Eur Heart J.* 2010;31(7):1533-1541.
- [2] Quarta G, Elliott PM. Diagnostic criteria for arrhythmogenic right ventricular cardiomyopathy. *Rev Esp Cardiol.* 2012;65(7):599-605.
- [3] Bosman LP, Verstraelen TE, van Lint FHM, *et al.* The Netherlands Arrhythmogenic Cardiomyopathy Registry: design and status update. *Neth Heart J.* 2019;27(10):480-486.
- [4] Mast TP, James CA, Calkins H, *et al.* Evaluation of structural progression in arrhythmogenic right ventricular dysplasia / cardiomyopathy. *JAMA Cardiol.* 2017;2(3):293-302.
- [5] Bhonsale A, te Riele ASJM, Sawant AC, *et al.* Cardiac phenotype and long-term prognosis of arrhythmogenic right ventricular cardiomyopathy/dysplasia patients with late presentation. *Heart Rhythm.* 2017;14(6):883-891.
- [6] Priori S, Blomstro C, Blom N, *et al.* 2015 ESC Guidelines for the management of patients with ventricular arrhythmias and the prevention of sudden cardiac death. *Eur Soc Cardiol.* 2015;17:1601-1687.
- [7] Shimizu W, Takagi M, Aiba T, Taguchi A, Kurita T, Kamakura S. Body surface distribution and response to drugs of ST-segment elevation in Brugada Syndrome: clinical implication of eighty-seven-lead body surface potential mapping and its application to twelve-lead electrocardiograms. *J Cardiovasc Electrophysiol.* 2000;11(4):396-404.
- [8] Ibanez B, James S, Agewall S, *et al.* 2017 ESC Guidelines for the management of acute myocardial infarction in patients presenting with ST-segment elevation. *Eur Heart J.* 2018;39(2):119-177.

Address for correspondence:

Janna Ruisch

Heidelberglaan 100, 3584 CX, Utrecht, The Netherlands

Email: j.ruisch@umcutre